

**POLITECNICO DI MILANO**

**Scuola di Ingegneria Industriale e dell'Informazione**

Corso di Laurea Magistrale in Automation and Control Engineering



Voltage and Frequency secondary control of islanded  
Low Voltage Inverter-Based Microgrid

Relatore: Prof. Sergio Bittanti

Correlatore: Ing. Riccardo Lazzari

Tesi di Laurea Magistrale di:

Davide Morena

Matricola 838178

Anno accademico 2017 - 2018



# Ringraziamenti

*Desidero ringraziare in primis l'ingegner Ricardo Lazzari, per la supervisione, la disponibilità ed il prezioso aiuto che mi ha fornito durante tutto il periodo di sviluppo e stesura di questa tesi.*

*Vorrei ringraziare il professor Bittanti per avermi concesso l'opportunità di svolgere l'attività di tirocinio presso RSE e ringrazio, inoltre, l'ingegner De Marco per la smisurata passione che è riuscito a trasmettermi.*

*Vorrei ringraziare i miei genitori per avermi supportato moralmente ed economicamente durante la mia carriera scolastica.*

*Ringrazio mio fratello per avermi rallegrato e consolato nei momenti più difficili di questi anni universitari.*

*Ringrazio, infine, tutti i miei parenti, amici e persone che mi sono state vicini in questi anni.*

# Abstract

Nowadays the energy production is moving towards a more sustainable ways to satisfy the increasing attention to environmental issues. Renewable energy sources have been establishing themselves as a valid alternative to the classic fossil-fuel oriented energy production; in this context, an interest in Microgrids design and control is growing more and more. In fact, the microgrid concept represents an appealing alternative for overcoming the challenges of integrating Distributed Energy Resource units, including renewable energy sources, in the current power systems. A microgrid can work either connected to the main grid, in grid-connected mode, or can separate from it and work alone, in islanded-mode. Major issues occur exactly in this case; the stochastic nature of both renewable sources and loads could create unbalances between the total generated power and the absorbed one. While in the grid-connected mode any power mismatch is compensated by a power exchange with the main grid, unbalance in islanded mode has a considerable impact on the network electrical variable, which can significantly deviate from their nominal value. The main objective of this work is to design a centralized controller for the coordination of the energy storage systems, interfaced to the microgrid through voltage controlled voltage source inverters. The control objective is to restore the frequency of the microgrid to its nominal value of 50 Hz and to keep, as close as possible, the nodal voltage magnitudes to a nominal value of 400 V, after a renewable source or load disturbance. Moreover, a power distribution logic among the storage systems is implemented, in order to take into account their state of energy. To this purpose, a hierarchical control architecture has been devised. First a voltage control in synchronous axis is developed for the single controller, then a primary control level, based on the largely studied *Droop Control*, is designed. This control strategy relies on a decentralized control action that promptly minimizes the power unbalances in the microgrid, by varying the inverter output voltage magnitude and frequency values. A secondary control level instead has the function to both restore voltages and frequency to their nominal values and efficiently distribute the generated and absorbed powers among the energy storage systems. The designed secondary layer is composed by two control action: one provided by Proportional-Integral with Smith Predictor controllers, which ensure the convergence of the microgrid frequency to its nominal value; and one provided by a multi-objective control strategy, that at each iteration defines the optimal output voltage magnitude of each converter.

The proposed secondary control level, besides improving the performances with respect to those provided by the primary control one alone, allows the better exploiting of the energy of each storage system. The results show the performances of the whole hierarchical control structure, when it is tested over a pre-defined powers profile of the microgrid.

# Sommario

Al giorno d'oggi, la produzione di energia si sta spostando verso nuovi modi più sostenibili di soddisfare una crescente attenzione per i problemi ambientali. Le fonti di energia rinnovabile stanno diventando una valida alternativa alla classica produzione di energia, incentrata sui combustibili fossili. In questo contesto, un interesse nel design e controllo delle Microreti sta crescendo sempre più. Infatti, la microrete rappresenta un'alternativa interessante per superare le difficoltà nell'integrare fonti di energia distribuita, incluse le fonti di energia rinnovabile, negli attuali sistemi di potenza. Una microrete può lavorare o connessa alla rete principale, in modalità rete-connessa, o può separarsi da essa e funzionare da sola, in isola. I problemi principali avvengono esattamente in questo caso; la natura aleatoria delle fonti rinnovabili e dei carichi può creare squilibri fra la potenza generata totale e quella assorbita. Mentre, quando la microrete è in modalità rete-connessa, squilibri di potenza possono essere risolti scambiando potenza con la rete principale, in isola, ciò non accade e gli squilibri di potenza possono far deviare la frequenza di rete e la tensione dei nodi dai loro valori nominali. L'obiettivo principale di questo elaborato è progettare un controllo centralizzato per il coordinamento dei sistemi di immagazzinamento di energia, interfacciati alla microrete attraverso convertitori controllati in tensione. Inoltre, una strategia per la distribuzione delle potenze fra le unità di immagazzinamento è implementata, in modo da tener conto del loro stato di energia. Il compito principale del controllo è quello di ristabilire la frequenza di microrete al valore di 50 HZ e delle tensioni dei nodi a 400 V, dopo disturbi dovuti alle fonti di energia rinnovabile o dei carichi. A questo proposito è stato ideato un controllo gerarchico. Prima un controllo di tensione su assi sincronizzati e in seguito un controllo primario, basato sul *Droop Control*, sono stati sviluppati. Questa strategia di controllo è implementata attraverso un controllo decentralizzato che immediatamente varia il valore della frequenza e della tensione di uscita dei convertitori, a seconda degli squilibri di potenza misurati.

Un livello secondario ha invece la funzione di riportare la frequenza e le tensioni ai loro valori nominali e, allo stesso tempo, di distribuire la potenza attiva assorbita o generata dai convertitori, a seconda dello stato di carica delle batterie.

Il livello secondario progettato è composto da due azioni di controllo: una fornita da regolatori Proporzionali-Integrali con Predittore di Smith, che assicurano la convergenza della frequenza della microrete al suo valore nominale; ed una fornita da un controllo ottimo che ad ogni iterazione definisce i valori ottimi di tensione e frequenza di uscita per ogni convertitore.

Il controllo secondario proposto, oltre a migliorare le prestazioni rispetto ad un solo controllo primario, permette di sfruttare al meglio l'energia di ciascuno dei sistemi di immagazzinamento. I risultati mostrano il comportamento dell'intera struttura gerarchica di controllo, quando è testata con un profilo di potenze predefinito.



# Contents

<b>ABSTRACT</b> .....	<b>IV</b>
<b>SOMMARIO</b> .....	<b>V</b>
<b>CONTENTS</b> .....	<b>VII</b>
<b>LIST OF FIGURES</b> .....	<b>IX</b>
<b>TABLES INDEX</b> .....	<b>XII</b>
<b>CHAPTER 1 INTRODUCTION</b> .....	<b>1</b>
1.1 MOTIVATION .....	1
1.2 MICROGRID CONCEPT.....	2
1.3 ISLANDED AC MICROGRID CONTROL.....	4
1.4 HIERARCHICAL CONTROL.....	6
1.4.1 Zero Level (Inner Control) .....	7
1.4.2 Primary Control Level .....	8
1.4.3 Secondary Control Level.....	10
1.4.4 Tertiary Control Level.....	10
<b>CHAPTER 2 SECONDARY CONTROL STATE-OF-ART</b> .....	<b>11</b>
2.1 SECONDARY CONTROL MOTIVATIONS.....	11
2.2 CENTRALIZED APPROACH .....	17
2.3 DISTRIBUTED APPROACH.....	33
2.4 SECONDARY CONTROL BENEFITS AND PROBLEMS .....	40
<b>CHAPTER 3 PRIMARY CONTROL</b> .....	<b>45</b>
3.1 ISLAND-MODE PROBLEMS .....	45
3.2 ZERO CONTROL LEVEL .....	47
3.3 DROOP CONTROL.....	51
3.3.1 Droop laws.....	52
3.3.2 Droop control structures.....	56
3.4 PRIMARY CONTROL DESIGN .....	57

3.5 CONVENTIONAL DROOP IMPLEMENTATION.....	60
3.5.1 Zero Control Level .....	61
3.5.2 Steady state droop test .....	63
3.6 CONCLUSIONS.....	66
<b>CHAPTER 4 SECONDARY CONTROL .....</b>	<b>69</b>
4.1 INTRODUCTION .....	69
4.2 RSE MICROGRID .....	70
4.3 SIMULATION SPECIFICATIONS .....	74
4.4 PRIMARY CONTROL: IMPLEMENTATION AND TEST .....	76
4.5 SECONDARY FREQUENCY CONTROL.....	81
4.5.1 Control description.....	81
4.5.2 Secondary frequency control simulation .....	85
4.6 SECONDARY VOLTAGE CONTROL .....	90
4.6.1 Secondary voltage control description .....	90
4.6.2 Secondary voltage control simulation.....	95
4.7 OVERALL SECONDARY CONTROL LEVEL.....	98
4.7.1 Secondary control considering the SOC's of the ESSs .....	100
4.8 CONCLUSIONS.....	107
<b>CONCLUSION AND FUTURE DEVELOPMENTS .....</b>	<b>109</b>
<b>APPENDIX A .....</b>	<b>115</b>
<b>BIBLIOGRAPHY .....</b>	<b>117</b>

# List of figures

Figure 1.1 Different Microgrid control structure	4
Figure 1.2 Hierarchical control structure	7
Figure 1.3 Example of inner control loop	7
Figure 1.4 $P$ - $Q$ circle and $P$ - $f$ and $Q$ - $E$ droop primary control relationship	9
Figure 2.1 Simplified scheme of two parallel converters supplying a common load	12
Figure 2.2 Voltage deviation in a typical droop characteristic	13
Figure 2.3 Classical secondary control	14
Figure 2.4 Secondary control action	15
Figure 2.5 Centralized and distributed secondary control	17
Figure 2.6 Centralized control structure	18
Figure 2.7 Scheme of direct control method	19
Figure 2.8 Gain-Scheduling control structure	20
Figure 2.9 Scheme of Multi-Objective control	23
Figure 2.10 Harmonic compensation secondary control	24
Figure 2.11 Voltage restoration loop	25
Figure 2.12 Fuzzy secondary control scheme.	26
Figure 2.13 Secondary control diagram for Active power sharing.	28
Figure 2.14 Secondary control diagram for Reactive power sharing.	28
Figure 2.15 Overall control scheme.	29
Figure 2.16 Primary control loop scheme	30
Figure 2.17 Scheme of MPC control	31
Figure 2.18 Scheme of Neural-Network control	32
Figure 2.19 ANN control scheme	32
Figure 2.20 MAS based control scheme	35
Figure 2.21 Scheme of consensus-based control	37
Figure 2.22 Two-layer example	38
Figure 2.23 Cooperative distributed scheme.	39
Figure 3.1 Electric scheme of the converter.	47
Figure 3.2 Control Scheme of the internal current Synchronous Framework	49

Figure 3.3 Voltage control scheme in synchronous frame	50
Figure 3.4 Space vectors in Park's representation	51
Figure 3.5 Simple electrical network.	53
Figure 3.6 Phasor representation of nodal voltages.	53
Figure 3.7 Conventional Resistive Droop	56
Figure 3.8 Inverse Resistive Droop	57
Figure 3.9 Resistive conventional droop characteristics	58
Figure 3.10 Simple network.	59
Figure 3.11 Direct and Quadrature voltage components.	60
Figure 3.12 Block diagram representation for voltage and frequency conversion	61
Figure 3.13 Current open loop Bode diagram	62
Figure 3.14 Voltage open loop Bode diagram	63
Figure 3.15 Test scheme for the steady state droop test	63
Figure 3.16 Simulated droop characteristics	64
Figure 3.17 Dynamics of a grid connected conventional droop	64
Figure 3.18 Reactive power dynamic performances	65
Figure 3.19 Active power dynamic performances	66
Figure 4.1 Picture of the RSE microgrid	70
Figure 4.2 Schematic of the RSE microgrid considered in the simulation.	71
Figure 4.3 Active power profile used for the secondary control simulations	75
Figure 4.4 Reactive power profile used for the secondary control simulations	75
Figure 4.5 Conventional Resistive Droop.	77
Figure 4.6 Schematic representation of droop control and Inverter	78
Figure 4.7 Inverters output active powers	78
Figure 4.8 Inverters output reactive powers	79
Figure 4.9 Nodal voltage response	80
Figure 4.10 $V_{PCC}$ voltages response	80
Figure 4.11 Inverters output frequencies	80
Figure 4.12 Possible frequency secondary control actions	81
Figure 4.13 Secondary frequency control scheme	82
Figure 4.14 Secondary frequency control with SP	83
Figure 4.15 Eigenvalues of the secondary control closed-loop.	84
Figure 4.16 SFC Active powers response	86
Figure 4.17 SFC Reactive powers response	86
Figure 4.18 SFC nodal voltages response	87
Figure 4.19 SFC $V_{PCC}$ response	87
Figure 4.20 SFC frequency response.	88

Figure 4.21 Droop gain modification	89
Figure 4.22 Microgrid frequency response with different control strategies	89
Figure 4.23 Possible secondary voltage control actions	90
Figure 4.24 Representation of a line	92
Figure 4.25 Powers scheme of the microgrid.	93
Figure 4.26 SVC active powers response	96
Figure 4.27 SVC reactive powers response	96
Figure 4.28 SVC nodal voltages response	97
Figure 4.29 SVC PCC voltage response	97
Figure 4.30 SVC microgrid frequency response	97
Figure 4.31 Overall secondary control active powers response	98
Figure 4.32 Overall secondary control reactive powers response	98
Figure 4.33 Overall secondary control nodal voltages response	99
Figure 4.34 Overall secondary control PCC voltage response	99
Figure 4.35 Overall secondary control microgrid frequency response	99
Figure 4.36 Balance SOCs active powers response	104
Figure 4.37 Balanced SOCs PCC voltage response	104
Figure 4.38 Balanced SOCs nodal voltages response	104
Figure 4.39 Balance SOCs response	105
Figure 4.40 Unbalanced SOCs active powers response	106
Figure 4.41 Unbalanced SOCs nodal voltages response	106
Figure 4.42 Unbalanced PCC nodal voltages response	106
Figure 4.43 Unbalanced SOCs response	107

## Tables index

Table 2.1 Advantages and disadvantages of secondary control methods.	41
Table 3.1 PI regulators parameters	62
Table 3.2 Parameters of dynamic simulation	65
Table 4.1 Maximum power of microgrid devices.	72
Table 4.2 List of line impedances parameters.	73
Table 4.3 ESSs parameters.	74
Table 4.4 Active and reactive power variations in kW and kVar.	76
Table 4.5 Primary control droop gains	78
Table 4.6 Parameters for the eigenvalues test.	84
Table 4.7 Frequency controller simulation parameters	85
Table 4.8 Initial SOCs	103

# CHAPTER 1

## INTRODUCTION

### 1.1 Motivation

Nowadays, world energy demand, especially in the electric field, is strongly increased. In this context, renewable energy resources (RES), directly connected to utility grid, are necessary to reduce pollution and the use of fossil fuels. Photovoltaic, micro-turbine, wind turbine and fuel cell put forward many promising applications with high efficiency and low emission. Together with power electronics technologies, these have provided an important improvement for the electrical grid with the origin of microgrid concept. A Microgrid is a contiguous section of the grid and its interconnected energy resources (i.e. generators, loads storage devices, electric vehicles) that can operate as an independent electrical island disconnected from the rest of the grid. Microgrids can provide more system capacity and control flexibility when several RESs with different electric behaviour are integrated in the same grid. The microgrid also offers other advantages to optimize RESs connected to the utility grid; additional, power quality requirements, system reliability and control flexibility would be achieved resorting to microgrid concept. To understand the current range of penetration of microgrids, that goes hand in hand with RES spreading, in the recent energy industry, the European example is taken in consideration. In [1] are reported the EU targets for the next decade, concerning renewable energy implementation and, so greenhouse gas emission reduction. In particular, as part of the climate and energy policy package for 2020, Directive 2009/28/EC on the promotion of the use of energy from renewable sources (known as the Renewable Energy Directive, RED) commits the EU to achieving a 20% share of renewable energy in gross final energy consumption by 2020 and a 10% share of renewable energy in transport energy consumption by the same year. For 2030, the European council agreed to increase the EU's renewable energy share to at least 27% gross final EU energy consumption [1].

## 1.2 Microgrid concept

Microgrids have been identified as a key component for the Smart Grid to improve power reliability and quality, to increase system energy efficiency, and to provide the possibility of grid-independence to individual end-user sites.

The DOE (Department of Energy of U.S.A) defines the microgrid as “a group of interconnected loads and distributed energy resources within clearly defined electrical boundaries that act as a single controllable entity with respect to the main grid. A microgrid can connect and disconnect, through the PCC (Point of Common Coupling), from main grid to enable it to operate in both grid-connected or island mode.”. Many other organizations define microgrids with very similar definitions, including the concept of a system constituted by multiple loads and generation, that can operate islanded from the grid. The benefits of microgrids include:

- Enabling grid modernization and integration of multiple Smart Grid technologies.
- Enhancing the integration of distributed and renewable energy sources that help to reduce peak load and reduce losses by locating generation near demand.
- Meeting end-user needs by ensuring energy supply for critical loads, controlling power quality and reliability at the local level, and promoting customer participation through demand-side management and community involvement in electricity supply.
- Supporting the grid by handling sensitive loads and the variability of renewables locally and supplying ancillary services at the bulk power system.

Microgrids are still advanced and challenging systems, whose enormous potentialities have been explored just recently; therefore together with the benefits, enlisted above, they introduce a set of drawbacks and technical shortcomings:

- *Intermittent power*: the most critical disadvantage of Variable Renewable Energy (VRE), such as solar and wind power, is for sure the unpredictability and the deficiency of full controllability of themselves. Their output powers mainly depend on weather conditions and on the different hours of the day. Lacks in power balances can be overcome exploiting energy stored into batteries, an efficient control of the ESS (Energy Storage Systems) must be realized, in order to manage the energy and the state of charge of the batteries. In general, batteries can absorb energy during peaks of generated power and release it when the requested power is greater than the produced one.
- *Low inertia*: Electrical grid is characterized by a huge number of synchronous generators that provide the main component of requested power and ensures an inertia component for the grid. Microgrids instead might show a very poor inertia, due to power electronic converters. This is an advantage in terms of dynamic response of the network, but could be a critical feature in case of

temporary power mismatches. Lower system inertia causes faster frequency deviations. In island operation this trend could be crucial.

- *Model uncertainty*: prevalence of three phase balanced conditions, nearly constant or predictable loads and well known primarily inductive transmission lines are common hypothesis used for traditional grids control. None of them is sure in low voltage microgrids.
- *Bidirectional power flows*: transmission lines have been designed for unidirectional power flow, from big power plants to loads (cities, industrial plants). Integration of distributed generation units at low voltage levels can cause reverse power flows and lead to complications in protection coordination and undesirable power flow patterns.

A typical and well-designed microgrid control system must be able to overcome the problems aforementioned to ensure a reliable and economically convenient behaviour of the microgrid. In particular, the required features are:

- *Inner control loops*: every DER (Distributed Energy Resource) must have an internal control able to properly follow the imposed reference of currents and voltages within required settling times. The control inside the microgrid is performed by the power electronic converters, needed to connect most of the distributed generators to the bus of the microgrid. Indeed Photovoltaic (PV) plants, small wind generators and other renewable sources generate electricity at different voltages and frequencies and they must be converted to the standard ones. Furthermore ESS, that can hold DC voltages, need a conversion stage.
- *Power balance*: DER units must guarantee the internal power balance in island mode, suddenly compensating excesses or shortages to keep voltage and frequency inside acceptable ranges. In case of grid-connected configuration instead they must be able to provide power references imposed by the higher control. In this sense a core role is performed by ESS that can be used to manage power.
- *Demand Response*: when possible, control of the loads (or at least part of them) can enhance the stability and improve the economic management of the microgrid.
- *Economic dispatch*: to reduce losses and to increase profits, an appropriate dispatch of DERs efforts must be taken into account. Also for the stability point of view it's important to have every generator available far from its saturation limits; this can be achieved only through a smart cooperation of generators and storage units.

### 1.3 Islanded AC microgrid control

Microgrid contains various renewable DGs such as PV arrays and wind turbines. It is well-known that energy production of renewable energy source is difficult to be predicted. Power flow between microgrid and main grid needs to be controlled, in grid-connected mode, to ensure seamless transition and microgrid should have the ability to survive after disconnecting with main grid. Also most renewable energy resources have stochastic generation behaviors and therefore, proper control techniques are necessary for a generic microgrid to perform properly. Three approaches can be identified in the microgrid control: centralized, decentralized and distributed control. A fully centralized control relies and elaborates data gathered from many points of the grid, computing the control actions for any electronic device. The opposite case is the decentralized control, in which every power device has its own controller that measures only local quantities and doesn't communicate to any other controller of the grid. The last one, the distributed control structure, stands in the middle of the previous two methods. Each power unit has its own controller, as in the decentralized control, but, in this case, there exists a communication systems, as in the centralized control, that allows the controllers to exchange information between them, in order to perform the control action on the microgrid. In Figure 1.1 are schematically represented the three aforementioned structure.

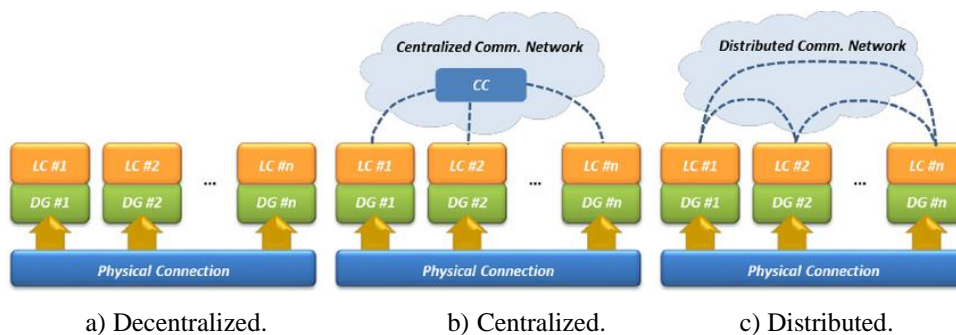


**Figure 1.1 Different Microgrid control structure**

A very fast, reliable and accurate communication is needed in the first and in the third approach, which is not feasible for grids with components connected far one from each other, in terms of costs and technical complications related to the distance. Furthermore the control is not robust and flexible: in fact in case of extension of the grid or temporary changes, the control law must be modified; in case of controller failure instead, the whole grid would collapse. At the same time, also decentralized approach as many difficulties: it is hardly implementable due to strong interactions between different control units and power dispatch can't be tuned online.

In the following the main centralized, decentralized and distributed control methods are introduced and briefly described:

- *Master-slave control:* while microgrid is connected to the main grid, all sources including the master converter follow grid voltage and frequency as reference. A power-frequency droop is used in this mode to adjust power for each DG. When microgrid switches from grid-connected to islanded mode, one source will behave as master controller under voltage mode control meanwhile providing voltage and frequency reference to the other sources which are working under current control [3]. In this way, loads are automatically re-distributed among master DG and other DGs. Microgrid central controller works as master controller, which adjust the set points for DGs when frequency and voltage violate defined settings. However, master controlling DG is considered to avoid be fully loaded to handle disturbance of the microgrid, because a failure of master controller can lead to whole system shutdown. The master converter is under the voltage control mode and providing voltage as well as current references to the slave converter while the slave converter has two control loops with an outer control loop as the current controller and an inner control loop as the voltage controller. Master-slave control can be implemented in both centralized and decentralized structure. Centralized control requires fast communication links between master and slave controllers and the reliability of communication links determines the controller dynamic response.
- *Peer-to-peer control:* unlike master-slave control, all DGs are acting in the same role, namely each of DGs performs a local control according to its own droop characteristics when microgrid is working in the islanded mode. During a load transient, each of DGs will rebalance the load variation based on the droop characteristics and the system will automatically reach a new balancing point [4]. In this method, when one energy source is connected or disconnected from the system, the microgrid will continuously operate without any additional reconfiguration, thus, “plug and play” feature is achieved. Droop control was initially used in power system to manage load sharing between multiple generators, namely, primary frequency control. By adjusting real power, frequency can be regulated and similarly voltage can be controlled by correspondingly adjusting reactive power. This method is a decentralized control method for the microgrid.
- *Hierarchical control:* as name suggests, this control method contains a maximum of three control levels, which are primary control, secondary control and tertiary control. Primary control is basically on the converter control level, where P/Q droop method is usually used to share active and reactive power between DGs. Secondary control is used to compensate frequency and voltage deviations caused by the primary control, also it ensures synchronization process with the main grid. Tertiary control is the highest control level which takes the economy concern into account and determines when to sell or buy power to or from the main grid. Furthermore, power flow between microgrid and main grid is also managed in this control level. Each level of the hierarchical control can be implemented

according to the three aforementioned structures: centralized, decentralized and distributed. Nevertheless, the most frequently implemented configuration consists of a decentralized control at the primary level (“droop control”), a distributed or centralized structure at the secondary level and a centralized control at the third and last level.

- *Multi-agent system control:* Multi-agent system (MAS) is an emerging technology that allows each micro-source or load to be represented as an agent and can exchange information with neighboring agents to collaborate for a mutual objective [5]. MAS control can be actually be classified as one member of peer-to-peer control family and it could be a distributed control method. Each agent in the microgrid in an autonomous entity to a certain extent that it can make decisions based on its status without external command. Compared to a traditional centralized control system, Mas system have very small number of data to manipulate because an agent only need to care about its own status and information from neighboring agents. Since any controller of DGs or energy storage or load can easily integrate with existing MAS controlled microgrid by following the same rule, thus, a plug and play ability is realized.

## 1.4 Hierarchical control

From now on it will be taken into account only the hierarchical control because it represents a satisfactory trade-off between a decentralized and a centralized control strategy. The considered hierarchical control consists of many local controllers coordinated by a high level control system. In this way fast dynamics of voltage and frequency are managed by local controllers, while an economical dispatch can be done by the centralized controller that operates on a slower dynamics. The communication between centralized controller and local controllers doesn't need to be so fast and robust, cause even in case of temporary problems in data transmissions, the grid stability is guaranteed by a primary control action, performed by the local controllers. The communication is only used for the restoration of nominal voltage and frequency (secondary control) and for the control of the power flows inside the grid and between microgrid and utility grid (tertiary control). In Figure 1.2, it is presented schematically an example of hierarchical control.

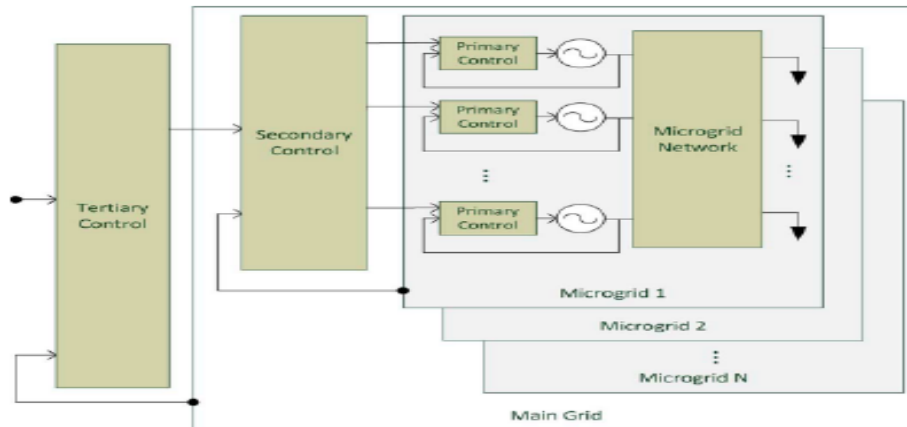


Figure 1.2 Hierarchical control structure

### 1.4.1 Zero Level (Inner Control)

The use of intelligent power interfaces between the electrical generation sources and the microgrid is mandatory. These interfaces have a final stage consisting of dc/ac inverters (voltage source inverte, VSI), which can be classified as current-controlled-voltage-source-inverters (CCVSIs), consisting of a single current control loop, and voltage-controlled-voltage-source-inverters (VCVSIs), consisting of an inner current control loop and an external voltage loop. In order to inject current to the grid, CCVSIs are commonly used, while in island or autonomous operation, VCVSIs are needed to keep the voltage stable.

VCVSIs are very interesting for microgrid applications since they do not need any external reference to stay synchronized. Furthermore, VCVSIs are convenient since they can provide to distributed power generation systems performances like ride-through capability and power quality enhancement. When these inverters are required to operate in grid-connected mode, they often change its behavior from voltage to current sources. Nevertheless, to achieve flexible microgrid, i.e. able to operate in both grid-connected and island mode, VCVSIs are required to control the exported or imported power to the mains grid and to stabilize the microgrid.

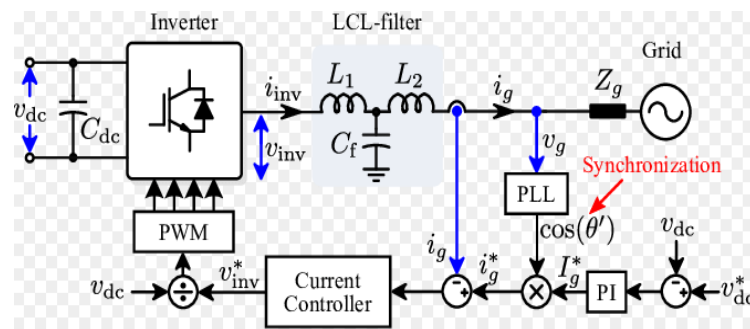


Figure 1.3 Example of inner control loop

VCVSIs and CCVSIs can cooperate together in a microgrid. The VCVSIs are often connected to energy storage devices, fixing the frequency and voltage inside the microgrid. The CCVSIs are often connected to photovoltaic or small wind turbines that require for maximum power point tracking algorithms, although those DG inverters could also work as VCVSIs if necessary. Thus, we can have a number of VCVSIs and CCVSIs, or only VCVSIs, connected in parallel, forming a microgrid. Generally the zero level is a very high bandwidth control, with very good performances, but it's only the individual control of the actuators acting in the grid; it doesn't take into account the whole system structure or the interaction between them.

## 1.4.2 Primary Control Level

When connecting two or more VCVSIs in parallel, circulating active and reactive powers can appear [2]. This control level adjusts the frequency and amplitude of voltage reference provided to the inner current and voltage control loops, to allow the parallel working in the microgrid of multiple inverters. The main idea of this control level is to mimic the behaviour of a synchronous generator, which reduces the frequency when the active power increases. This principle can be integrated in VCVSIs using a P/Q droop

$$f = f^* - G_P(s) * (P - P^*) \quad (1.1)$$

$$E = E^* - G_Q(s) * (Q - Q^*) \quad (1.2)$$

where  $f$  and  $E$  are the frequency and amplitude of the output voltage reference,  $f^*$  and  $E$  are their references,  $P$  and  $Q$  are the active and reactive powers exchanged with the grid,  $P^*$  and  $Q^*$  are their references,  $G_P(s)$  and  $G_Q(s)$  are their transfer function, respectively, which are typically proportional droop terms, i.e.,  $G_P(s) = m$  and  $G_Q(s) = n$ . The use of pure integrators in the droop law is not allowed when the microgrid is in islanded mode, since the total load will not coincide with the total injected power, but they can be useful in grid-connected mode to have a good accuracy of the injected  $P$  and  $Q$ . Nevertheless, this control will be achieved by the secondary control level.  $m$  and  $n$  can be designed as follows:

$$m = \frac{\Delta f}{P_{max}} \quad (1.3)$$

$$n = \frac{\Delta V}{Q_{max}} \quad (1.4)$$

where  $\Delta f$  and  $\Delta V$  are the maximum frequency and voltage allowed and  $P_{max}$  and  $Q_{max}$  are the maximum active and reactive powers delivered by the inverter, respectively. If the inverter can absorb active power, since it is able to charge batteries like a line-interactive UPS, then  $m = \Delta f/2 P_{max}$ . Figure 1.4 shows the relationship between the  $P$ - $Q$  circle of a DG unit and  $P$ - $f$  and  $Q$ - $E$  droops. In that

case, the DG is able to generate active power ( $P > 0$ ) and to store energy ( $P < 0$ ) and, at the same time, is able to supply reactive power ( $Q > 0$ , acting like a capacitor) or ( $Q < 0$ , acting like an inductor).

In the conventional droop method used by large power systems, it is supposed that the output impedance of synchronous generators, as well as the line impedance, is mainly inductive. However, when using power electronics, the output impedance will depend on the control strategy used by the inner control. Furthermore, the line impedance in low-voltage applications is near to be pure resistive. Thus, the control droops (1) and (2) can be modified according to the park transformation by the impedance angle  $\theta$  ( $\sin\theta = R/Z$  and  $\cos\theta = X/Z$ ) [2]:

$$f = f^* - G_p(s)[(P - P^*) \sin\theta - (Q - Q^*) \cos\theta] \quad (1.5)$$

$$E = E^* - Q(s)[(Q - Q^*) \cos\theta - (P - P^*) \sin\theta] \quad (1.6)$$

The primary control, designed according to the droop method above, is a decentralized control, that is every power electronic device has its own controller that rely only on local measurements. No communications are available between controllers, due to speed and reliance requirements. The distributed control structure permits also to split the computational cost among the controllers, avoiding the need of advanced hardware requirements for a central controller. The primary control layer is responsible of dealing with the fast dynamics of the overall grid, in particular it is designed to quickly stabilize frequency and voltage of the microgrid during large variations of powers or during islanded operation, by mean of droop characteristics. In this regard the system is stable if a steady state can be reached, in which the fundamental components of all voltages in the microgrid have constant amplitudes and constant relative phase angle difference. Finally, primary control doesn't aim to keep voltages and frequency in their nominal values, but just to stabilize the grid as fast as possible. Without, higher control in islanded condition, the grid would maintain constant steady state error.

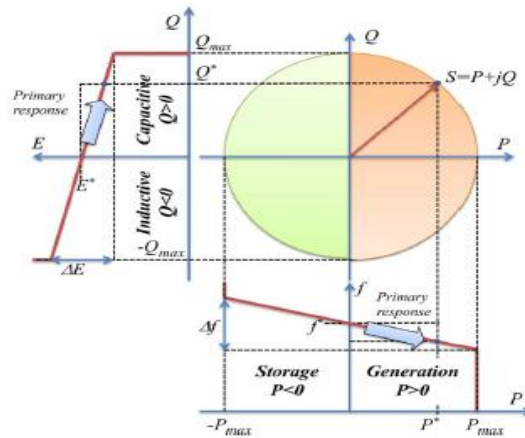


**Figure 1.4**  $P$ - $Q$  circle and  $P$ - $f$  and  $Q$ - $E$  droop primary control relationship

### 1.4.3 Secondary Control Level

Primary control, as discussed above, may cause frequency and voltage deviation in steady state. Therefore the goal of restoring the frequency and the voltage deviations from the nominal values is assigned to the level immediately above in the hierarchical control structure: the Secondary Control. The control of this level is developed according to a centralized configuration, that is the Microgrid Central Controller (MGCC) receive information from each DER through Low-bandwidth communications links (LBCL) and then compute the reference values for each primary control, by mean of a specific control law. Also, this control can be used for microgrid synchronization to the main grid before performing the interconnection, transiting from islanded to grid-connected mode. Originally, frequency deviation from the nominal measured frequency grid brought to logically implement an integrator for each DG along with the Primary control. For some parallel sources, this displacement cannot be produced equally because of measured errors. In addition, if the power sources are connected in islanded mode through the main grid at different times, the load behaviour cannot be completely ensured because all the initial conditions (historical) from the integrators are different. Hence, it is necessary that an external secondary control be able to measure the frequency and amplitude and send the necessary references to push up or down the droop characteristics of each DG. A deeper study on the secondary control and its state of the art is proposed in the next chapter.

### 1.4.4 Tertiary Control Level

The purpose of this control level is to manage the power flow by regulating the voltage and frequency when the MG is in grid-connected mode. By measuring the P/Q through the PCC, the grid's active and reactive power may be compared against desired reference. Hence, grid active power can be controlled by adjusting the MG's reference frequency. This control level is the last and slowest level of control, and ensures optimal operation of the microgrid, not only technically, but also economically [7]. Technically, if a fault or any-non plane islanding issue arise for the MG, then the tertiary control will attempt to absorb P from the grid in such a way that, if the grid is not present, the frequency will begin to decrease. When the expected value is surpassed, the MG will be disconnected from the grid for safety, and the tertiary control disabled. At the same time, when faults don't occur, the third control level considers the economic concerns for optimal operation of the microgrid and manages the power flow between microgrid and main grid.

# CHAPTER 2

## SECONDARY CONTROL STATE-OF-ART

### 2.1 Secondary control motivations

The secondary control, in the typical hierarchical control structure of a microgrid, works to compensate for voltage and frequency errors and to regulate the values in the operational limitations of the microgrid. In other words, the secondary control ensures, in island-mode, that the frequency and voltage deviations are regulated toward zero following each load or generation change in the MG. Recently new objectives for the secondary control related to voltage control and power quality has been investigated, such as voltage unbalance and harmonic compensation or increasing accuracy in reactive and active power-sharing among DGs. In some cases secondary level could also be in charge of economical administration of the powers generated by the inverter units within the microgrid, operating in island mode [7].

Secondary control is the highest hierarchical level in microgrids operating in island mode and it usually operates sending reference values to the lower level: the primary control level. It works on a slower time frame as compare to the primary control in order to:

- reduce the communication bandwidth by using sampled measurements of the microgrid variables
- allow enough time to perform complex calculations
- decouple secondary control from primary control

In order to better understand the functions of the secondary control and its contribution to the overall control of the microgrid, a simplified system with two converters DG1 and DG2, connected in parallel, is considered. The system is represented in Figure 2.1:

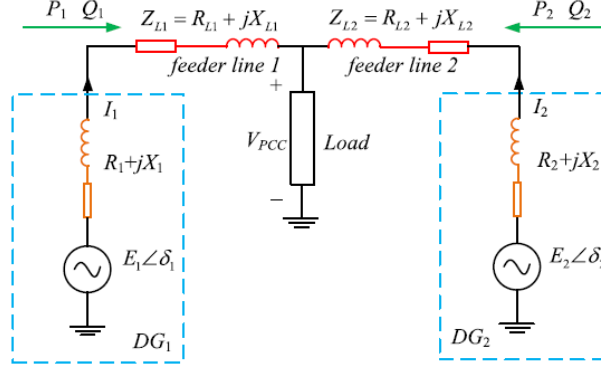


**Figure 2.1 Simplified scheme of two parallel converters supplying a common load**

When medium/large system are considered, the impedance is approximately inductive and the primary control level is implemented as power-frequency (P-f) and reactive-voltage (Q-V) droop control:

$$\omega = \omega_i^* - m_i P_i \quad (2.1)$$

$$E_i = E_i^* - n_i Q_i \quad (2.2)$$

where  $i$  is the index representing each converter,  $\omega_i^*$  and  $E_i^*$  are the nominal angular frequency and voltage amplitude of each converter,  $m_i$  and  $n_i$  are active and reactive droop coefficients.  $P_i$  and  $Q_i$  are the generated or absorbed active and reactive power of the converter  $i$ . In the case of the figure above,  $P_i$  and  $Q_i$  are (for  $i = 1, 2$ ) [6]:

$$P_i = \frac{(X_i + X_{L_i})(E_i V_{PCC} \cos \delta_i - V_{PCC}^2) + (R_i + R_{L_i})E_i V_{PCC} \sin \delta_i}{(X_i + X_{L_i})^2 + (R_i + R_{L_i})^2} \quad (2.3)$$

$$Q_i = \frac{(X_i + X_{L_i})(E_i V_{PCC} \cos \delta_i - V_{PCC}^2) - (R_i + R_{L_i})E_i V_{PCC} \sin \delta_i}{(X_i + X_{L_i})^2 + (R_i + R_{L_i})^2} \quad (2.4)$$

It is clear from the figure that  $X_i$ ,  $X_{L_i}$  and  $R_i$ ,  $R_{L_i}$  represent the reactances and the resistances of each feeder impedances for each generator  $i$ ,  $E_i$  and  $\delta_i$  represent the voltage of each DG and the phase angle difference between  $E_i$  and  $V_{PCC}$ . The power angle  $\delta_i$  is usually very small and it can be assumed that  $\sin \delta_i = \delta_i$  and  $\cos \delta_i = 1$ . When the reactance is much larger than the resistance of the feeder impedance, the equations above can be simplified and rearranged,

$$P_i = \frac{E_i V_{PCC} \delta_i}{(X_i + X_{L_i})} \quad (2.5)$$

$$Q_i = \frac{V_{PCC}(E_i - V_{PCC})}{(X_i + X_{L_i})} \quad (2.6)$$

Hence, in the conventional droop control, by combining the droop equation (Q-V) and the equation for the reactive power, the following relation is obtained:

$$Q_i = \frac{V_{PCC}(E_i^* - V_{PCC})}{(X_i + X_{L_i}) + n_i V_{PCC}} \quad (2.7)$$

where the reactive power of the DG is related to the feeder impedance, PCC voltage and reactive droop coefficient. From the equation above, we can say that even if DG1 and DG2 have the same capacity and reactive power droop coefficients, the reactive power of each DG could be different under a mismatched feeder impedance condition  $X_1 \neq X_2$  or  $X_{L_1} \neq X_{L_2}$ . In Figure 2.2, it is shown the voltage deviation problem of the reactive power sharing in the conventional droop control method.

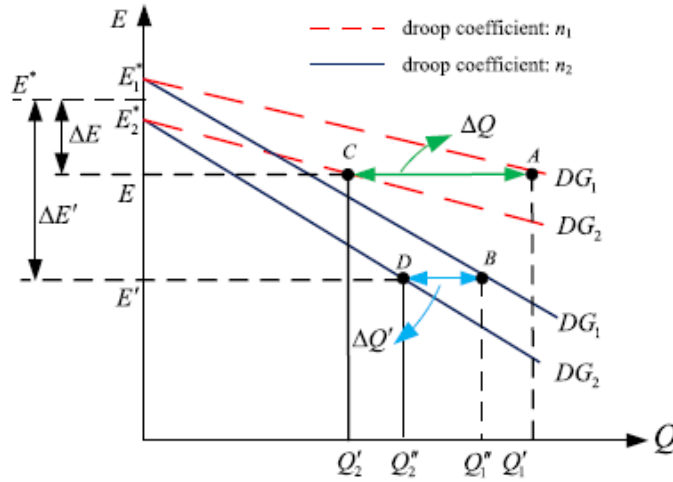


**Figure 2.2 Voltage deviation in a typical droop characteristic**

$E^*$  is the reference voltage and  $E_1^*$  is larger than  $E_2^*$ . When the reactive droop coefficient is  $n_1$ , DG1 and DG2 operate at  $E$ , while DG1 and DG2 operate at  $E'$  when the reactive droop coefficient is  $n_2$ . A and B indicate that the reactive power of DG1 is  $Q'_1$  (droop coefficient  $n_1$ ) and  $Q''_1$  (droop coefficient  $n_2$ ), respectively. C and D indicate that the reactive power of DG2 is  $Q'_2$  (droop coefficient  $n_1$ ) and  $Q''_2$  (droop coefficient  $n_2$ ), respectively. The reactive power difference of DG1 and DG2 is  $\Delta Q = Q'_1 - Q'_2$  when they operate at  $E$ , and the difference is  $\Delta Q' = Q''_1 - Q''_2$  when they operate

at  $E'$ . Although  $\Delta E$  is smaller than  $\Delta E'$ ,  $\Delta Q$  is larger than  $\Delta Q'$  (when  $n_2 > n_1$ ). Therefore, there exist two way to improve bus voltage magnitudes and reactive power sharing accuracy according to Q-V droop characteristic of droop-controlled DER units: 1) changing voltage reference; 2) changing Q-V droop coefficient. Nevertheless, Q-V droop coefficient has to be varied within a certain range otherwise it will impact the stability, transient operation, and steady state of islanded MG. Therefore the first method is chosen here to shift up and down the Q-V droop characteristics of droop-controlled DER units by receiving the optimal voltage references from the units, assigned to the voltage control of the microgrid.

In order to overcome the problem of voltage deviation in the droop control method, the classical secondary control is introduced to eliminate the deviation of frequency and voltage values at PCC. A classical secondary control scheme for two parallel-DGs in an islanded MG is presented in Figure 2.3.

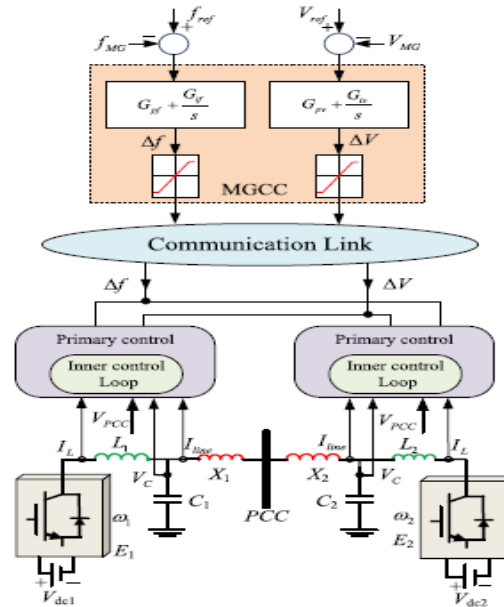


**Figure 2.3** Classical secondary control

The frequency ( $f_{MG}$ ) and the voltage value ( $V_{MG}$ ) measured at the PCC are sent as references value to two proportional-integral controllers (PI), which will adjust the frequency/voltage deviation ( $\Delta f/\Delta V$ ) of the primary control. Both PI controllers and the saturation blocks compose the MGCC (Microgrid Central Controller), whose outputs are sent to the primary and inner control loop through communication lines to regulate the initial voltage and frequency references. However, the classical secondary control presents a major drawback: when the voltage is regulated to eliminate the droop voltage deviation, introduced by the primary level, the reactive power sharing among the different DGs is really poor; on the other hand, when the secondary control performs a perfect reactive power sharing, the voltage deviation is not completely removed. This situation is clearly synthesized in the Figure 2.4,

representing the E-Q droop characteristics of the two parallel DG units, depicted in Figure 2.2, with and without a conventional secondary control.

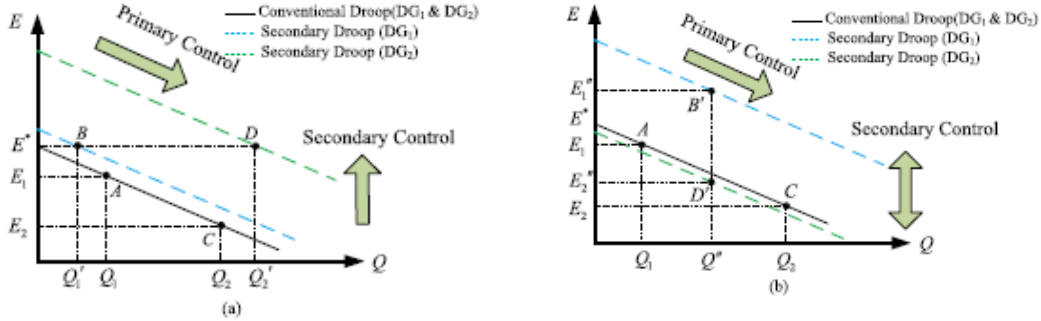


**Figure 2.4 Secondary control action**

In Figure 2.4 (a), points  $A(Q_1, E_1)$  and  $C(Q_2, E_2)$  represent the output voltage of DG1 with the injection of reactive power is  $E_1$  and the voltage of DG2 with  $Q_2$  is  $E_2$  in the conventional droop control, respectively.  $B(Q'_1, E^*)$  and  $D(Q'_2, E^*)$  represent the output reactive power of DG1 is  $Q'_1$  and DG2 is  $Q'_2$  when the voltage is restored to the rated value in the conventional secondary control. However, the reactive power deviation between DG1 and DG2 increases ( $Q'_1 < Q_1 < Q_2 < Q'_2$ ). In Figure 2.4 (b), is presented a situation where the reactive power is regulate as  $Q_1 = Q_2 = Q''$  (a special situation of proportional reactive power sharing) in the conventional secondary control,  $B'(Q'', E_1)$  and  $D'(Q'', E_2)$  are the output voltages of DG1 and DG2, respectively. It can be seen that, even if we have a perfect reactive power sharing, the voltages of DG1 ( $E_1''$ ) and DG2 ( $E_2''$ ) cannot be restored to the rated values and the voltage difference is larger compared to the primary control ( $E_2 < E_2'' < E_1 < E_1''$ ). Therefore, the conventional secondary control cannot regulate the voltage accurately while sharing the reactive power equally or proportionally [6].

To summarize what it has been discussed so far: in the conventional secondary control, the reactive power sharing cannot be achieved when the voltage amplitude and frequency are restored to the rated value in islanded MGs with mismatched feeder impedance; on the other hand, the real power sharing capabilities are not affected by feeder mismatches, as the frequency at steady-state is constant throughout the whole microgrid, provided that the local load demand does not exceed the maximum apparent power rating of the inverters connected to the microgrid. Furthermore, the additional reactive current supplied by each inverter reduces the maximum real power that can be supplied by the inverters. Considering the problems of the classical secondary control method just described, new secondary level control strategies must be investigated in order to provide better microgrid performances.

Another aspect that must be taken into account in the development of the secondary level control, it's the recent introduction of ESSs (Energy Storage Systems) in the design of microgrids. This is due to the fact that ESSs can provide a range of services, particularly when distributed throughout the power network (e.g. at the distribution level, collocated with loads). ESSs services can be broadly grouped into four categories:

- *Energy Shifting*: energy generated during periods of excess supply can be stored and shifted to periods of high demand. This can add significant value to intermittent renewable sources.
- *Peak Shaving*: short-term load spikes can be supplied by local ES systems, reducing the peak demand seen at higher levels in the power network hierarchy. This lowers the required capacity of generation/transmission infrastructure and avoids peak power fees.
- *Power Quality Regulation*: ES systems can be used to address network power quality issues such as voltage/ frequency offsets, harmonics, voltage unbalance and low power factor.
- *Spinning Reserve*: ES systems can provide backup power in case of islanding, increasing availability.

Hence, considering the attached benefits, a proper control strategy must be developed in order to allow an efficient and reliable use of ESSs. In particular, the microgrid controller should guarantee balance discharge rates among the ESSs, especially when the ESS capacities in an MG are different. In the development of a microgrid control strategy, it must be taken into account, regarding the problem of power-sharing control among DG units, that the ESSs in different DG units could have different discharge rates according to their states-of-charge (SoCs) and capacities. A powerless DG unit can be shut down first when its SoC is below the threshold, and the remaining DG units have to supply more power to the total loads. This situation would probably cause overcurrent and unintentional outages. Furthermore, it could degrade the stability and reliability of the [7]. All aspects of the coordinated power output control strategy, such as the SoC and ESS capacities, should be considered. The unit with the highest SoC should supply more power to the common load to ensure a balance discharge rate. Therefore, in order to design an efficient and reliable hierarchical control strategy, control problems, related to the presence of ESSs in the microgrids, must be taken into account.

Considering all the problems involved in the control of a microgrid and considering the current state-of-the-art [6]-[8], there exist two main approaches to implement a secondary control: centralized approach and distributed approach. The former relies on the presence of a central controller, the Microgrid Central Controller (MGCC), that gathers all the necessary information to perform the specific control; the latter instead, consists of an interaction of the various units within the microgrid in order to facilitate a distributed decision making process. In Figure 2.5, high-level diagrams of these control strategy architectures for an AC microgrid are shown.

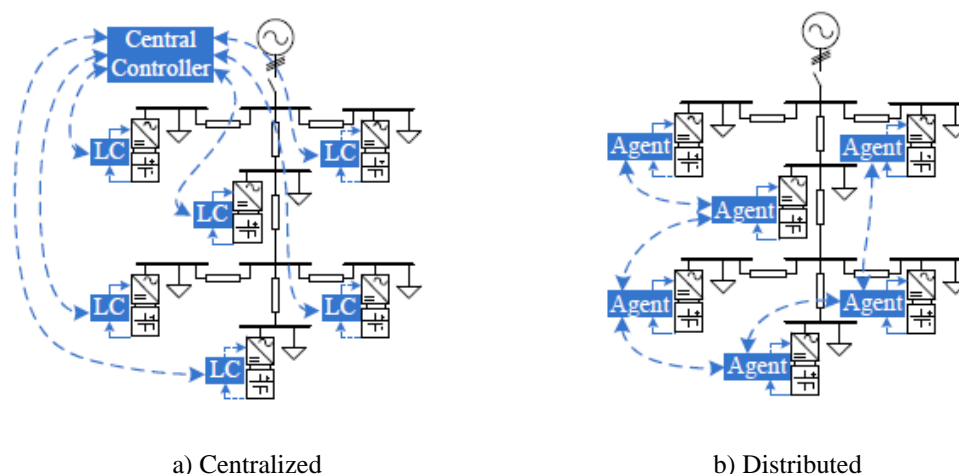


**Figure 2.5 Centralized and distributed secondary control**

The centralized approach architecture allows the implementation of on-line optimization routines and a high level of coordination of the DGs compared to a distributed control structure, having the MGCC a complete view over the microgrid. On the other hand, the distributed architecture can easily incorporate new DER units without need to make continuous changes to the controller settings (plug-and-play feature) and it presents a better robustness to faults in the secondary control devices and in the communication system. However, the inability of controlling the system during the transient and persistent faults that cause blackout situations in microgrids without an MGCC and some of the other management functions of the MG are challenges to implementing a fully decentralized control system. In general, centralized approaches are more suitable for isolated microgrids with critical demand-supply balances and a fixed infrastructure, as they are more likely to provide continuous operation of the system while dealing with variable generation and load, without main grid support. Distributed approaches are more suitable for grid-connected microgrids, with multiple owners and fast-changing number of DER units.

## 2.2 Centralized Approach

In Figure 2.6, it is represented the typical structure of a centralized secondary control. It consists of a central controller (MGCC), that collects all the required information from every DER units and load within the microgrid, and the network itself (e.g., cost functions, technical characteristics/limitations, network parameters and modes of operation), as well as the information from forecasting systems (e.g., local load, wind speed, solar irradiance), in order to perform the chosen control for the specific microgrid. Low-bandwidth communication channels are used to support the information exchange between the MGCC and the local controllers in the secondary control level. Even though a variety of high-level communication infrastructures including Ethernet, Internet WiMax, and WiFi are

increasingly implemented for microgrid communication, when centralized secondary control is used in active and reactive power sharing strategies to eliminate the frequency and voltage deviation, the delays and drops in communication lines cannot be ignored in order to design an efficient and reliable centralized controller. Output variables of the secondary controller are the reference values of the primary control system (e.g., output power and/or terminal voltage) for each dispatchable DER unit, together with decision variables for controlling loads for load shifting or shedding.

The performance of the generic centralized control system strongly depends on the efficiency of the communication system adopted to gather and to deliver information. Furthermore, the communication system must guarantee coordination between the protection and control system and more important the integration of the microgrid with the host power system. Nowadays, in order to overcome these requirements the IEC 61850 is often applied to the microgrid level. This standard has been designed by the International Electrotechnical Commission (IEC) Technical Committee 57, for the automation of electrical substations, and can be implemented over TCP/IP networks using the existing infrastructure (in some cases with some specific hardware), featuring response times within the range required for protection applications. The standard defines abstract data models that can be mapped to several protocols such as Generic Object Oriented Substation Events (GOOSE) and Manufacturing Message Specification (MMS). IEC 61850-7-420 describes the communication systems for DER that can be used in microgrid control applications.

In [26] are described the major features of IEC 61850 and the significant benefits achieved adopting this standard with respect to the legacy approach. Finally, an example of the implementation of IEC 61850 is treated in [27]

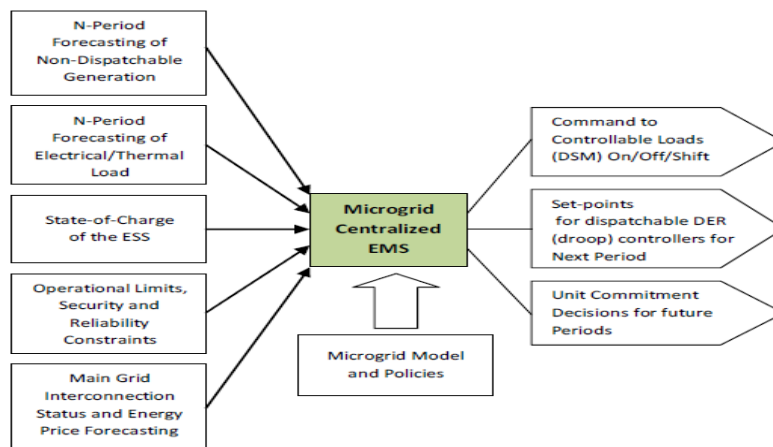


**Figure 2.6 Centralized control structure**

In the following, they are described different secondary centralized control strategies currently implemented in microgrid control.

### ***Direct control methods for the Reactive power sharing***

In [23] it is described a simple control method that tries to overcome the mentioned problem of reactive-power sharing of inverters in an islanded microgrid. The inverters cannot compensate for mismatches in their reactive power outputs while provided only with local voltage and current information, since the operating parameters of the others inverter are unknown. Hence, the main task of direct control methods is to collect the required information in each DG, do the sum of these values, and then assign adjusted powers to each DG on average (weighted average). Each converter is responsible for providing the information of the required reactive power to the MG via LBCs links, then the MGCC collects all these values and carries out all the necessary calculations. The reactive power demand for each inverter can be calculated by:

$$Q_i^* = \frac{\sum Q_i}{n_i(\sum_{n_i=1}^k \frac{1}{n_i})} \quad (2.8)$$

where  $\sum Q_i$  is the total reactive power supplied by all the inverters,  $Q_i^*$  is the reactive power demand supplied by the  $i_{th}$  inverter and  $n_i$ , is the droop gain of the  $i_{th}$  inverter. Once the reactive power references are determined, the MGCC regulates the reactive power of each inverter via PI controllers Figure 2.7.

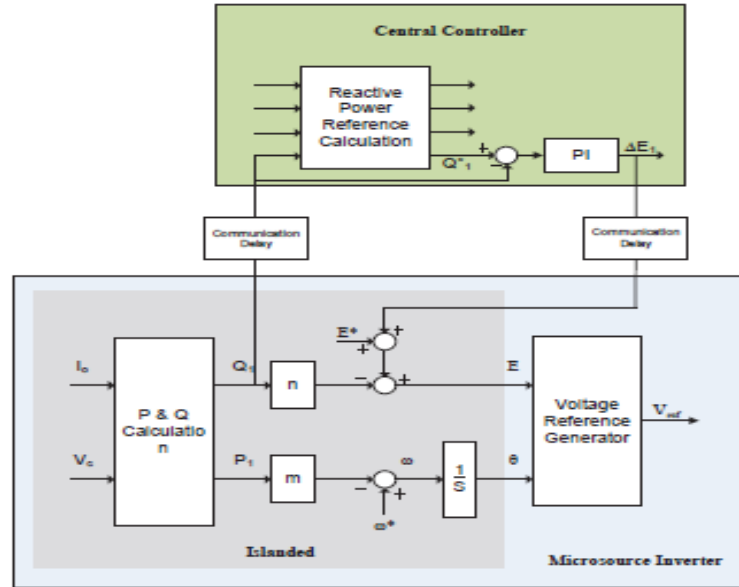


**Figure 2.7 Scheme of direct control method**

The communication delay blocks are modelled with the *t.f.*  $G_d(s) = 1/(T_d s + 1)$ .

### ***Secondary control with Gain Scheduler***

In [24], it is presented a gain scheduling control strategy, whose goal is to compensate the effects of communication delay on the secondary frequency control to guarantee the active power sharing and stable operation of the MG. As previously mentioned, the delay in communication lines between local controllers and the MGCC is an important detail to be consider in order to implement an effective secondary control strategy; in [24] the effects of delay on microgrid performance are studied as well. The characteristic of the delay can be constant, bounded or random in terms of the network structure. In Figure 2.8, it is represented the architecture of the proposed secondary controller.

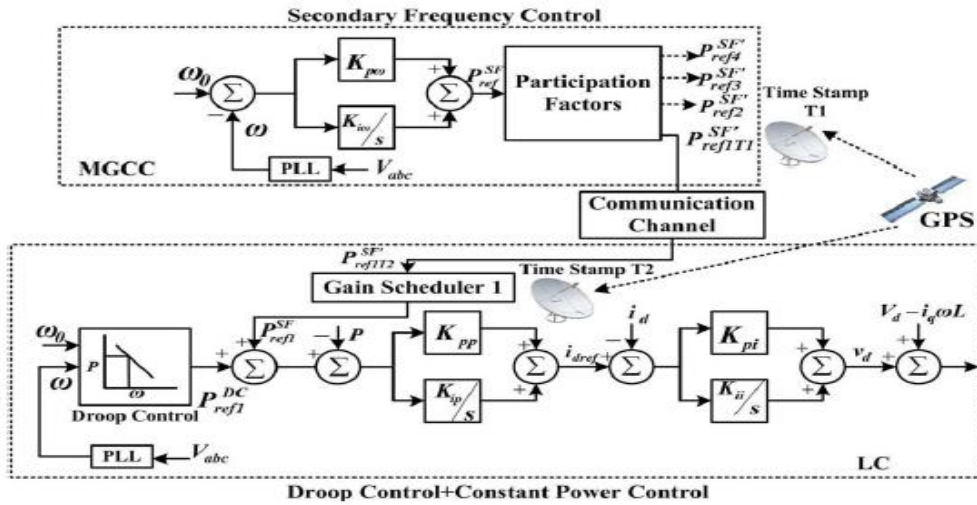


**Figure 2.8** Gain-Scheduling control structure

The primary level is implemented locally for each DG as a frequency droop control, through a  $P$ - $\omega$  characteristics:

$$P_{refi}^{DC} = K_{\omega i}(\omega_0 - \omega_i) \quad (2.9)$$

where  $K_{\omega i}$  is the droop control gain,  $P_{refi}^{DC}$  is the corrective power set point due to frequency variations.

The secondary frequency control is:

$$P_{refi}^{SF} = \left( K_{p\omega i} + \frac{K_{i\omega i}}{s} \right) (\omega_0 - \omega_i) \quad (2.10)$$

where  $P_{refi}^{SF}$  is the supplementary power set point of the  $i$ th DG assigned by the secondary frequency controller,  $K_{p\omega i}$  and  $K_{i\omega i}$  are proportional and integral control gains, respectively;  $\omega_0$  is the nominal frequency reference; and  $\omega_i$  is the instantaneous frequency obtained from a phase-locked loop (PLL). What really distinguish this control scheme from a classical one is the presence of the Gain scheduler, which represents an attempt to overcome the problem of time delay in communication channels. The presence of communication delays, which are usually time varying in the microgrid frequency control loop [24], may degrade its performance. Hence, a gain-scheduling approach is proposed to reduce the

error on dynamic performance of the islanded microgrid, which is caused by communication delays. The gain-scheduling logic is defined by the following equations:

$$K_{i\omega i}^* = \beta_{i\omega i} K_{i\omega i} \quad (2.11)$$

$$K_{p\omega i}^* = \beta_{p\omega i} K_{p\omega i} \quad (2.12)$$

where  $K_{i\omega i}$  and  $K_{p\omega i}$  are considered to be fixed since the secondary frequency controller in MGCC. The variable parts are  $\beta_{i\omega i}$  and  $\beta_{p\omega i}$  located in each local DG controller.  $\beta_{i\omega i}$  denotes an integral gain scheduler and  $\beta_{p\omega i}$  a proportional gain scheduler.  $K_{i\omega i}^*$  and  $K_{p\omega i}^*$  represent the equivalent gains of the secondary frequency controller after gain schedulers are equipped in each LC. The gain scheduler varies only one gain variable, either  $\beta_{p\omega i}$  or  $\beta_{i\omega i}$ . Hence, the equations of the equalized load frequency controller:

$$P_{refi}^{SF} = (K_{p\omega i}^* + \frac{K_{i\omega i}}{s})(\omega_0 - \omega_i) \quad (2.13)$$

$$P_{refi}^{SF} = (K_{p\omega i} + \frac{K_{i\omega i}^*}{s})(\omega_0 - \omega_i) \quad (2.14)$$

where  $P_{refi}^{SF}$ , as previously mentioned, is the new supplementary power set point of the  $i$ th DG assigned by the secondary frequency controller.

The equations above, can be utilized to investigate the root locus of time-delay small-signal model to find optimal  $\beta_{p\omega i}$  and  $\beta_{i\omega i}$  and the stable operation of the microgrid system could be guaranteed under different LBC delay conditions. In addition, the cost function  $J$  is built to find the relationship between the gain-scheduler variables and the system performance of the MG, which is defined as:

$$J = \frac{1}{T} \int_{t=0}^T (\omega_{i,d}(t) - \omega_i(t))^2 \quad (2.15)$$

where the frequency of the  $i$ th DG when the microgrid operates with and without communication delays are presented by  $\omega_{i,d}(t)$  and  $\omega_i(t)$ , respectively. Considering relationship between the time delay  $\tau_i = T2-T1$  (difference between 2 time stamp) and its corresponding feasible gain  $\beta_{i\omega i}^{\tau_i} / \beta_{p\omega i}^{\tau_i}$ , a proper cost index is needed to be built in order to obtain the gain value of different MGs. The detailed procedure of the gain-scheduling approach is summed up in the following steps.

- *Step 1:* The secondary frequency controller in the MGCC calculates real-power set points for each DG to restore their frequencies to the nominal one and sends them to local inverters. These set

points are denoted by  $P_{refiT1}^{SF'}$ , where T1 is the time stamp generated when they are sent by the MGCC.

- *Step 2:* After LCs in the local inverters receive their set points from the MGCC, the set points are marked as  $P_{refiT2}^{SF'}$ , where T2 is the time stamp generated when they are received by LCs.
- *Step 3:* LCs calculate the communication delay by comparing the time stamps of two signals  $P_{refiT2}^{SF'}$  and  $P_{refiT1}^{SF'}$ . The time delay is  $\tau_i = T2 - T1$ .
- *Step 4:* For a given cost index, by looking up the relationship between the time delay  $\tau_i$  and its corresponding feasible gain  $\beta_{i\omega_i}^{\tau_i}$  or  $\beta_{p\omega_i}^{\tau_i}$  built by the offline analysis, the local gain scheduler adjusts its gain value according to the measured communication delay.

### ***Multi-Objective method***

In [15] it is proposed an optimal secondary voltage control strategy, that consists of a Multi-objective optimal function, power flow equality and three sets of inequality constraints. The secondary controller, designed here, aims to maintain several critical bus voltages in permitted ranges and to minimize the reactive circulating current among corresponding DER units in islanded mode. It also tries to integrate its action not only with droop-controlled DER units with storage devices, but also with photovoltaic grid-connected units (PV units) and other PQ-controlled DER units to satisfy the reactive power demands of customers, while limiting the investment of reactive compensation power devices.

For further clarifications, the proposed optimal secondary strategy, in order to perform an effective multi-bus secondary voltage regulation and an economical reactive power distribution, acts on the primary control level by appropriately changing the voltage references of the Q-V droop characteristics of the droop controlled DER units and on the PQ controlled units by setting the dispatched reactive power commands. In the figure below is represented the described control system.

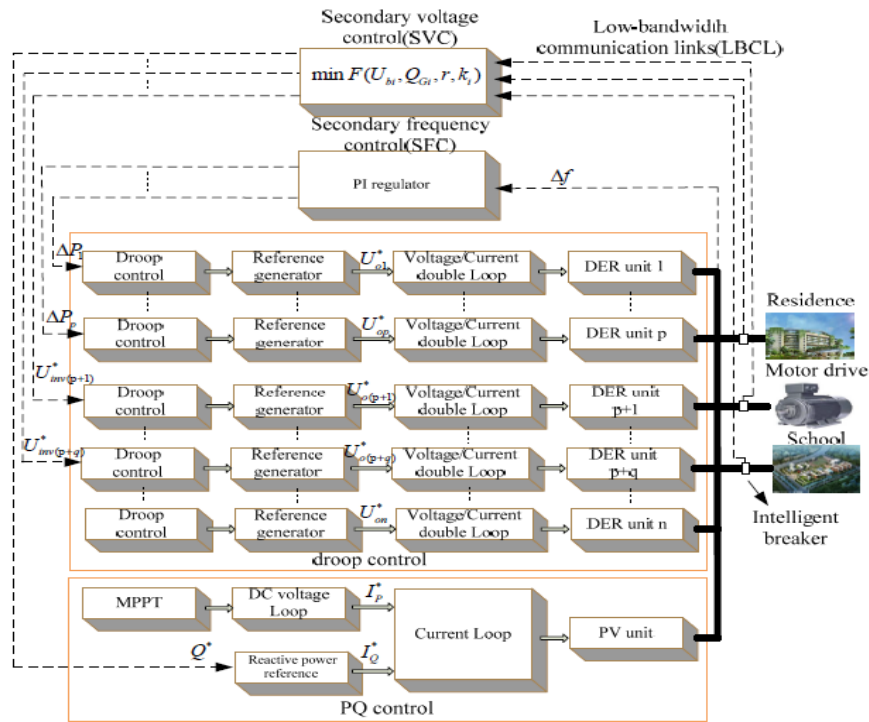


**Figure 2.9 Scheme of Multi-Objective control**

In Figure 2.9, the primary control of droop-controlled DER unit is a multi-loop control scheme including the droop control loop and voltage, current double-loop. Considering that the inner double-loop responds much faster than the secondary control, it is assumed that the inner double-loop has already achieved steady state when the secondary control is executed.

In [16], [17] and [18] are described Objective-function approaches with different heuristic optimization techniques and different constraints, to handle the problem of optimal energy management in a microgrid. Finally [19] and [20] differs from the Multi-objective methods, described so far, because in the constraints they address the problem of emissions reduction.

In [25] it is proposed a strategy in order to compensate the error in reactive power sharing among the inverters of the microgrid, in particular the active and reactive powers can be share among inverters by combining the virtual impedance and secondary control. This control strategy must be considered as a variation of the multi-objective one previously described. As already mentioned, the frequency and voltage deviations from the nominal values due to the droop algorithm depend on various factors including the load impedance of the single inverter, the number of inverters connected to the microgrid and the droop gains used. Due to the decentralized operation, the inverters can only measure the local voltage and current waveforms. The stability of the microgrid can be compromised if the inverters adjust their output voltages and frequencies in an attempt to restore the microgrid without any feedback from the other inverters in the microgrid while operating autonomously. The proposed secondary control is represented in the Figure 2.10, together with the primary and inner control.

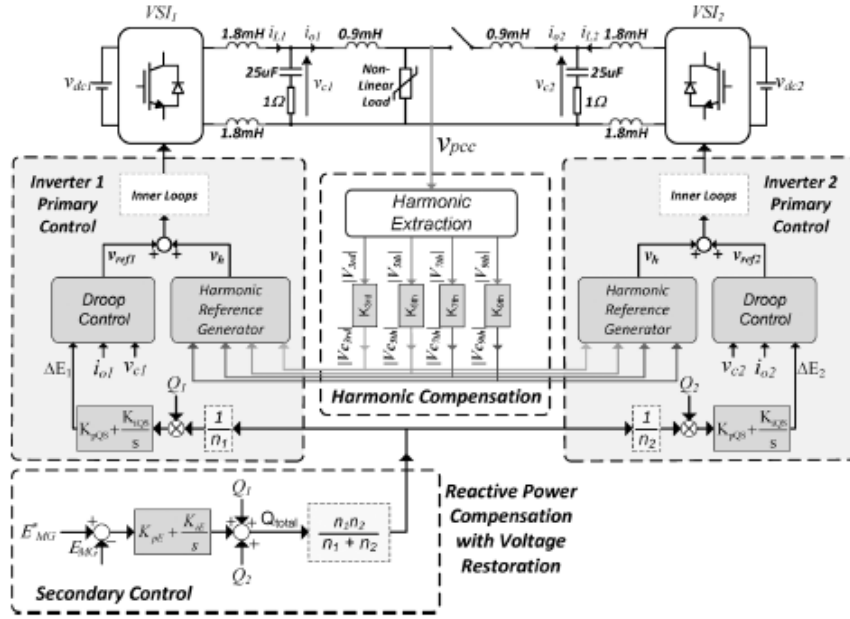


Figure 2.10 Harmonic compensation secondary control

The MGCC is essentially composed by four components:

- *Reactive power compensation loop*: The MGCC gathers the information about reactive power values from each inverter and then determines the total reactive power ( $Q_{total}$ ) supplied by all the inverters in the microgrid, taking into account the different droop coefficients. This reactive power value is broadcasted to each inverter, whose task is to determine its own reactive power demand, according to the following equation:

$$Q_x^* = \frac{Q_{total}}{n_x \sum_{i=1}^k \frac{1}{n_i}} \quad (2.16)$$

where  $n_x$  is the droop gain of inverter  $x$ , and  $\sum_{i=1}^k \frac{1}{n_i}$  is the summation of the inverter droop gains of the inverters connected to the microgrid. When a new inverter is connected to the microgrid, it must transmit to the MGCC the value of its droop gain, so as to enable an accurate estimation of the reactive power demand. The reactive power value  $Q_x^*$  just found, is then used to estimate, by mean of a PI controller, the additional voltage amplitude change of each inverter, that allows the reactive power sharing among the inverters:

$$\Delta E_x = k_{pQS}(Q_x^* - Q_x) + k_{iQS} \int (Q_x^* - Q_x) dt \quad (2.17)$$

where the  $k_{pQS}$  and  $k_{iQS}$  are the gains of the PI controller,  $Q_x$  is the current value of reactive power for the  $x$  inverter and  $\Delta E_x$  is the additional voltage deviation that must be added to the droop control output.

- *Voltage restoration loop*: A voltage restoration algorithm is implemented in the MGCC in cascade with the reactive compensation one. The MCGG collects the required value of voltage and then

applies a control action, by mean of a classical PI controller. In particular, the PI provides an additional change in the reactive power demand  $\Delta Q_{rest}$  that is added to the total reactive power calculated by the reactive power compensation loop. The additional  $\Delta Q_{rest}$  introduces an additional offset in the output voltage of all the inverters, thereby increasing /decreasing the microgrid voltage. The amplitude restoration compensator can be expressed by:

$$\Delta Q_{rest} = k_{pE}(E_{MG}^* - E_{MG}) + k_{iE} \int (E_{MG}^* - E_{MG})dt \quad (2.18)$$

where  $k_{pE}$  and  $k_{iE}$  are the gains of the PI controller,  $E_{MG}^*$  is the desired microgrid voltage and  $E_{MG}$  is the voltage measure at the point PoL, represented in Figure 2.11.

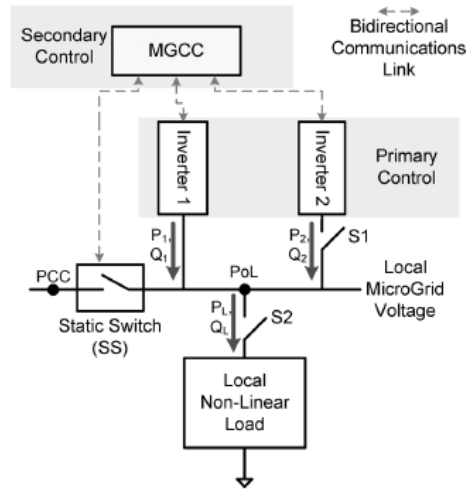


**Figure 2.11 Voltage restoration loop**

- *Frequency restoration loop:* The MGCC gathers the information on frequency at the PCC and then regulates the frequency of the microgrid, by mean of a PI controller. The frequency restoration compensation is expressed by the equation below:

$$\Delta \omega_{rest} = k_{p\omega}(\omega_{MG}^* - \omega_{MG}) + k_{i\omega} \int (\omega_{MG}^* - \omega_{MG})dt \quad (2.19)$$

where  $k_{p\omega}$  and  $k_{i\omega}$  are the gains of the PI controller,  $\omega_{MG}^*$  is the desired microgrid voltage and  $\omega_{MG}$  is the voltage measure at PCC.

- *Harmonic compensation loop:* The harmonic compensation loop is used to improve the power quality and stability of the MG. Specifically, the harmonic caused by the nonlinear load are compensated by harmonic controller, and a resistive virtual impedance  $R_V$  is used to improve the stability of the microgrid. The transfer function of virtual impedance can be obtained as:

$$Z_d(s) = R_V - \sum_{n=3,5,7,9,\dots} \frac{\omega_{cn} k_{cn}}{s^2 + \omega_{cn} s + \omega_n^2} \quad (2.20)$$

where  $Z_d(s)$  is the virtual impedance transfer function.  $k_{cn}$  are the harmonic resonant gains,  $\omega_{cn}$  are the harmonic resonant bandwidth and  $\omega_n$  is the  $n$ th harmonic frequency. The voltage across the capacitor of the output filter can be expressed as:

$$V_h(s) = V_{ref}^*(s) - i_k(s)Z_d(s) \quad (2.21)$$

where  $V_{ref}^*(s)$  is the reference voltage that is determined by the outer droop control loop.  $V_h(s)$  is the compensated input to the inner loops and  $i_k(s)$  is the output current of the  $k$ th inverter. The harmonic compensation is used to damp the voltage harmonics of at the PCC.

### ***Fuzzy logic control***

In [13] and [14] it is proposed a secondary control that exploits a MGCC designed according to the fuzzy logic. The designed Fuzzy Secondary Controller (FSC) manages multiple control inputs, keeping the voltage and the frequency of the microgrid within acceptable limits in the stand-alone mode or supplying active and reactive power to the utility grid in the grid-connected mode. The major benefit given by the Fuzzy control approach is the fact that it still exploits the advantages of the primary droop control and it is able to restore the system frequency and voltage values, using local measurements and minimum communication links in stand-alone mode. In Figure 2.12, it is presented a possible implementation of FSC.

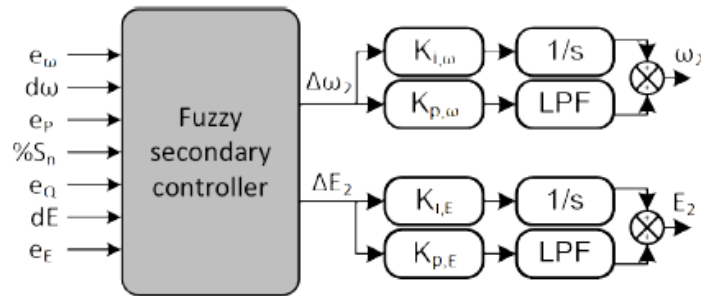


**Figure 2.12 Fuzzy secondary control scheme.**

The inputs were chosen to use only local measurements as the frequency and voltage deviations ( $e_\omega$  and  $e_E$ ), the frequency and voltage gradients ( $d\omega$  and  $dE$ ), the active and reactive power errors ( $e_p$  and  $e_q$ ) and the microgrid nominal power rate ( $\%S_n$ ). All the required information for the computation of these input variables are gathered at the PCC point of the micorgrid. The outputs of the controller are the frequency and voltage incremental droop offsets,  $\Delta\omega_2$  and  $\Delta E_2$ , respectively. After

inferring, the output variables go through a filter and an integer to finally be summed and become  $\omega_2$  and  $E_2$ , the inputs for the following primary droop control.

$$\omega = \omega_i^* - m_i P_i + \Delta\omega_2 \quad (2.22)$$

$$E = E_i^* - m_i P_i + \Delta E_2 \quad (2.23)$$

Thus, the droop characteristics present an off-set, determined by the values of  $\omega_2$  and  $E_2$ , outputs of the secondary fuzzy control.

### ***ESSs secondary control methods***

In the following are considered control methods specifically designed to deal with microgrids characterized by the presence of Energy Storage Systems (ESSs). The introduction of ESSs is a recent addition to the architecture of a microgrid, but thanks to the several benefits they provide to stability and energy sharing performance in microgrids, they are more often considered as a fundamental feature in the design of MGs. Therefore it seems clear that new control methods, that are able to exploit properly the ESSs present in the microgrid, must be investigated.

In [28] it is proposed a hierarchical control that takes into account the different SoC (State of Charge) of each ESS, performing its control action. At the primary level a modified droop control is employed. The coefficients in the conventional droop method are adjusted according to the SoC of each energy storage module. The modules with higher SoC deliver more active power, while those with lower SoC deliver less. Meanwhile, the reactive power is equally share in the energy storage system. The modified droop control equations are the followings:

$$f = f^* - (m_0 / SoC^n) * p_{ACLPF} \quad (2.24)$$

$$E = E^* - n * q_{ACLPF} \quad (2.25)$$

where  $f$  and  $E$  are the frequency and amplitude of the local AC output voltage,  $p_{ACLPF}$  and  $q_{ACLPF}$  are the filtered active and reactive power in the AC side of the converter,  $m_0$  is the droop coefficient for the active power when the SoC is 1 and  $n$  is the reactive power droop coefficient.

The secondary control instead is employed to restore the deviation of voltage and frequency in the AC-bus, caused by the droop control method. For the active power sharing, the secondary control diagram is depicted in the Figure 2.13.

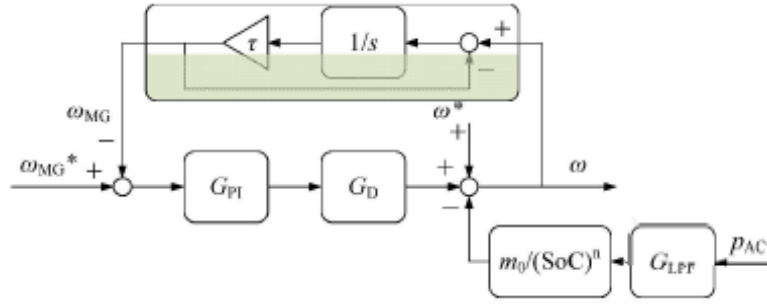


**Figure 2.13 Secondary control diagram for Active power sharing.**

where  $\omega_{MG}$  is the angular frequency at the PCC,  $\omega^*$  and  $\omega$  are the reference and actual values of the local frequency,  $G_{PI}$  is the secondary controller.  $G_D$  is the first-order t.f. of the time delay,  $G_{PLL}$  represents the transfer function of the synchronization part, where  $\tau$  is the time constant of the system. For the reactive power sharing the secondary control is depicted in the Figure 2.14

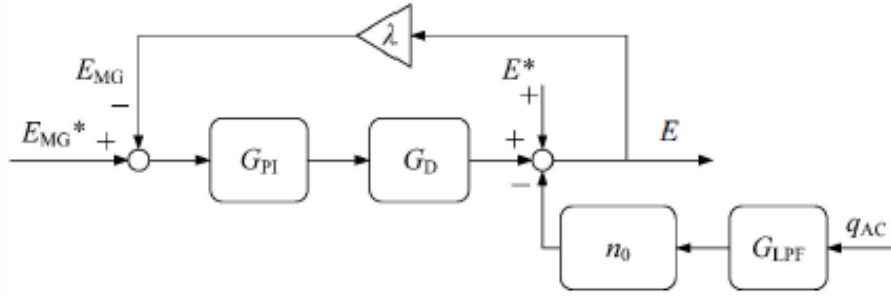


**Figure 2.14 Secondary control diagram for Reactive power sharing.**

where the coefficient  $\lambda$  represent the ratio between the local voltage amplitude and PCC voltage amplitude and it is in relation with the system [28].  $G_{PI}$  is the secondary controller and  $G_{LPF}$  is the t.f. of a low-pass filter.

By using SoC-based droop method, the energy storage with higher SoC generates more active power, and the one with lower SoC generates less. The droop coefficients for active power sharing are inversely proportional to  $\text{SoC}^n$ . Meanwhile, the conventional droop control is employed for equal reactive power sharing and for DGs that are not storage units. In order to restore the deviation caused by the SoC-based droop control, secondary control is involved to restore the frequency and amplitude of the AC-bus voltage, considering the changing SoC and different exponents.

In [29] it is proposed a coordinated control approach based on an autonomous current-sharing control strategy for balancing the discharge rates of energy storage systems (ESSs) in islanded ac microgrids. The proposed coordinated controller can prevent overcurrent incidents and unintentional outages in DG units by regulating the power outputs of the DG units according to their SoCs. The control strategy aims to adjust the VRs (Voltage Ranges) of the voltage-controlled inverters (VCVSI) at the secondary level in terms of SoC and ESS capacities. An autonomous current-sharing controller is

integrated in primary control to ensure a fast and accurate load sharing performance of paralleled VCVSIs. The proposed coordinated secondary controller can provide a larger stability margin than the conventional droop controller. The controller structure is presented in the Figure 2.15.

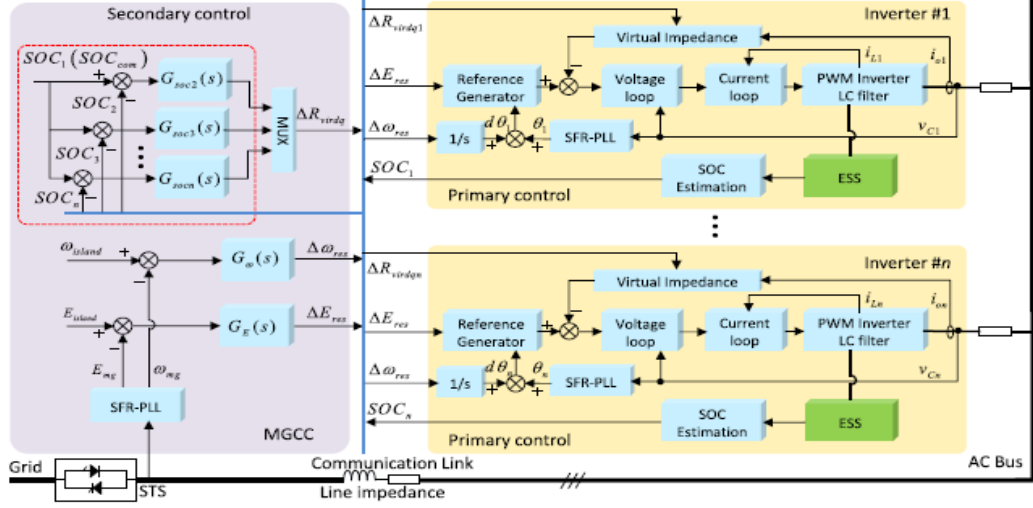


Figure 2.15 Overall control scheme.

where  $\Delta\omega_{res}$  and  $\Delta E_{res}$  are used for restoring voltage and frequency deviation. At the secondary level, an additional control loop action is added to the classical secondary one, in order to balance the discharge rate among DGs. The output of the SoC estimation loop is communicated to the secondary level by mean of a communication link. One of the DG units is selected as the common reference ( $SoC_{com}$ ), whereas the remaining DG units adjust their VRs based on the differences between  $SoC_i$  and the common reference  $SoC_{com}$  with a proportional-integral differential PID controller. The output of the PID controller is regarded as incremental control component to reduce the power oscillation among DG units. Therefore, the adaptive VRs of each DG can be represented as follows:

$$R_{vir_i} = R_{vir\_base} + \Delta R_{vir_i} \quad i = 2,3,4 \dots N \quad (2.26)$$

where  $R_{vir_i}$  is the VR of the  $i$ -th DG,  $R_{vir\_base}$  is the preassigned VR, and  $\Delta R_{vir_i}$  is the incremental of the PID action.

As previously mentioned, the secondary control acts on a primary level controller developed according to a current-sharing control strategy Figure 2.16.

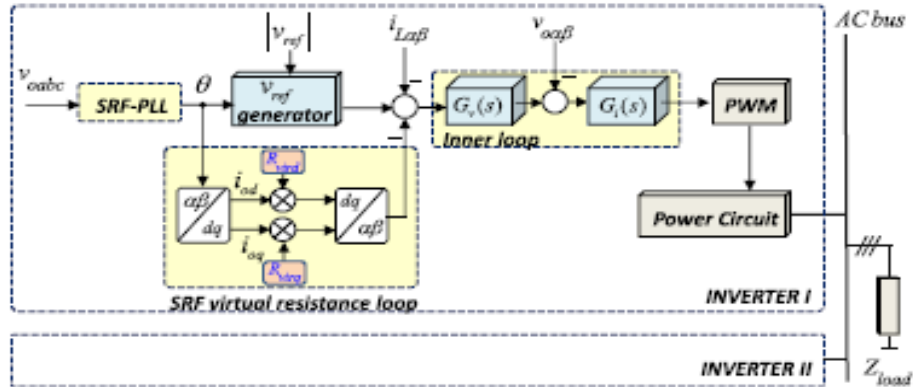


**Figure 2.16 Primary control loop scheme**

This proposed secondary controller can effectively prevent overcurrent in DG units by regulating the power outputs of DG units according to their SoC values. In addition, the autonomous current-sharing control strategy that is employed at the primary control level provided a faster transient response, more accurate output-current-sharing performance, and larger stability region than the earlier power droop control-based coordinated SoC control method.

### ***Model predictive control***

In [6], it is briefly mentioned, among the several approaches to implement the secondary control, a controller that uses the recent MPC logic. The Model predictive control has been introduced in the control of microgrids in order to address at the same time the problem of network variables restoration after the action of primary control and the problem of optimal power management of the microgrid. This secondary controller allows the restoration of frequency and voltage values in a particular node of the microgrid (problem of frequency/voltage deviation) and also allows to optimally distribute the power production of the controllable units taking into account some predictions, if available, of the non-dispatchable power profiles (renewable sources, loads, and so on) as well as to implement different resources management strategies by properly tuning the MPC cost function.

MPC is able to overcome both problems during the critical stand-alone operation since in this case power unbalances can result in unstable behaviors. The MPC approach is an optimization-based control strategy where an optimization problem is formulated and solved at each discrete time-step, and it is an integral part of a centralized control approach. It operates in the following way: at each time-step, the solution to the optimal control problem is solved over a certain pre-defined horizon using the current state of the system as the initial state. The optimization calculates a control sequence for the whole horizon such that the selected objectives are minimized, but only the control action for the next time step is implemented; the process is then repeated at the next time-step.

The optimality of the control depends also on the accuracy of the system model and disturbances. Uncertainties of the real parameters, such as wrong information about uncontrollable

renewable sources or load trend or wrong values of the line impedances, imply that the hierarchical control structure will rely on a slightly wrong system model and consequently the computed control actions may be not the optimal ones to implement.

In Figure 2.17, is represented a typical implementation of a secondary MPC control over a primary control performed with the droop control method.

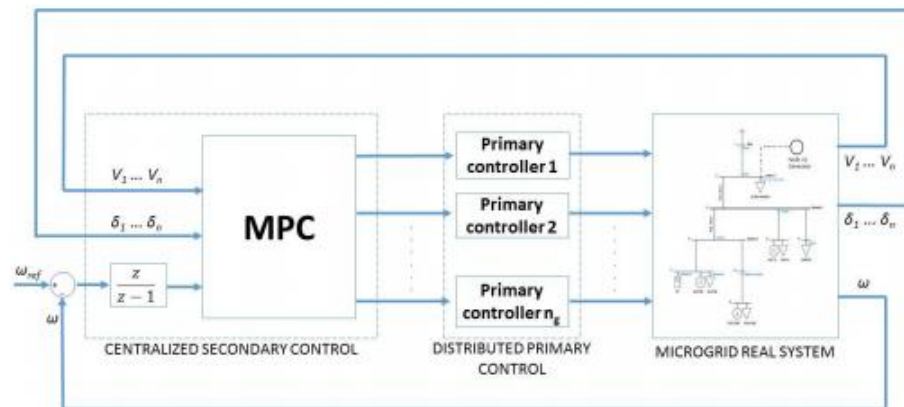


**Figure 2.17 Scheme of MPC control**

In [9] and [10] are proposed two examples of this control applied to a specific microgrid. The secondary control acts on the power references of the droop primary control in order to shift up or down the droop characteristics of each DER units.

### ***Neural Network***

The methods introduced here are Non-model based methods because they don't require a detailed model of the system in order to perform properly. For this particular feature they are becoming more and more appealing for the developing of secondary microgrid control. Respect to conventional design methods such as model based design and simulation-based optimization, they allow plug-and-play operation and are robust to system parameters change. In [11] it is proposed a second control with a Central Controller that uses a Neural Network (NN) in order to optimize the schedule of generators and responsive loads. The designed NN-MGCC predicts for each hour of the day the optimal schedule of generation and the optimal load management without using the classical one-day ahead scheduling. The most important benefit deriving from the NN application is that it does not require the definition of a functional relation between input and output variables and that it tries to reproduce the behavior learnt during the training phase.

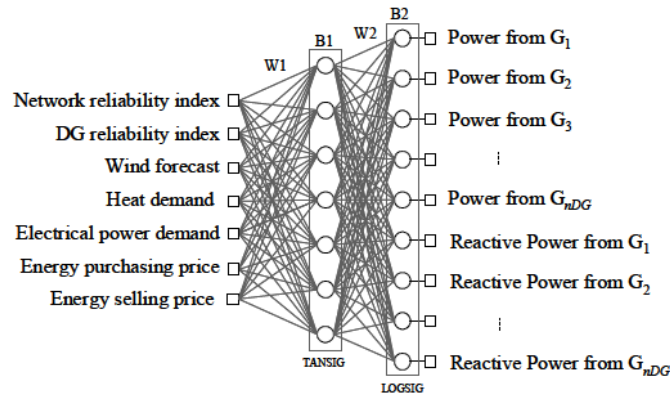


**Figure 2.18 Scheme of Neural-Network control**

NN approach is very easy to implement, it has high computational skills and it needs short processing time. However, the NNs require to be opportunely trained and it is necessary to create a suitable training set of examples. The training process is a periodical off-line procedure, that is usually made to test the NN performances and when there are significant variations in the microgrid characteristics.

In [12] the NN theory is used to implement an ANN (Artificial Neural Network)-Based Microgrid Central Controller. The secondary control designed here operates after the action of the primary control in order to restore the system frequency and voltage to the nominal values. In particular, this control is performed by conventional PI controllers, whose coefficients are regulated by an ANN-based intelligent control unit.

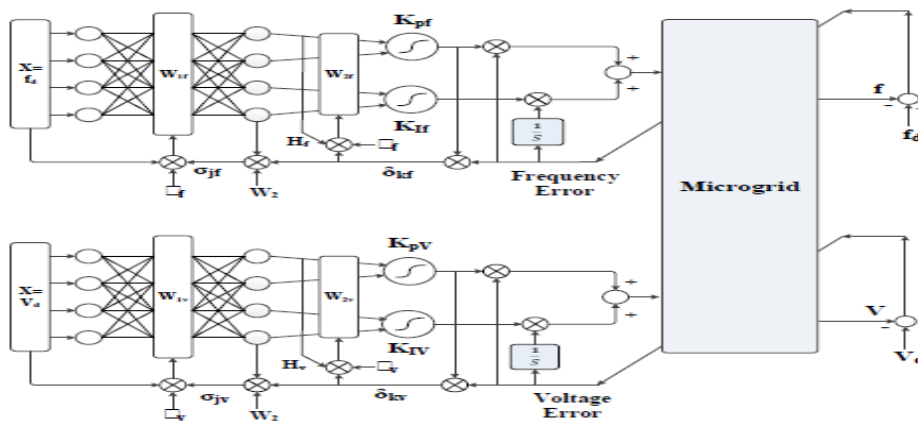


**Figure 2.19 ANN control scheme**

In Figure 2.19, it is shown a schematic diagram of the proposed central controller scheme for the ANN-based online tuning MG voltage and frequency control. When operating conditions of the MG change due to changes in loads or outgoing in a DG, the voltage and frequency of the MG are deviated from its nominal values. To avoid this problem and for better performance of the MG under events and

sudden changes in load, an ANN-based intelligent controller collects the information about the voltage and frequency of all DGs and Loads. The collected data are considered as the ANN inputs. The ANN plays role of an online optimizer for the PI control parameters. By getting input-output data based on some certain ANN learning rules namely the back-propagation rules, the weights are adjusted and an appropriate control signal is recommended to each DG control structure. Hence, the PI regulators act on the primary control of each DG unit, shifting the droop characteristics.

## 2.3 Distributed Approach

A distributed secondary control intends to solve the energy management problem for a microgrid while providing the highest possible autonomy for different DER units and loads. Although this approach can still use a hierarchical structure for data exchange, decisions on the control variables are made locally. The autonomy of the local controllers (LCs) of each DER unit implies that they are intelligent and can communicate with each other to form larger intelligent entity. In distributed control, the main task of each controller is not necessarily to maximize the revenue of the corresponding unit but to improve the overall performance of the microgrid. These features indicate that a multi-agent system (MAS) can be prime candidate to develop a distributed microgrid control. Conceptually, the MAS is an evolved form of the classical distributed control system with capabilities to control large and complex entities. A main features of the MAS that distinguishes it from the classical distributed control techniques is that the software within each agent can imbed local intelligence. Each agent uses its intelligence to determine future actions and independently influences its environment. This type of system requires a fairly advanced communication system with capabilities similar to the human speech, e.g. the Agent Communication Language (ACL) that provides an environment for information and knowledge exchange. The need for a high-level communication environment can be shown by considering the communication needs of two agents within a microgrid. For example at a given time one may have an instantaneous surplus of 1,500W and other may need 500w. It is neither efficient nor required to provide the exact values, since the situation can change within a short time. The ACL provides the environment to exchange messages of the form “ I have currently some watts and do not expect to use them in the next 30 minutes” or “I need a few extra watts in the next 30 minutes”.

The agents not only exchange simple values and on-off signals but also knowledge, commands, beliefs, and procedures to be followed through the ACL. In the following the main decentralized method to develop the secondary control are briefly described. All these control methods tries to give a solution to the typical problems concerning the secondary control.

### ***Reactive power sharing method for MAS-based microgrid***

The decision-making architecture that manages microgrid assets is formulated from dispersed agents that comprise a distributed MAS: These agents must adapt to changing conditions without a

central controller directing their actions. Specifically, as mentioned before, a microgrid will operate in two distinct states: interconnected with larger utility network or islanded from it. When interconnected, agents must control generation, load, and storage assets primarily from the standpoint of power flows. When islanded, voltage and frequency regulation, as well as power balancing are of critical importance. Within each state, the distributed agents must self-organize and cooperate towards the best operational situation possible. In order to design a microgrid according to the agents theory, the microgrid components are divide into four asset classifications. Different microgrid assets are grouped according to operational capabilities and can be assigned appropriate control agents. The microgrid component classes are:

- *Generation*: capable of sourcing real and/or reactive power.
- *Load*: consumes real power; leading or lagging power factor
- *Storage*: can source or consume real power.
- *Node*: Point of connection w/ measurable connected quantities.

It could be guessed that in order to perform properly the MAS control requires an efficient communication system between the distributed agents. By utilizing the Foundation for Intelligent Physical Agents (FIPA) guidelines for agent-based communication, the interoperability and communication protocols for the microgrid MAS are standardizes [30]. Once the MAS structure is defined, the most changeling aspect of distributed MAS without a centralized supervisor is system organization and prioritization. In other words, at each instant, the agents that comprise the MAS must evaluate their local situation, determine a local best solution to the problem dictated by the goals assigned to the unique agent, communicate their intended action to MAS, participate in the prioritization of the MAS, and adjust its action based on the decision of the collective group. Determining rules for negotiation, however, is challenging. When M agents engage in cooperative acts, there is no supervisory agent that imposes a prioritization and task assignment based on its superior knowledge of the whole system. In a distributed agent collective where no agent has complete information about the entire microgrid and a predefined decision-making priority is not present, the agents must possess a level of intelligence to self-organize when seeking solutions to the problem to hand [31].

In [32] an example of distributed secondary MAS control is applied. According to the network considered, a set of control laws are developed for each agent by the secondary control and only local information are required.

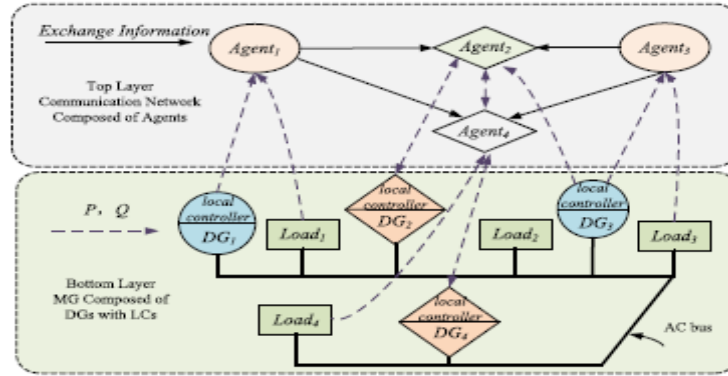


**Figure 2.20 MAS based control scheme**

The control scheme of the MG is divided in two layers as depicted in the Figure 2.20. The top layer is encompassed by the agents and the communication network, the bottom one is composed of DG units with local controllers. The agents connected to an uncontrollable or partially controllable DG (represented by circle) are called controllable and partially controllable agents, respectively. The other agents are called uncontrollable agents (represented as diamonds). When the output power of the RES starts to change, uncontrollable agents receive information from their corresponding uncontrollable DGs and then send the information to adjacent controllable agents according to the present control method. These controllable agents adjust the corresponding controllable DGs to get desired active and reactive power. The active power production of DG1 depends on environment(e.g., PV panel depends on sunlight) and it will be larger once the intensity of sunlight increases. Since the controllable DG2 is adjacent to DG1, Agent1 and Agent3 will send the information to Agent2 (neighbours Agent1 and Agent3), respectively. And the output power of the controllable DG2 is regulated by Agent2, making the total active power to the desired value.

### ***Consensus based method***

The Consensus-based control method [21] is entirely based the Graph Theory. The foundation of Graph Theory and the criterion to build a communication graph from a general microgrid are exhaustively discussed in [22]. In the following they will be only mentioned the important equation and the two theorems, which establish the Consensus-based control method. Each agent (node) of the graph is considered as a single-state system ( $\dot{x}_i = u_i$ ):

$$\dot{x}_i = \sum_{j \in N_i} a_{ij}(x_j - x_i) \quad (2.27)$$

where  $a_{ij}$  is the  $(i,j)$  element of the adjacency matrix  $A$  and  $x_j$  is the state of the neighboring agents of agent  $i$  and  $N_i$  the number of nodes in the graph. The consensus control problem is to find  $u_i$  such that all the states  $x_i$  converge to a common equilibrium point. In particular, considering the consensus protocol above ( $u_i$ ), it can be derived that the entire system can be written as  $\dot{x} = -Lx$  where  $L$  is the Laplace

matrix of the communication graph. The first of the two theorems establishes that the consensus will be achieved:

*Theorem I:* if there is a spanning tree in the communication graph, consensus control can be reached and the Laplace matrix  $L$  has a simple zero eigenvalue and all the other eigenvalues have positive real part.

If we consider a configuration of the graph with a control node, the system could be forced to converge to a desired external control input rather than some initial-dependent value. The control node can deliver a control signal  $v$  to a subset of nodes  $B$  in the system. Then, the state function is updated to:

$$\dot{x}_i = \sum_{j \in N_i} a_{ij}(x_j - x_i) + b_i(v - x_i) \quad (2.28)$$

where  $b_i = 1$ , if  $i \in B$  and  $b_i = 0$  otherwise. In this modified case, the consensus is guaranteed by the second theorem:

*Theorem II:* if there is a spanning tree in the communication graph, consensus control can be reached and a root node  $i$  satisfying  $i \in B$ , all agents' states will converge to the external control signal  $v$ .

Considering the bases of the consensus logic just introduced, the primary and secondary control levels are modified accordingly. In the droop control, in order to make sure  $Q_i$  is proportional to  $n_{Q,i}$  (droop coefficient), the protocol should be set to drive all the  $\frac{Q_i}{n_{Q,i}}$  to be identical. Therefore, in the equation (2.27),  $x_i$  is replaced by  $\frac{Q_i}{n_{Q,i}}$ . However, in order to realize this substitution,  $Q_i$  must be directly controlled, this is not possible since all DGs are operating in  $V-f$  mode. To overcome this problem, control protocol is set to be based on a controllable quantity  $\dot{V}_i$  instead of  $\frac{Q_i}{n_{Q,i}}$ :

$$\dot{V}_i = \sum_{j \in N_i} a_{ij} \left( \frac{Q_j}{n_{Q,j}} - \frac{Q_i}{n_{Q,i}} \right) \quad (2.29)$$

The second protocol introduced above allows sending a control signal  $v$  to a set of networked agents with only sparse communication links. Therefore, a consensus based secondary control can be designed.

$$\delta \dot{V}_i = \sum_{j \in N_i} (\delta V_j - \delta V_i) + b_i(\delta V - \delta V_i) \quad (2.30)$$

where  $\delta V$  is the control signal calculated at the an MGCC, according to the equation of the classical secondary control implemented by a PI regulator ( $\delta V = k_p (V_{std} - V_{pcc}) + K_i \int (V_{std} - V_{pcc}) dt$ ),  $\delta V_i$  is a locally secondary control signal that tracks  $\delta V$  through the consensus protocol introduced above, and  $b_i = 1$  for the DGs with direct communication to the MGCC  $b_i = 0$  elsewhere. According to *theorem II*, all local  $\delta V_i$  converge to  $\delta V$ .

Combining the secondary control signal with the primary one previously calculated, the inverter voltage reference in the equations below.

$$\dot{V}_{ref,i} = \dot{V}_i + \delta\dot{V}_i \quad (2.31)$$

$$\dot{V}_{ref,i} = \sum_{j \in N_i} a_{ij} \left( \frac{Q_j}{n_{Qj}} - \frac{Q_i}{n_{Qi}} \right) + \sum_{j \in N_i} (\delta V_j - \delta V_i) + b_i (\delta V - \delta V_i) \quad (2.32)$$

In Figure 2.21, it is represented a typical implementation of the consensus-base control method.

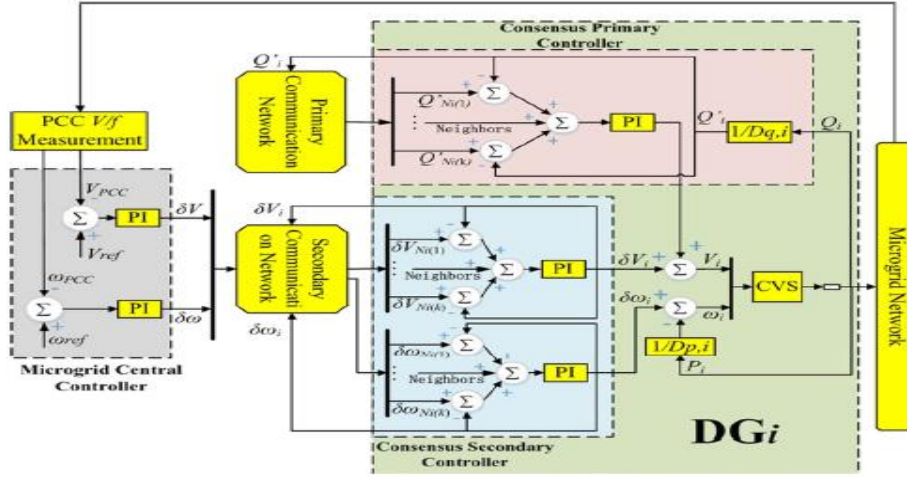


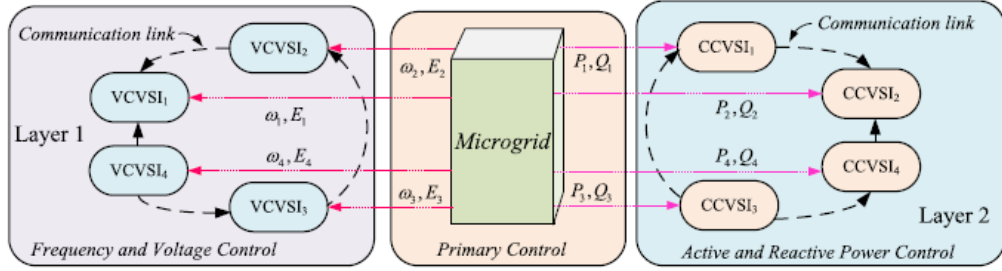
Figure 2.21 Scheme of consensus-based control

Even if it is present a MGCC, typical of a centralized secondary control architecture, this control strategy must be considered a distributed one; in fact the MGCC is only used to re-establish the nominal value of frequency and voltage at the PCC, but the main part of the secondary control action is performed by a distributed multi-agent control system.

### ***Indirect method for the reactive power sharing***

In [33] it is described and then applied in a particular case of study a distributed secondary control. The control structure is composed by two layers: one voltage source inverters (VCVSI) of the microgrid, the other one put in charge of Active and Reactive control of current controlled voltage source inverters (CCVSI).

Each control layer is associated with a limited and sparse communication network. The communication topology for each layer should be a graph containing a spanning tree in which the implemented controller at each DG only requires information about that DG and its direct neighbors in the communication graph. According to the physical structure of the microgrid, proper connecting graphs are designed, following optimization criteria (minimal length of communication links, maximal use of existing communication links, minimal number of links, and so on.). In Figure 2.22, it is depicted a scheme of the two-layers distributed control just mentioned.


**Figure 2.22 Two-layer example**

The optimal reactive power sharing is achieved by performing a frequency control action on VCVSIs and a reactive power control on CCVSI.

- *Frequency Control of VCVSIs*: The main objective of this control action is to synchronize all VCVSI frequencies to the nominal frequency. Furthermore, it should allocate the output active power of VCVSIs based on their active power ratings:

$$\frac{P_1}{P_{max1}} = \dots = \frac{P_{Nv}}{P_{maxNv}} \quad (2.33)$$

$$m_{p1}P_1 = \dots = m_{pNv}P_{Nv} \quad (2.34)$$

where  $N_v$  is the number of VCVSIs and  $m_{p_i}$   $i = 1, \dots, N_v$  are the droop coefficients. Differentiating the frequency-droop characteristics in (2.1) yields to:

$$\dot{\omega}_{ni} = \dot{\omega}_i + m_{p_i}\dot{P}_i = v_{fi} \quad (2.35)$$

where  $v_{fi}$  is an auxiliary control to be designed. Equation (2.35) is a dynamic system for computing the control input  $\omega_{ni}$  from  $v_{fi}$ . The auxiliary control should be designed such that VCVSI frequencies synchronize to the reference frequency  $\omega_{ref}$ , and (2.33) is satisfied. According to (2.35), the secondary frequency control of a microgrid including  $N_v$  VCVSIs is transformed to a synchronization problem for a first-order and linear multi-agent system:

$$\begin{cases} \dot{\omega}_1 + m_{p1}\dot{P}_1 = v_{f1} \\ \dot{\omega}_2 + m_{p2}\dot{P}_2 = v_{f2} \\ \vdots \\ \dot{\omega}_{Nv} + m_{pNv}\dot{P}_{Nv} = v_{fNv} \end{cases} \quad (2.36)$$

To achieve synchronization, it is assumed that VCVSIs can communicate with each other through the prescribed communication diagraph. The auxiliary control  $v_{fi}$  are chosen based on each VCVSI's own information, and the information of its neighbors in the communication diagraph as:

$$v_{fi} = -c_{fi} \left( \sum_{j \in Ni} a_{ij} (\omega_i - \omega_j) + g_i (\omega_i - \omega_{ref}) + \sum_{j \in Ni} a_{ij} (m_{p_i} P_i - m_{p_j} P_j) \right) \quad (2.37)$$

where  $c_{fi}$  is the control gain. It is assumed that the pinning gain  $g_i \geq 0$  is nonzero for one VCVSI that has the reference frequency  $\omega_{ref}$  information. The control input  $\omega_{ni}$  is defined by :

$$\omega_{ni} = \int v_{fi} dt \quad (2.38)$$

- *Reactive Power Control of CCVSI*: The reactive power of CCVSI is set based on their Reactive power ratings as:

$$\frac{Q_1}{Q_1^*} = \dots = \frac{Q_i}{Q_i^*} = \alpha Q_{ref} \quad (2.39)$$

According to each CCVSI and its adjacent information, the auxiliary control  $v_{Qi}$  can be chosen as:

$$v_{Qi} = -c_{Qi} \left( \sum_{j \in Ni} a_{ij} \left( \frac{Q_i}{Q_i^*} - \frac{Q_j}{Q_j^*} \right) + g_i \left( \frac{Q_i}{Q_i^*} - \alpha Q_{ref} \right) \right) \quad (2.40)$$

where  $\alpha Q_{ref}$  represents the pre-specified reactive ratio reference, and  $C_{Qi}$  and  $g_i$  are the control gains. Considering the consensus principle in (2.27),  $Q_i/Q_i^*$  can be synchronized to a reference value, and equivalent or proportional reactive power sharing can be achieved. Although the algorithm in two layer control is complex, it is not affected by the feeder impedance and it is suitable for sharing the reactive power in islanded MG with unbalanced and nonlinear loads.

### *Distributed cooperative method*

In [34] and [35], it is presented a secondary level reactive power control, that is developed as a one distributed cooperative control algorithm for each DG. The basic idea of the proposed distributed control is to share information among neighboring units via incorporating local communication networks, as schematically depicted in Figure 2.23.

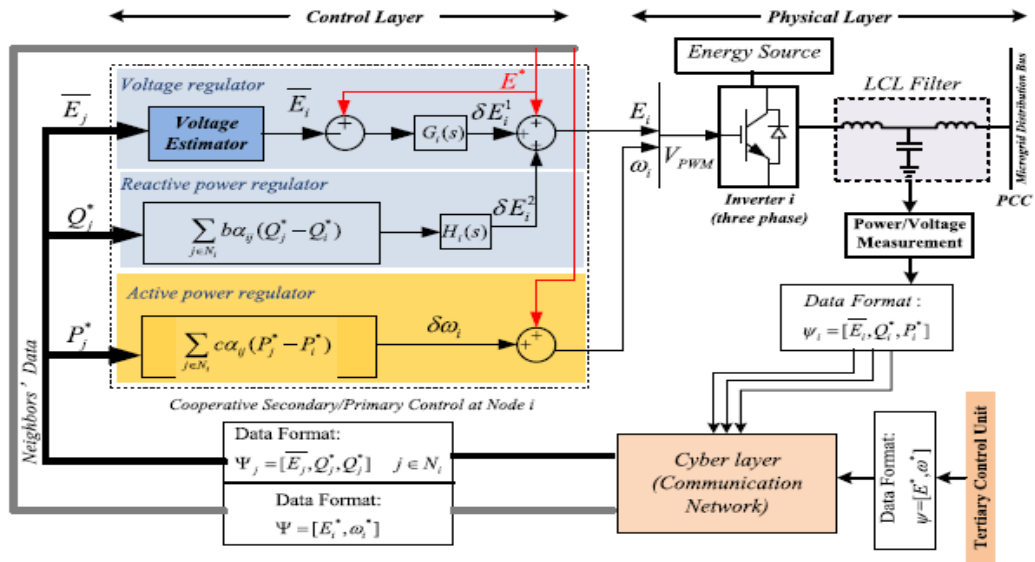


Figure 2.23 Cooperative distributed scheme.

In the proposed control structure, each inverter is considered as an agent of a multi-agent system to exchange data with a few other neighbor inverters, and process the information to update its local voltage set points and synchronize their normalized power and frequency. Moreover, global voltage regulation, frequency synchronization and proportional load sharing can be achieved by the cooperation among voltage, reactive power and active power regulators effectively in a fully distributed control strategy, and the stability and robustness of MG can be improved. Specifically, the node  $i$  receives the information  $\psi_j$  from its neighbors node  $j$ , and regulate the neighbor and local data  $\psi_i$  to update its voltage and frequency references ( $E_i^*$  and  $\omega_i$ ). The voltage reference is obtained by two voltage correction terms ( $\delta E_i^1$  and  $\delta E_i^2$ ) from the voltage and reactive power regulators, and the reactive power and frequency can be regulated by eliminating the reactive power and frequency deviations among the neighbors through PI controllers. Then, the reference voltage  $E_i^*$  of DG $_i$  can be obtained as:

$$E_i^*(t) = E^* + \delta E_i^1(t) + \delta E_i^2(t) \quad (2.41)$$

$$m_{Q_i} = \sum_{j \in N_i} b\alpha_{ij}(Q_j^* - Q_i^*), \quad \delta\omega_i = \sum_{j \in N_i} c\alpha_{ij}(P_j^* - P_i^*) \quad (2.42)$$

where  $E^*$  is the rated voltage magnitude of the MG. The voltage regulator at node  $i$  is compared with the rated voltage, where the difference is fed to a PI controller to generate the first voltage correction  $\delta E_i^1$ ,  $b$  and  $c$  are gain coefficients. The neighborhood reactive loading mismatch  $m_{Q_i}$ , which measures the difference between the normalized reactive power of the source  $I$  and the average value of its neighbors, and the mismatch in (2.42) is fed to a PI controller to adjust the second voltage correction term  $\delta E_i^2$ . The frequency correction term  $\delta\omega_i$  represents the information of neighborhood active loading mismatch.

Due to the performance of the PI regulator, all reactive powers will be synchronized to the same value and reactive power sharing is achieved. The active power regulator module keeps the frequency at the rated value, and precisely tunes the phase angle reference  $\delta\omega_i^*$  to reroute the active power across the MG and mitigates the neighborhood active power mismatch.

In the cooperative distributed control strategy, MG can run at the rated voltage and angular frequency, combining the active power regulator, the voltage and reactive power regulators. The cooperative distributed controller can realize the equivalent reactive power sharing under the mismatched feeder impedance and nonlinear load condition when the LBC delay is within the delay margin, but proportional active and reactive power sharing cannot be achieved.

## 2.4 Secondary control benefits and problems

In the following table are recapped the advantages and disadvantages of the secondary control methods introduced in the previous sub-section.

**Table 2.1 Advantages and disadvantages of secondary control methods.**

	Techniques	Advantages	Disadvantages
CENTRALIZED	DIRECT CONTROL METHOD FOR POWER SHARING	<ul style="list-style-type: none"> <li>• The equivalent/proportional power sharing is achieved</li> <li>• Method is easy to expand</li> <li>• First order communication delay is considered</li> <li>• Suitable for linear and nonlinear load conditions</li> </ul>	<ul style="list-style-type: none"> <li>• Cannot share power in islanded microgrids with more complex loads</li> <li>• Without considering communication delay</li> <li>• Without considering data droop in communication lines</li> </ul>
	GAIN SCHEDULING	<ul style="list-style-type: none"> <li>• Provides a general model</li> <li>• Reduce the cost by providing a reasonable cost function</li> <li>• The system can guarantee a good power sharing in the delay margin</li> </ul>	<ul style="list-style-type: none"> <li>• Gain coefficients are not easy to select</li> <li>• Communication delay in reactive power controllers is not considered</li> <li>• Data droop is not considered</li> </ul>
	MULTI-OBJECTIVE CONTROL	<ul style="list-style-type: none"> <li>• Reactive power sharing achieved</li> <li>• Possibility of accounting different object for the control</li> <li>• Provides model of the system</li> </ul>	<ul style="list-style-type: none"> <li>• Affected by communication delay</li> <li>• Affected by data droop in communication lines</li> <li>• Poor expandability</li> </ul>
	FUZZY LOGIC AND NEURAL NET	<ul style="list-style-type: none"> <li>• Reactive power sharing achieved</li> <li>• Possibility of accounting different object for the control</li> <li>• Provides model for the system</li> </ul>	<ul style="list-style-type: none"> <li>• Affected by communication delay</li> <li>• Affected by data droop in communication lines</li> <li>• Poor expandability</li> <li>• Affected by uncertainty in the model</li> </ul>

	ENERGY STORAGE SYSTEMS METHODS	<ul style="list-style-type: none"> <li>• Consider harmonic voltage effectively</li> <li>• The stability of the system is enhanced</li> <li>• The equivalent proportion power sharing is achieved</li> <li>• Influence on nonlinear load is considered</li> </ul>	<ul style="list-style-type: none"> <li>• The influence of feeder impedance mismatch is not considered</li> <li>• Not suitable for large scale MGs</li> <li>• Poor expandability of the control strategy</li> <li>• The reactive power sharing is influenced by LBC delay</li> </ul>
	MODEL PREDICTIVE CONTROL	<ul style="list-style-type: none"> <li>• Good robustness to a constant communication delay</li> <li>• Provides a general model of the system</li> <li>• The system can guarantee a good power sharing in the delay margin</li> </ul>	<ul style="list-style-type: none"> <li>• The algorithm is complex</li> <li>• Poor expandability (must change the model of the system)</li> <li>• Cannot deal with the problems brought by random delay</li> </ul>
DECENTRALIZED	MAS-BASED METHOD	<ul style="list-style-type: none"> <li>• Be suitable for a complex MG</li> <li>• Active power sharing is achieved</li> <li>• Frequency deviation is eliminated</li> <li>• Reactive power sharing is realized without high bandwidth communication</li> <li>• The control law can be simplified by graph theory</li> <li>• Organize information autonomously computational entities</li> <li>• Be beneficial to exchange information</li> </ul>	<ul style="list-style-type: none"> <li>• The programming algorithm is difficult to be designed in a complex MG</li> <li>• Delay/data droop in algorithm need to be considered</li> <li>• Delays in algorithm need to be considered</li> <li>• Communications delay in LBC lines</li> <li>• Good protocol in agents is difficult to be designed</li> <li>• The active and reactive power sharing are poor when data drop exists in the pre-set algorithm</li> </ul>

	<p>CONSENSUS BASED</p>	<ul style="list-style-type: none"> <li>• The two-layer secondary controllers described are fully distributed and they will not affect each other</li> <li>• The model is suitable for a complex MG</li> <li>• The control method is suitable for islanded MG with nonlinear load conditions</li> <li>• The control law can be simplified by graph theory Reactive power sharing is realized without high bandwidth communication</li> <li>• Active power sharing is achieved</li> </ul>	<ul style="list-style-type: none"> <li>• The algorithm is complex</li> <li>• Without considering LBC delay</li> <li>• The performance of controller is affected by data droop</li> <li>• Control equation need to be further optimized in the MG with complex loads</li> <li>• Proportional reactive power sharing is difficult to achieve</li> </ul>
	<p>INDIRECT CONTROL METHOD FOR POWER SHARING</p>	<ul style="list-style-type: none"> <li>• The equivalent/proportional reactive power sharing is achieved</li> <li>• Method is easy to expand</li> <li>• First-order communication delay is considered</li> <li>• Be suitable for linear nonlinear load conditions</li> <li>• The two layer control is fully distributed and will not affect each other</li> <li>• The proportional reactive power sharing can be achieved the model is suitable for a complex MG</li> <li>• The control method is suitable for islanded MG</li> </ul>	<ul style="list-style-type: none"> <li>• Cannot share the reactive power in islanded microgrid with more complex loads</li> <li>• Without considering communication delay</li> <li>• Without considering data drop in communication lines</li> <li>• Total generation cost of MGs not considered</li> <li>• The algorithm is complex</li> <li>• Without considering LBC delay</li> <li>• The performance of controller is affected by data droop</li> </ul>

		with nonlinear load conditions	
	DISTRIBUTED COOPERATIVE	<ul style="list-style-type: none"> <li>• The equivalent active and reactive power sharing can be achieved under complex load conditions</li> <li>• Good plug-and-play capability</li> <li>• Have resiliency to a single communication link failure</li> <li>• Good robustness to the constant communication delay</li> </ul>	<ul style="list-style-type: none"> <li>• The algorithm is complex</li> <li>• Poor expandability</li> <li>• Cannot deal with the problems brought by random delay</li> <li>• Data drop is not considered</li> <li>• Cannot deal with the problems brought by random delay</li> <li>• The proportional reactive power cannot be realized</li> </ul>

# CHAPTER 3

## PRIMARY CONTROL

### 3.1 Island-mode problems

Every electrical network operate according to the principle, stated in the Tellegen's theorem [36], that is the sum of lost, generated and absorbed powers in the network must be zero. This statement is formalized in (3.1) and (3.2) by considering separately active (P) and reactive (Q) powers.

$$\sum_{k=1}^n P_k^{generated} + \sum_{k=1}^n P_k^{lost} + \sum_{K=1}^n P_K^{absorbed} = 0 \quad (3.1)$$

$$\sum_{k=1}^n Q_k^{generated} + \sum_{k=1}^n Q_k^{lost} + \sum_{K=1}^n Q_K^{absorbed} = 0 \quad (3.2)$$

where  $n$  corresponds to the number of nodes of the network.

In grid-connected mode this law is always satisfied since any unbalance between generated and absorbed power in the microgrid is compensated by an exchange of powers, in and out, with the main grid, that act as an infinite source of powers. On the other hand, during islanded operating mode the microgrid is in a critical situation for the absence of the connection with the main grid and because generated and absorbed powers easily mismatch due to the intermittent and stochastic nature of most renewable sources, generally present in the structure of the microgrid.

It's worth noticing that the electrical power, especially if related to transmission losses and to loads, is not a fixed quantity but it depends on the network variables such as voltages ( $V$ ), currents ( $I$ ) and frequency ( $w$ ). For this reason, it would be more correct to rewrite equations (3.1) and (3.2) as in (3.3) and (3.4), explicating the dependence of the power from the network variables. In these equations, frequency is not defined as a nodal variable because at steady state the whole network reaches a unique system frequency, therefore it is a global variable. It is important to underline that, since the lost powers are mainly related to line losses, they do not depend only on the electrical variables of their own node

but they are defined from the voltages of all interconnected nodes, as well as from the system frequency.

$$\sum_{k=1}^n P_k^{generated}(V_k, \omega) + \sum_{k=1}^n P_k^{lost}(V_1, \dots, V_n, \omega) + \sum_{k=1}^n P_k^{absorbed}(V_k, \omega) = 0 \quad (3.3)$$

$$\sum_{k=1}^n Q_k^{generated}(V_k, \omega) + \sum_{k=1}^n Q_k^{lost}(V_1, \dots, V_n, \omega) + \sum_{k=1}^n Q_k^{absorbed}(V_k, \omega) = 0 \quad (3.4)$$

Therefore it can be noticed that the dependence between powers and network variables has a considerable impact on the management of an island microgrid. From Tellegen's theorem, when a power unbalance occurs, for example due to sudden load peak, voltages and microgrid frequency vary in order to bring the microgrid to a new equilibrium condition where (3.3) and (3.4) are satisfied again. However, depending on the size of the unbalance, microgrid voltages and frequency may largely deviate from their reference values, resulting in an equilibrium condition that it is not allowed for the system correct operation. In low voltage grids (LV grids) the network variables have to respect some predefined limitations to not compromise power quality, as well as not damage microgrid physical devices.

The Italian Electrotechnical Committee (CEI) defined several regulations for power quality of low voltage networks; a norm that can be applied in the islanded case is the CEI 0-21, that is related to the power quality of LV grid in real geographic islands; these in fact do not have connection with the main grid if located too far from the shore. The mentioned requirements are:

$$f = 50 \text{ Hz} \pm 5\%$$

$$V = 400 \text{ V} \pm 10\%$$

where  $f$  corresponds to the microgrid frequency and  $V$  to the amplitude of the line-to-line voltage in three phase interconnections. This means that the frequency can deviate only by 2.5 Hz around the nominal value, while line voltages are bounded between 440 V and 360V.

Given the aforementioned issues, a primary control level is needed to regulate the microgrid variables' values. This control acts on the VCVSIs by providing frequency and voltage amplitude references to the zero level control, according to the powers absorbed or generated by the inverter unit. Practically, this control layer consists in a decentralized structure that quickly modifies the voltage and frequency of each VCVSI, that can be approximated to an ideal voltage sources, so that the network power balance becomes feasible after an unexpected perturbation in the microgrid state of equilibrium. As previously mentioned, the primary level is developed according to a "droop control" logic.

## 3.2 Zero control level

The inverter is the fundamental electronic device of a microgrid, it represents the key unit over which the generic microgrid control is developed. The basic action of an inverter is to transform a DC power source, that could be a DC current source or a DC voltage source, in an AC one. Even though the literature provides a detailed description of its physical structure and control [2], it is not of interest for this work to go into a detailed explanation. To sum up, the inverter circuit consists on a series of power electronic devices that, through an accurate control, can generate a three phase sinusoidal voltage waveform starting from a DC power source. Moreover, there are some configuration that implements also an AC/AC conversion through the sequence of an AC/DC stage and a DC/AC stage; in this way it is possible to decouple two distinct AC power sources that work at different frequencies, as well at different wave amplitudes.

As it is represented in figure Figure 3.1, the type of inverter, taken in consideration for the development of this work, is a three phase voltage source inverter (VSI) composed by a IGBT bridge, a three phase transformer and an LCL filter (the first inductance of the filter is incorporated into the transformer). The bridge, fed by a constant voltage source, is controlled through a Pulse Width Modulation (PWM) technique. The transformer raises the voltages produced by the bridge and remove the bias terms. The output filter is required to reduce the harmonic contributions of voltages and currents produced by the electronic converter. In general, distorted signals can cause significant malfunctions of other sensible grid connected devices, so it's very important to keep the lowest possible level of Total Harmonic Distortion (THD), by properly selecting the right parameter for the LCL filter. In any case, the right choice of the LCL filter parameters is out of the purpose of this thesis work, a proper pre-tuned filter is used to develop the following study.

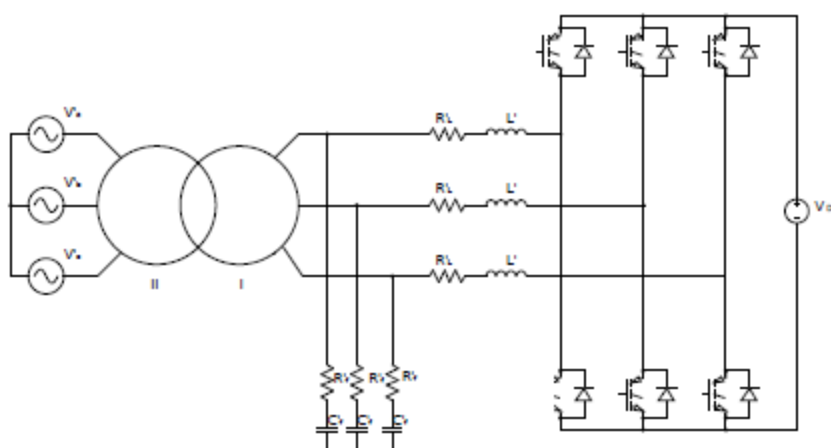
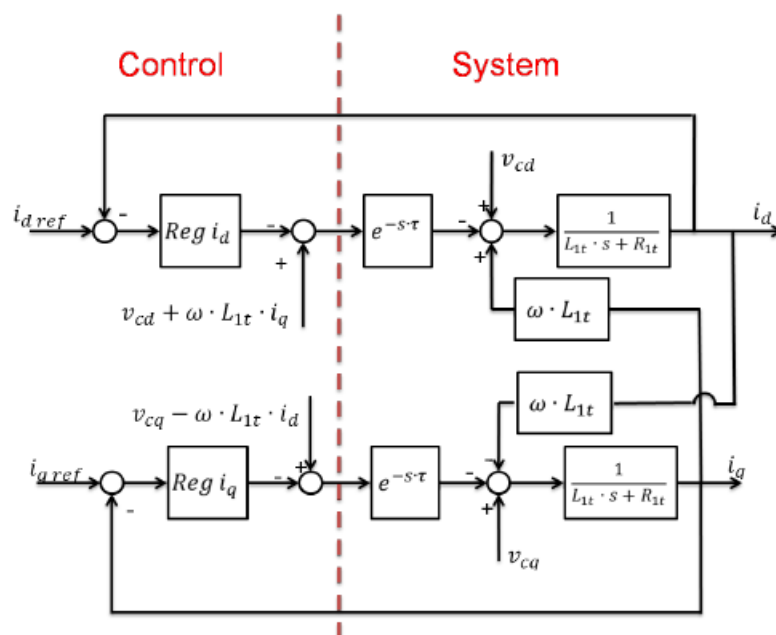


Figure 3.1 Electric scheme of the converter.

After that briefly description of the inverter purpose and structure, it should be clear why the inverter represents a fundamental block in the development and correct functioning of a microgrid. In fact, the major part of energy sources in a generic microgrid, produces DC power (energy storage units and photovoltaics), while others, such as wind turbines, produce AC power that is not synchronous with the established microgrid frequency. Moreover, if it is properly regulated, this electronic interface allows to independently shape the output voltage waveform of each power source, based on the set-points imposed by the primary level “droop” control. To accomplish this task, series of cascade loops and modulation techniques are designed that act on the inverter switching valves in order to track the chosen output variable, such as the output voltage. In the typical hierarchical control structure of a microgrid, this stage is usually defined as zero control level. The zero control level structure for a Grid Forming Converter is composed by two fundamental blocks, disposed in a cascade structure [2]:

- *Output filter currents control or grid following configuration:* thanks to the action of the inner current control loop an inverter could be considered as an ideal current control source. As depicted in Figure 3.2, this control action is performed in the d-q synchronous frame. The control variables are the direct and quadrature components of the voltage provided by the IGBT (Insulated-Gate Bipolar Transistor) bridge ( $S_d$  and  $S_q$ ), while the outputs, the current components  $I_d$  and  $I_q$ , coincide with the state variables of the controlled system and are, as well, the d-q components of the current flowing in the capacitor of the LCL filter.  $V_{Cd}$  and  $V_{Cq}$  are the components of the capacitor voltage, in this control scheme are measurable disturbance and they can be easily compensated by an appropriate control action; the same holds for the terms  $\omega L_{1t} * i_q$  and  $-\omega L_{1t} * i_d$ , being  $i_d$  and  $i_q$  and  $\omega$  available measurements and  $L_{1t}$  the first inductance of the LCL filter, so a known parameter. To make the model more realistic the actuation delay has also been considered in the scheme.



**Figure 3.2 Control Scheme of the internal current Synchronous Framework**

The control action is performed by two PI regulators, one for each  $d$ - $q$  component, which are tuned placing the zero at the same frequency of the slow pole of the system and adjusting the gain to have a crossover frequency  $\omega_c$  around 3000 rad/sec (nearly 500 Hz). In this way  $\omega_c$  is one decade slower than  $\omega_s = 2 \cdot \pi \cdot fs$  ( $fs = 50$  Hz), so it's possible to consider the switching dynamics frequency of the bridge decoupled from those of the current loop.

- *Output filter voltages or grid forming configuration:* The aim of this control is to regulate the frequency and amplitude of the voltage on the capacitor of the LCL filter. It is the external control loop, in the typical cascade configuration of the zero level control, and its output represents the set points for the internal current control loop previously described.

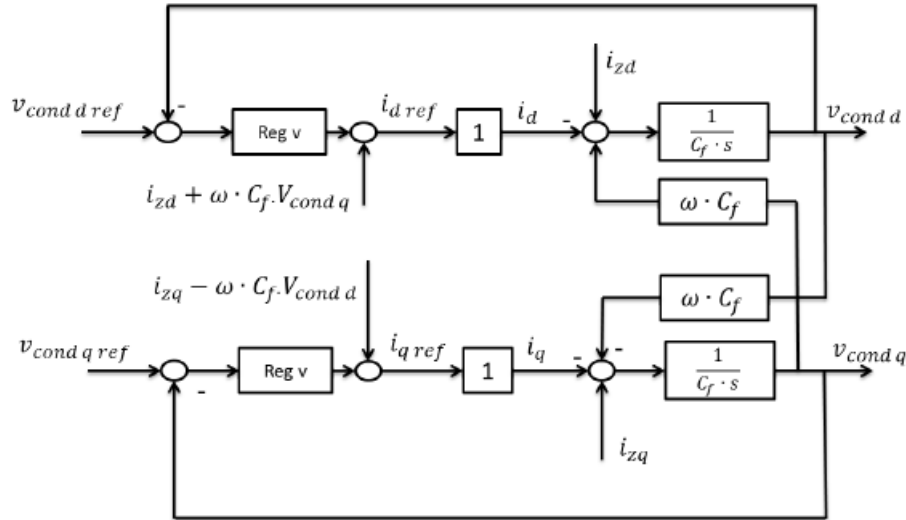


**Figure 3.3 Voltage control scheme in synchronous frame**

In the control structure of Figure 3.3,  $V_{condq}$ ,  $V_{cond d}$  and  $\omega$  represents measurable disturbances, which can be compensated properly tuning the voltage regulators. On the other hand,  $i_{zq}$  and  $i_{zd}$ , currents flowing in the second inductor, are not available measurements but they can be extracted with some electric computation, exploiting the measurements of the internal current and the voltage measured on the capacitor pins. The control variables of the voltage regulators, summed to the disturbances  $i_{zd} + \omega \cdot C_f \cdot V_{condq}$  and  $i_{zd} + \omega \cdot C_f \cdot V_{cond d}$ , represents the set-points for the internal current control loop in the cascade configuration. The control action is performed by two PI regulators, one for each d-q component of the voltage capacitor, on the system t.f.:

$$G_v(s) = -\frac{1}{C_f * s} \quad (3.5)$$

It can be seen that the system under control presents a negative gain, so the PI must have a negative gain too, in order to have a final phase margin between  $-180^\circ$  and  $0^\circ$ . The zero of the regulators is placed more than two decades before the crossover frequency, obtaining a phase margin equal to  $90^\circ$  and a crossover frequency of 300 rad/s. As it is shown in Figure 3.3, the internal current control loop is considered as a unitary gain, this is due the fact that the voltage control has been tuned such as the crossover frequency of the open loop transfer function is one decade lower than the current one, hence the dynamics of the current regulation don't affect the dynamics of the voltage regulation. As it can be noticed, the use of the synchronous representation of the electrical variable of the inverter is recurrent in the design of the zero control level. This is due to the fact that it results easier to handle DC electric variables instead of AC ones.

The Synchronous framework approach exploits the state vector representation of the electric variables of the grid, expressing it through two components that are the projections of the space vector

onto an orthogonal framework dq, that rotates at the same angular velocity of the space vector. These components can be easily obtained applying the Park's transformation, having an estimation of the angle  $\theta$  and of the frequency  $f$  of the electric quantity. Under the hypothesis of symmetric voltages and equilibrated currents, at steady state the terms are converted into two components as shown in Figure 3.4.

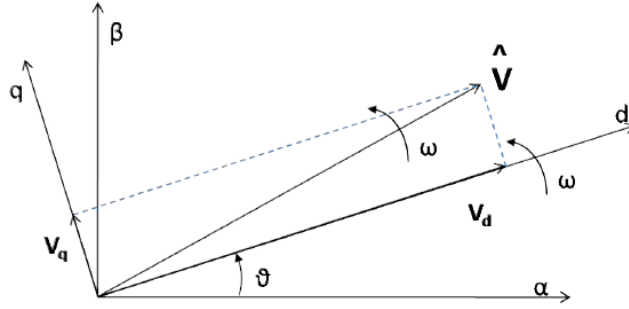


**Figure 3.4 Space vectors in Park's representation**

The Park transformation of a voltage term is obtained through the equation (3.6).

$$\begin{aligned}
 V_{dq0} &= T(\vartheta(t)) * v_{abc}(t) = \\
 &= \frac{2}{3} \begin{bmatrix} \cos(\vartheta) & \cos(\vartheta - \frac{2}{3} * \pi) & \cos(\vartheta + \frac{2}{3} * \pi) \\ \sin(\vartheta) & -\sin(\vartheta - \frac{2}{3} * \pi) & -\sin(\vartheta + \frac{2}{3} * \pi) \\ \frac{1}{\sqrt{2}} & \frac{1}{\sqrt{2}} & \frac{1}{\sqrt{2}} \end{bmatrix} \begin{bmatrix} v_a(t) \\ v_b(t) \\ v_c(t) \end{bmatrix} \quad (3.6)
 \end{aligned}$$

### 3.3 Droop control

In order to overcome the problems of island operation, mentioned in paragraph 3.1, a distributed control is taken into account to develop the primary control layer. Instead of entrusting the stability of the microgrid to a single converter operating as a voltage source, with its own controller, this task is given to every power converter connected to the microgrid, adopting a technique called Droop control [7]. The droop method, developed as a proportional control action, ensures a rapid regulation of the inverter that minimizes power unbalances and consequently the system frequency and voltages. This is a relevant feature since, the inverter interface implies a low system inertia, resulting in fast dynamics that must be properly managed.

The power reference or voltage reference for the droop control (it depends on how the droop control is developed) are provided by the higher layer in the hierarchical control structure of the

microgrid, responsible for the secondary control. In any case, the stability of the microgrid isn't affected by the values of this reference: indeed, even in case of missing signals or great discrepancies between the overall power reference and the power actually absorbed by the microgrid, every local converter automatically modifies the ejected power in order to satisfy the current power request, keeping the frequency and voltages inside the prescribed limits, as previously mentioned.

The theory on which the droop control is based has been briefly introduced in paragraph 2.1, to explain the motivation for a secondary control layer. In the following this theory is reconsidered and the process to deduce its algebraic laws is discussed.

### 3.3.1 Droop laws

There are three possible way to couple the electrical variables involved in the droop laws: the resistive coupling, the inductive coupling and the mixed one.

- *Resistive*: The active power variation is linked to the nodal voltage one, while the reactive power variation to the network frequency one (P-V, Q- $\omega$ ).
- *Inductive*: The active power variation is linked to the network frequency one, while the reactive power variation to the nodal voltage one (Q-V, P- $\omega$ ).
- *Mixed*: In this case both active and reactive power variations have an impact both on frequency and voltages; although this can express more realistic cases, this relationship is not very used given its complex definition.

The droop relationship are usually chosen based on the line impedance [2], and, in particular, the key factor is represented by the ratio between the resistance and the inductive impedance of the line, known as the R/X factor. A network characterized by a predominance of the resistance part of the line impedance will present a bigger value of the R/X factor, compared to a network whit the predominance of the inductive impedance. The former case suggests the implementation, for the droop control, of the P-V and Q- $\omega$  relationship; the latter one exploits the Q-V and P- $\omega$  relationship. Being the resistive characteristic typical of small grid systems like the one considered in this work, the resistive droop relationship will be considered for the development of the rest of the thesis.

To better understand the concept that is behind the droop control method a shorter and intuitive explanation is given in the following, based on the scheme depicted in Figure 3.5

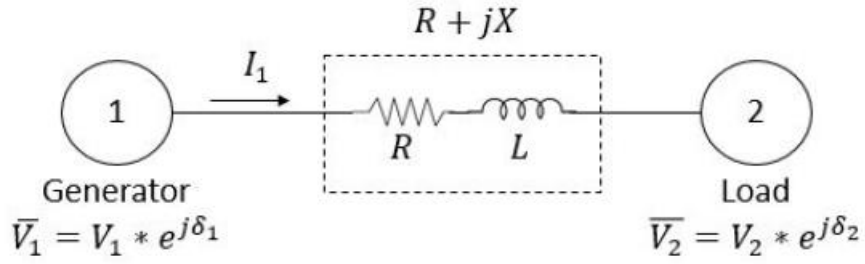


**Figure 3.5 Simple electrical network.**

The network is composed of one generator and one load, interconnected through a line with a defined impedance. It is assumed that this AC network has already reached the steady state condition, therefore each variable has a sinusoidal waveform that pulsates at the steady state frequency,  $\bar{\omega}$ . This allows to study the system in the phasor domain, where each voltage can be represented in the complex plane as a phase vector that rotates at the steady state frequency, as reported in Figure 3.6.

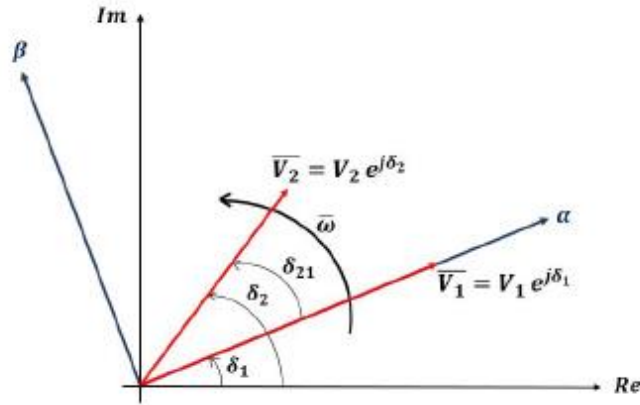


**Figure 3.6 Phasor representation of nodal voltages.**

Node 1 is assumed to be the reference node, called also *slack node*. This means that all phasor vectors are defined with respect to a new coordinate system  $(\alpha, \beta)$  which is synchronous and aligned with  $\bar{V}_1$ . Therefore:

$$\bar{V}_1^{\alpha\beta} = V_1 \quad (3.7)$$

$$\bar{V}_2^{\alpha\beta} = V_2 e^{j\delta_{12}} \quad (3.8)$$

Given the nodal voltages and the line impedance, the line current can be easily computed:

$$\begin{aligned}
 \bar{I}_1^{\alpha\beta} &= \frac{(\bar{V}_1^{\alpha\beta} - \bar{V}_2^{\alpha\beta})}{R + jX} = \frac{(V_1 - V_2 \cos(\delta_{21}) - jV_2 \sin(\delta_{21}))}{R + jX} \\
 &= \frac{-RV_2 \cos(\delta_{21}) + RV_1 - XV_2 \sin(\delta_{21})}{R^2 + X^2} \\
 &\quad + j \frac{XV_2 \cos(\delta_{21}) + XV_1 - RV_2 \sin(\delta_{21})}{R^2 + X^2}
 \end{aligned} \tag{3.9}$$

Knowing both voltage and output current of Node 1, it is possible to compute the complex delivered power:

$$\begin{aligned}
 S_1 &= \bar{V}_1^{\alpha\beta} * \bar{I}_1^{\alpha\beta} = \\
 &= V_1 \frac{-RV_2 \cos(\delta_{21}) + RV_1 - XV_2 \sin(\delta_{21})}{R^2 + X^2} \\
 &\quad + jV_1 \frac{XV_2 \cos(\delta_{21}) + XV_1 - RV_2 \sin(\delta_{21})}{R^2 + X^2}
 \end{aligned} \tag{3.10}$$

Finally, the output active and reactive power are computed by considering separately the real and imaginary part of the complex power:

$$P_1 = \text{Re}(S_1) = V_1 \frac{(R(V_1 - V_2 \cos(\delta_{21})) - XV_2 \sin(\delta_{21}))}{R^2 + X^2} \tag{3.11}$$

$$Q_1 = \text{Im}(S_1) = V_1 \frac{(X(V_1 - V_2 \cos(\delta_{21})) + RV_2 \sin(\delta_{21}))}{R^2 + X^2} \tag{3.12}$$

Starting from the expression of the active and reactive generated power with the explicit dependence on the network variables, now it is possible to understand why the resistive and the inductive relationship have these precise links between powers, frequency and voltages. Considering first the inductive droop coupling, it is applied when the R/X factor is very small. Therefore by considering  $X \gg R$  and by linearizing  $\delta_{21} \sim 0$  (in a single line interconnection it can be assumed that the voltages have nearly the same phase), we obtain:

$$P_1^{\text{inductive}} = -\left(\frac{V_2 V_1 X}{R^2 + X^2}\right) \delta_{21} \tag{3.13}$$

$$Q_1^{\text{inductive}} = V_1 \frac{(V_1 - V_2)X}{R^2 + X^2} \tag{3.14}$$

While for the resistive network, where  $R \gg X$ , it results that:

$$P_1^{\text{resistive}} = V_1 \frac{(V_1 - V_2)R}{R^2 + X^2} \tag{3.15}$$

$$Q_1^{inductive} = \left( \frac{V_2 V_1 R}{R^2 + X^2} \right) \delta_{21} \quad (3.16)$$

By looking to the equations (3.13) and (3.14), it is possible to see that an increment in the phase difference between the two nodes has an impact on the active power in the inductive case and on the reactive power in the resistive case. Actually, the phase difference is strictly related to the frequency. An increase of  $\delta_{21}$  means that  $V_2$  waveform tends dynamically to anticipate the  $V_1$  one, which in turn implies that the frequency of Node 2 tends to be higher with respect to the Node 1 [36]. Therefore, in order to control the frequency, for inductive microgrids it is better to vary the generated active power, while for the resistive case it is better to act on the variation of reactive power.

Regarding the voltages, it should be noted that in both cases, inductive and reactive, a voltage variation affects the active and reactive power, since, looking to eq. (3.13)-(3.16), it doesn't exist a perfect decoupling. However, for (3.13) and (3.15), the dependence between the relative power and the generation voltage  $V_I$  is a squared dependence. Although the effects are not completely decoupled as for the frequency, in the inductive case the generation voltage is linked with the delivered reactive power, while in the resistive case the generated active power is usually used to control the nodal voltage.

Even if the aforementioned relations don't presents a perfect decoupling of the effects of frequency and generation voltage over reactive and active powers, the approximation they provide is generally well accepted, since the aim of the droop control is not to perform a precise control action but only to allow the network to properly function without large deviations of variables.

For small scale networks it is not true that only line impedances have to be taken into account, but the whole system should be considered. Actually, since microgrids are characterized by short lines, load characteristics have a great impact on the relationship between network variables and generated powers. For example, linear RLCs loads are characterized by a resistive coupling ( $P-V$ ,  $Q-\omega$ ), while an asynchronous rotating motor, presents an inductive relationship ( $Q-V$ ,  $P-\omega$ ). So the prevailing load characteristics dictate the droop relation should be chosen for the control. Taking into account the study performed in [2], it can be stated that the resistive relationship is the one that ensures the system stability for the microgrid, taken into consideration for this thesis work, and in general for most types of microgrids. Actually, is quite difficult to have a small-scale network characterized by a prevailing inductive characteristic, since is not frequent to have rotating loads directly connected to the line but they are usually interfaced through inverters.

Once the relationship between voltage, frequency and powers is chosen, there are however different approaches to implement the droop control. Even if they all have the same objective, they are based on different control actions.

### 3.3.2 Droop control structures

Depending on the chosen controlled and control variables, two droop methods can be implemented: the Conventional and the Inverse droop.

The *Conventional droop* intervenes directly on the output voltage waveform of the inverter; in fact it directly varies, by mean of a proportional action, the output voltage magnitude and the frequency based on the variation of the delivered active and reactive power. This droop strategy is interfaced with Grid Forming Converter. As it can be seen in Figure 3.7, the conventional droop provides voltage magnitude and frequency set-points to the zero control level, whose control action, from the point of view of the primary control, makes the inverter an ideal voltage generator.

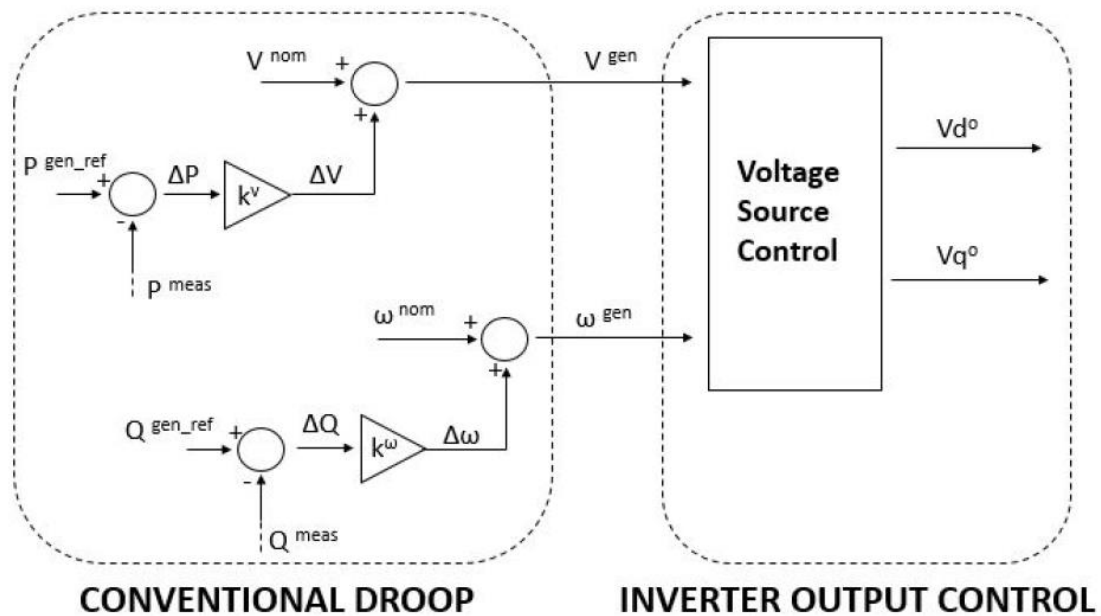


Figure 3.7 Conventional Resistive Droop

On the other hand, the *Inverse droop* control acts in the opposite way. It modifies the generated output power depending on the deviations of the nodal voltage magnitude and frequency from their nominal values. This droop strategy is usually implemented along with Grid Following Converter, since they are able to track active and reactive power set-points [2]. As stated before, the main difference between this strategy and the conventional one, is that whit this approach is not possible to have a direct control on the voltages and on the microgrid frequency, but they both will take the values that guarantee the power balance of the microgrid. A schematic representation of the Inverse Droop Control with resistive relationship is reported in Figure 3.8.

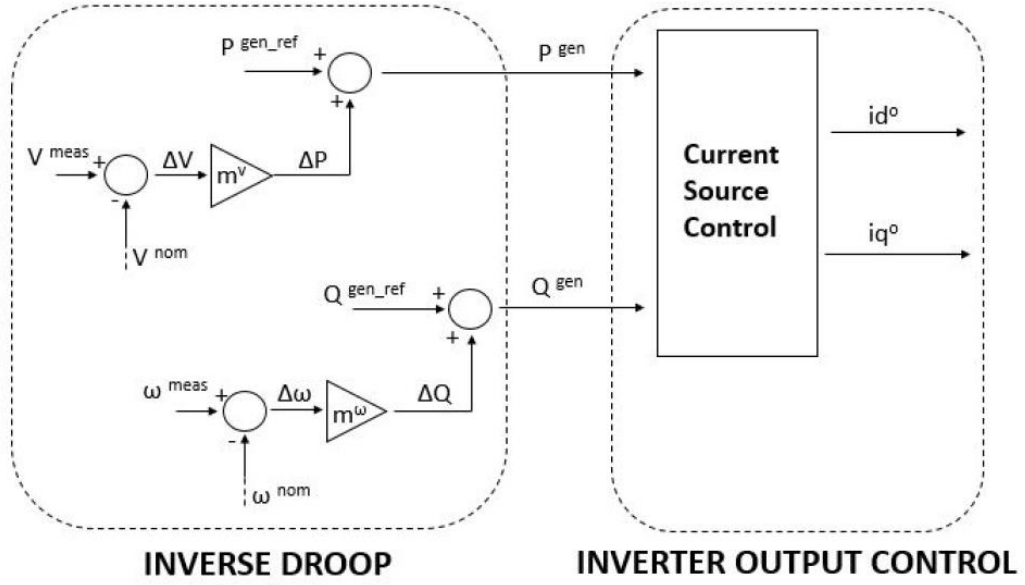


Figure 3.8 Inverse Resistive Droop

### 3.4 Primary control design

The primary microgrid control structure adopted for this master thesis work consists of a decentralized structure where at some node of the microgrid a Conventional Droop control is located, that is, as previously said, interfaced to the microgrid through a voltage controlled inverter. The nodes where a voltage controlled inverter is placed are considered as voltage controlled nodes. The resistive relationship ( $P$ - $V$ , $Q$ - $\omega$ ) is implemented since, as aforementioned, it guarantees the network stability form most types of loads. Therefore, the output voltage magnitude and the frequency of the inverter are defined by the droop control as the following:

$$V_j = -K_p^j(P_j - P^{ref}_j) + V^{ref}_j \quad (3.17)$$

$$f_j = K_Q^j(Q_j - Q^{ref}_j) + f^{ref}_j \quad (3.18)$$

where  $j$  ( $1, \dots, ncv$ ), with  $ncv$  number of controllable voltage units,  $P^{ref} = 0 W$  and  $Q^{ref} = 0 W$ ,  $P_j$  and  $Q_j$  are respectively the measured active and reactive powers generated/absorbed by the inverter, while  $K_p^j$  and  $K_Q^j$  represent the proportional coefficients of the droop control, defined as the following:

$$\begin{cases} K_p = \frac{2\Delta V_{max}}{P_{max} - P_{min}} \\ K_Q = \frac{2\Delta f_{max}}{Q_{max} - Q_{min}} \end{cases} \quad (3.19)$$

The values of  $\Delta f_{max}$  and  $\Delta V_{max}$  are the maximum frequency and voltage permanent deviations allowed by the standards, and in Italy, as already mentioned, for the low voltage islanded microgrids they correspond respectively to 2.5 Hz and 40 V (line to line rms value).  $P_{max}$  and  $Q_{max}$  are the maximum active and reactive powers that the considered converter can generate while  $P_{min}$  and  $Q_{min}$  are the maximum that the converter can absorb. This choice of the droop gains maximizes the power range on which the converter can regulate frequency and/or voltage through the droop characteristic inside saturation limits. Indeed if the references exceed the maximum allowed deviation they must be saturated to their limits. Being the droop control a linear relation, it can be easily represented in a graph, like the one depicted in Figure 3.9.

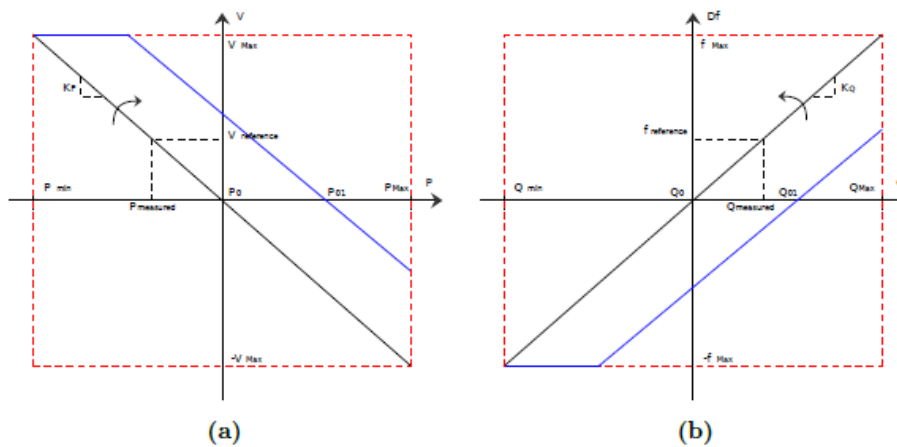


**Figure 3.9 Resistive conventional droop characteristics**

In the picture  $P_0$ ,  $P_{0l}$ ,  $Q_0$  and  $Q_{0l}$  represents different values of the power references  $P^{ref}$  and  $Q^{ref}$  of eq. (3.17) and (3.18). In particular, as it can be noticed, a variation of these reference values affects the offsets of the straight lines, on the contrary the droop gains affect the slopes. The measured power is considered positive if generated by the inverter and negative if absorbed.

Looking at the droop characteristics, it can be noted that two lines present an opposite effect on the outputs. On the one hand, the voltage magnitude is decreased with respect the reference value as the power deviation increases, while the inverter frequency variation is directly proportional to the power offset. An intuitive explanation of this choice can be given by considering a resistive network with a generator and a parallel RLC load, as schematically depicted in Figure 3.10.

In order to study this simple network, the absorbed power is firstly computed. Since microgrids are characterized by short interconnections and loads represent the most relevant power absorption, power line losses are neglected.

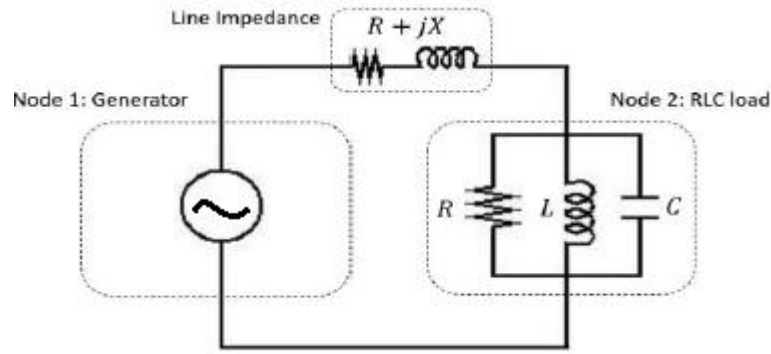


**Figure 3.10 Simple network.**

It's simple to evaluate the power absorbed by the load:

$$\begin{aligned}
 S^{load} &= V^{load} (I^{load})^* = V^{load} \left( \frac{V^{load}}{Z^*} \right) \\
 &= \frac{(V^{load})^2}{R} + j \frac{(V^{load})^2}{\omega L} - \omega C (V^{load})^2
 \end{aligned} \tag{3.20}$$

where the active and reactive power can be calculated as:

$$p^{load} = \text{Re}(S^{load}) = \frac{(V^{load})^2}{R} \tag{3.21}$$

$$Q^{load} = \text{Im}(S^{load}) = \frac{(V^{load})^2}{\omega L} - \omega C (V^{load})^2 \tag{3.22}$$

Through equation (3.21) and (3.22), it is possible to give an interpretation of the droop characteristics shown in Figure 3.9. Taking into account firstly the active power, generation peak occurs, there will be an initial unbalance where the generated power exceeds the absorbed one ( $P^{gen} > P^{load}$ ). Given the Tellegen's theorem, this will result in a voltage increase since it is the only way to raise the active absorbed power, as reported in (3.21), and so bring again the network in a stability condition  $P^{gen} = P^{load}$ . To counteract the effect of generated or absorbed power peaks of the inverter, the droop control directly regulates the magnitude voltage node, according to the measured active power deviation from the power reference. So if  $P^{gen} > P^{load}$ , a peak of generation, the voltage controlled inverter lowers the voltage magnitude in order to decrease the active power generated toward the power reference, on the contrary if  $P^{load} > P^{gen}$ , so we have a peak of absorption, the inverter raises the voltage magnitude to increase the inverter power and bring back the measured power to  $P_{ref}$ .

The same interpretation with the opposite logic is valid for the reactive power. In this case looking at (3.22), the frequency appears at the denominator of the equation (the capacitive load is neglected). So if  $Q^{gen} > Q^{load}$ , the inverter increases the frequency in order to decrease the reactive power generated

towards  $Q_{ref}$ , while if  $Q^{load} > Q^{gen}$  the voltage controlled unit lower the frequency to increase the reactive power absorbed and so return the measured reactive power to the reference. The reported explanation seems coherent with the two graph reported in Figure 3.9, where the left line has negative slope and the right one has positive slope. Although the droop strategy is studied for a simple case, the same principles can be applied to more structured microgrids

### 3.5 Conventional droop implementation

Droop characteristics must provide the references that a lower control level have to follow in order to perform a primary control, this is a peculiarity of a hierarchical microgrid control system: the upper control level set the references for the immediately lower one, that is implemented on a faster time scale. The lower is the level the faster is the control response time.

In the case of the conventional droop strategy, the references of frequency and voltage amplitude, given by the droop laws, must be converted to direct and quadrature components  $V_{dref}$  and  $V_{qref}$ , because those ones are the only input set-points that a grid forming converter, implemented in the synchronous framework, can accept. Direct and quadrature components are referred to a nominal value of phase, computed by integrating the main grid frequency. This is a trick in order to compute the quadrature and direct component of the voltage that in the scheme in Figure 3.12, otherwise will be sinusoidal. Calling  $\vartheta_{ref}$  the voltage reference phase,  $\vartheta_n$  the nominal one and  $\Delta\vartheta$  their difference,  $V_{dref}$  and  $V_{qref}$  can be easily computed exploiting (3.23), as shown in Figure 3.11.

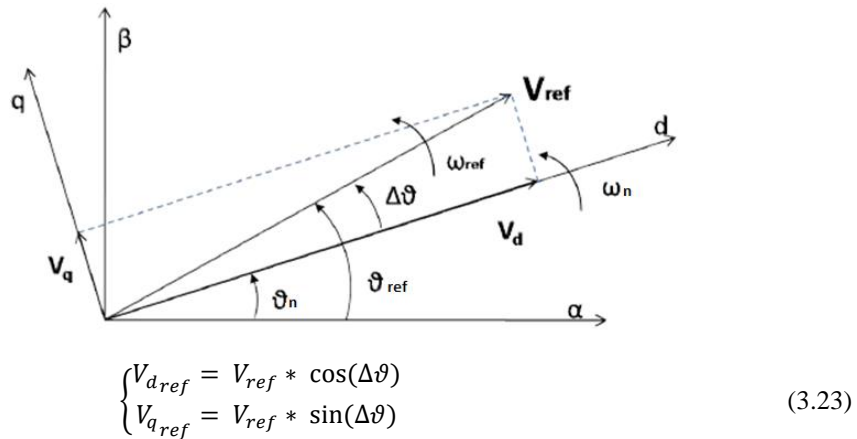


**Figure 3.11 Direct and Quadrature voltage components.**

Having that the reference phasor rotates at angular speed equal to  $\omega_{ref} = 2 * \pi * f_{ref}$ , the reference phase can be expressed as  $\vartheta_{ref} = \int \omega_{ref}(\tau) d\tau$ : final expression of  $\vartheta_{ref}$  can be summarized in (3.24).

$$\Delta\theta = \left[ \int (2 * \pi * f_{ref}(\tau) d\tau \right] - \vartheta_n \quad (3.24)$$

A schematic representation of the resistive conventional droop interface with the grid forming converter is depicted in Figure 3.12, where  $T_{connection}$  represents the time instant when the converter connect to the microgrid.

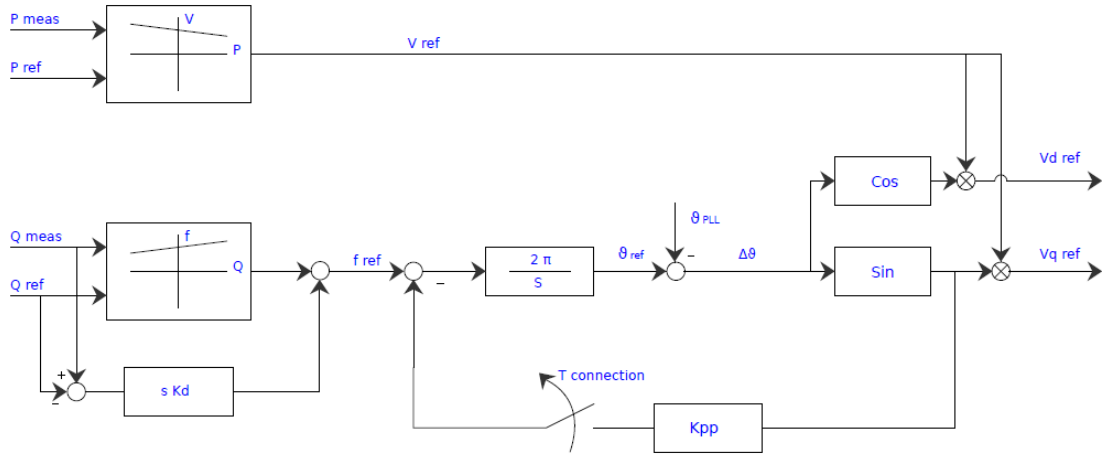


**Figure 3.12 Block diagram representation for voltage and frequency conversion**

As it can be seen from the scheme, a derivative action is applied on the reactive power deviation for the frequency branch. This is due to the capacity of the derivative action to speed up the reactive power reference tracking and to damp major oscillatory transients [2]. In the scheme is also implemented a closed loop with a proportional regulator  $K_{pp}$ , whose objective is to cancel the quadrature components during the connection of the converter as the following:

$$\frac{f_{ref}}{V_{q_{ref}}} = \frac{\frac{2\pi}{s} * \frac{1}{s^2 + 1}}{1 + K_{pp} \frac{2\pi}{s} * \frac{1}{s^2 + 1}} = \frac{2\pi}{s(s^2 + 1) + K_{pp} 2\pi} \xrightarrow{s=0} \cong \frac{1}{K_{pp}} \quad (3.25)$$

In this way, for high values of  $K_{pp}$ , the voltage reference is kept in phase with the grid voltage, because having null quadrature component means to have  $\Delta\theta = 0$ . During this first phase,  $\vartheta_n$  is provided by a PLL in order to synchronize the Converter with the main grid.

### 3.5.1 Zero Control Level

In this subsection the open loop transfer functions of the current and voltage loops are presented

Regarding the current regulator, looking at Figure 3.2 a time delay can be noted. To easily tune the controller, the first order Padé approximation is adopted, in order to have a clear idea of the upper limit of the crossover frequency  $\omega_c$ . This must be smaller than the pole frequency of  $1/\tau$  ( $\tau$  is the time delay) to maintain a positive phase margin. Being the current and voltage d-q reference signals constant (at least at steady state), the PI is the best controller choice because it guarantees zero steady state errors. Since they deal with the same process transfer function, both in the case of the voltage regulation and of the current one, the PI controller that regulate the d component is equal to the one put in charge of the q component regulation.

The current PI regulators are tuned to have an open loop crossover frequency  $\omega_c$  around 3000 rad/s (nearly 500 Hz), while the voltage ones are tuned for a crossover frequency a decade smaller, that is 300 rad/s (nearly 50 Hz).

The proportional and integral coefficient of the voltage and current regulators are enlisted in Table 3.1, along with the parameters of the considered inverter.

**Table 3.1 PI regulators parameters**

<i>Parameter</i>	<i>Value</i>
<b>Kp_c</b>	456.67
<b>Ki_c</b>	456.67*0.019
<b>Kp_v</b>	-0.035879
<b>Ki_v</b>	-0.035879*0.19
<b>Lt</b>	0.0022
<b>Rt</b>	0.0176
<b>Cf</b>	5e-5

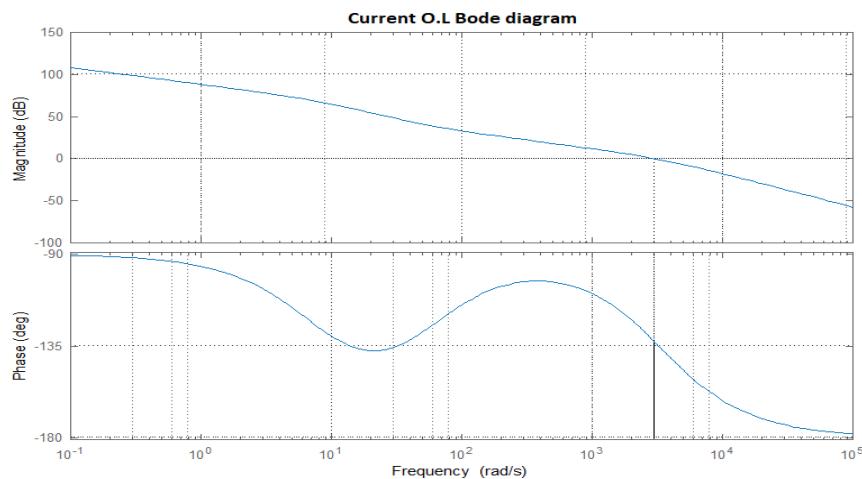


**Figure 3.13 Current open loop Bode diagram**

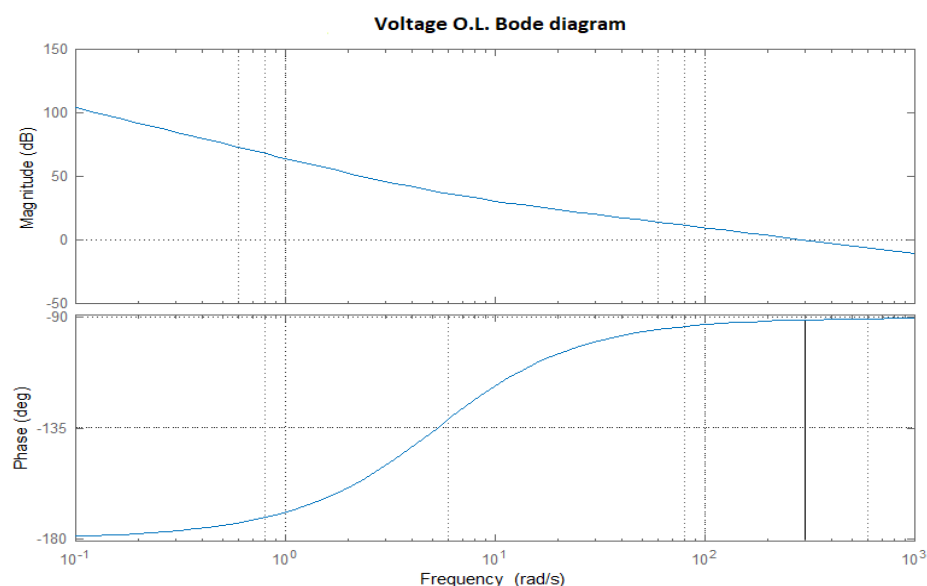


**Figure 3.14 Voltage open loop Bode diagram**

The results of the reference tracking performances of the voltage and current regulators are intentionally omitted here, since, in the next subsection, tests on the reference tracking of the primary control will be presented and the effectiveness of its control action depends on the correct function of the voltage and current regulation.

For a deepening on the effects of different PI parameters on the performances of the zero control level see [2].

### 3.5.2 Steady state droop test

First, the designed droop control is tested in steady state conditions in the trivial microgrid, represented in Figure 3.15. The trivial microgrid is composed of the converter connected to a three phase controlled current source that can emulate a load or power controlled energy source. Quasi-static diagrams of measured power, voltage and frequency are extracted from simulations and are exploited to draw the conventional resistive droop characteristics implemented in a power converter.

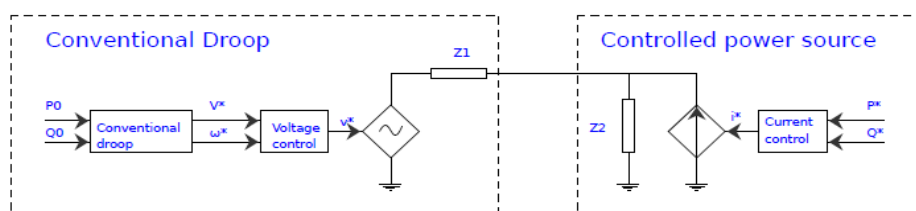


**Figure 3.15 Test scheme for the steady state droop test**

The simulations are carried out taking into consideration that the variations of absorbed/generated power of the current source, must be slow enough to consider negligible the internal dynamics of the converter control. Three different curves are extracted providing minimum, maximum and zero power references to the droop control and measuring amplitude  $V$  and frequency of the generated voltage.

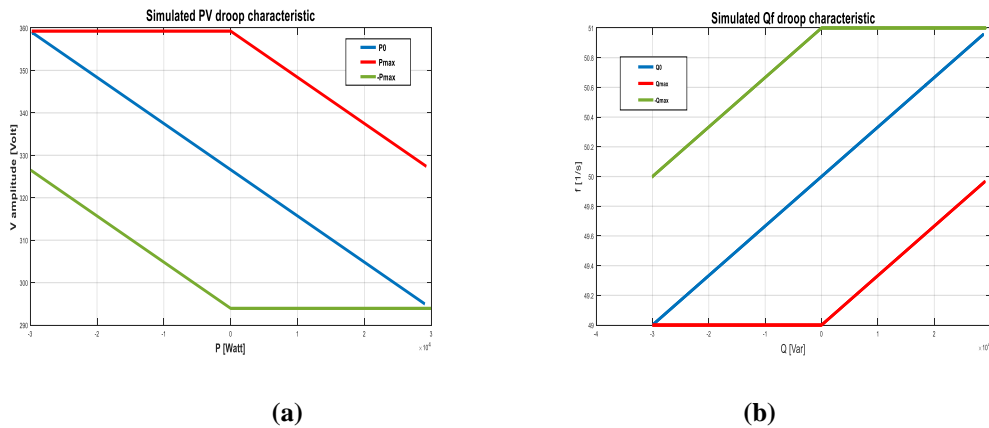


Figure 3.16 Simulated droop characteristics

Looking at Figure 3.16, both the curves represent what it is imposed by the droop control. The P-V characteristics is tuned over the phase voltage magnitude so  $V_n = 400\sqrt{2}/\sqrt{3}$  and  $\Delta V = 40\sqrt{2}/\sqrt{3}$ .

In this subsection the simulation results of a trivial microgrid composed by a converter connected to a main grid (simulated by an ideal voltage generator) are presented as shown in Figure 3.17. The aim of the simulation is to highlight the dynamic performances of the droop control tuned with the best parameters possible for the considered inverter. The dynamics of the droop control strongly depend on the values of parameters chosen to implement it, however the aim of this thesis work is not to investigate how they affect the control but rather to implement the best possible primary control. For a better view on how the droop control changes for different tunable parameters see [2].

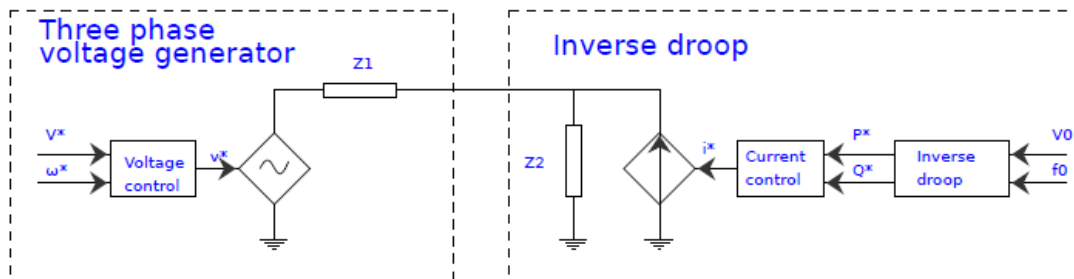


Figure 3.17 Dynamics of a grid connected conventional droop

The active and reactive power limits of the converter, taken into consideration for the simulation are equal to  $\pm 30kW$  and  $\pm 30kVar$ , as the one in the quasi-static case. Between the converter and the grid a series line impedance is modelled. Being this subsection and the overall thesis focused on low voltage microgrids, simulations are carried out with a line resistance that is dominant or at least comparable to the value of the line inductive reactance. A resistive conventional droop regulates the power converter, whose power references are modified during the simulation. The grid forming control is configured in synchronous framework with a set of tuning parameters for the voltage regulator and of electrical parameters for the microgrid listed in the following table.

**Table 3.2 Parameters of dynamic simulation**

<i>Parameter</i>	<i>Value</i>	<i>Unit</i>
<b>R<sub>lin</sub></b>	0.1	$\Omega$
<b>L<sub>lin</sub></b>	0	$\mu H$
$\Delta V_{max}$	$40\sqrt{2}/\sqrt{3}$	V
$\Delta f_{max}$	1	Hz
<b>k<sub>d</sub></b>	$1 * 10^{-5}$	
<b>k<sub>pp</sub></b>	$10^3$	

Instead of a pure derivative control scheme of Figure 3.12, a first order high pass filter is used to make the model realizable, with its pole placed in  $s = -1000 rad/s$ , this gimmick helps also to filter out high frequency noises.

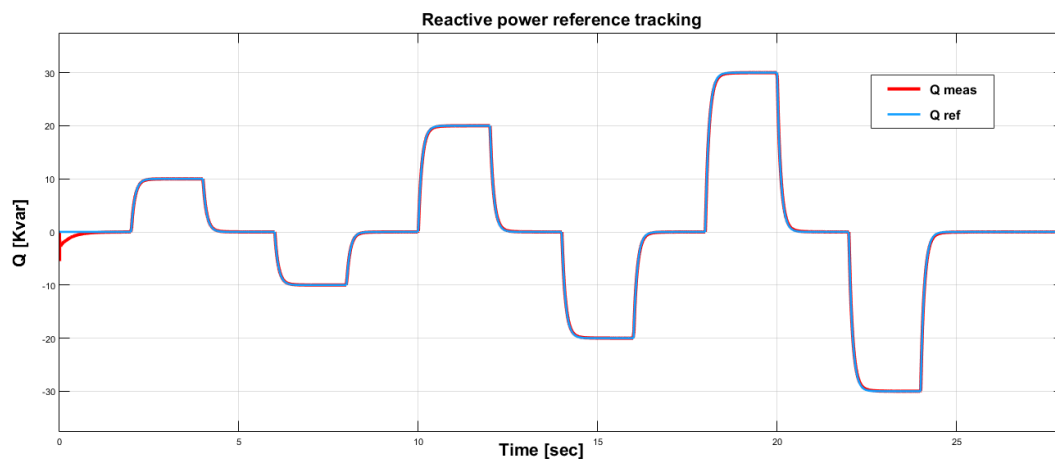


**Figure 3.18 Reactive power dynamic performances**

As it can be seen in Figure 3.18, the reactive power reference tracking in this configuration has greater performances with respect to those of the active power one, in Figure 3.19. This can be ascribed

to the fact that the resistive droop relates  $Q$  to the frequency, that in this case is constrained to its nominal value by the main grid. This doesn't hold for the voltage  $V$  measured downstream the converter, because it depends on the voltage droop caused by the series line impedance and in the end on the current flowing through the line. This is why at steady state the generated active power is different from its reference. Indeed, at second 17 a change in the power reactive reference is applied, the converter reacts by providing more current to generate also reactive power, so the active power error is much increased. This behavior highlights the fact that there is a coupling between generated reactive power and active power: indeed even if the line impedance used in simulation is purely resistive, the inductance of the LCL filter, in series with the line resistance, makes the resistive droop relation only an approximation of the real interaction between  $f$ ,  $V$  and  $P$  and  $Q$ . Hence changing the power angle with an RL series impedance generates not only a reactive power but also a component in the active power.

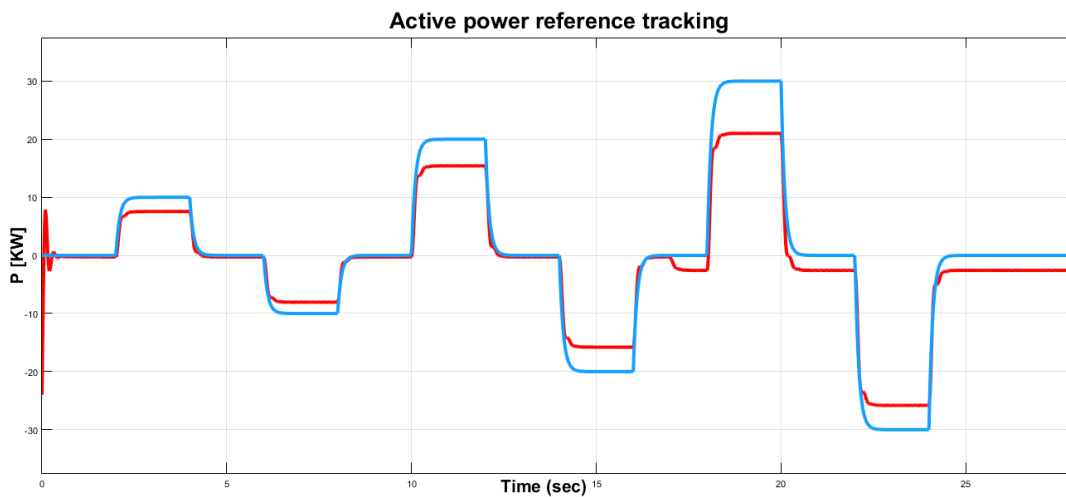


Figure 3.19 Active power dynamic performances

### 3.6 Conclusions

The designed distributed primary control level allows the microgrid to properly work in islanded mode even if power unbalances may occur. However, a control action based only on proportional gains, as already mentioned, doesn't ensure that the variables reach their nominal values [6], which is a desirable feature especially for the frequency. Moreover, at this stage both electrical references  $V_{ref}$  and  $f_{ref}$ , that power ones  $P_{ref}$  and  $Q_{ref}$  are fixed parameter. It would surely be better to have an additional control that tries to act on those references depending on the state of the microgrid. Indeed in this way, major deviations of the voltages and frequency can be limited in size, as well as the frequency of the microgrid and the nodal voltages can be kept in the desired range of values.

Finally, relying only on a primary control layer, each source is independently controlled and so it is not possible to have a high-level coordination between sources. This would be a relevant aspect since it

allows to implement several strategies based either on economic reasons or on green energy-oriented policies.

All the mentioned issues can be overcome by a supervising control layer, implemented as a centralized secondary controller. Its control action would consist in shifting the droop characteristics by varying  $V_{ref}$  and  $f_{ref}$ , based on an optimization algorithm.



# CHAPTER 4

## SECONDARY CONTROL

### 4.1 Introduction

In this chapter a centralized secondary control strategy is developed and then validated resorting to simulations carried out through a model of a real Low Voltage AC Microgrid. This work has been carried out in collaboration with RSE S.p.A, an Italian research institution which provide a microgrid test case. The considered microgrid corresponds to the real low voltage grid that RSE owns in order to develop studies and experimentations on Distributed Energy Resources and Microgrid solutions.

The proposed secondary control strategy consists of a PI control action for the regulation of the microgrid frequency and of a multi-objective optimal control for the regulation of the voltage amplitude of the microgrid nodes. Both control actions take full advantage of droop-controlled units connected in the MG; in particular, the multi-objective function aims to minimize the voltage errors of selected buses, while the PI control tries to recover the microgrid frequency to the nominal value of 50 Hz.

The power balance in the microgrid in islanded mode is guaranteed by the action of the primary and zero level control, previously described, which regulate the output voltage amplitude and frequency of the inverter, according to the active and reactive power generated/absorbed by the inverter itself. However, this control action is implemented at the cost of microgrid frequency and node voltage deviations, that, in some cases, can assume high values. Hence, a secondary control is designed to eliminate these deviations by shifting up and down the P-V and Q-f droop characteristics of conventional droop-controlled units, by acting on  $V_{ref}$  and  $f_{ref}$ .

The secondary control actuators for the RSE microgrid consists of three inverters, on which a conventional droop control, with resistive laws, is implemented. The DC side of each inverter is realized by the action of an ESS, which guarantees a constant and reliable flow of power towards the microgrid as long as its State Of Charge (SOC) is in a particular range. Therefore, the secondary control action must take into consideration, in some way, the SOC level of each battery, in addition to everything else. This chapter will evolve in the following way:

- A description of the microgrid model, taken into consideration for the development and simulation of the secondary control level is presented. As already mentioned, this model is a representation of the real RSE AC microgrid.
- Then, a description of each component of the secondary level control is provided and simulations are carried out to test its performances, following a pre-determined power profile of the microgrid.

## 4.2 RSE Microgrid

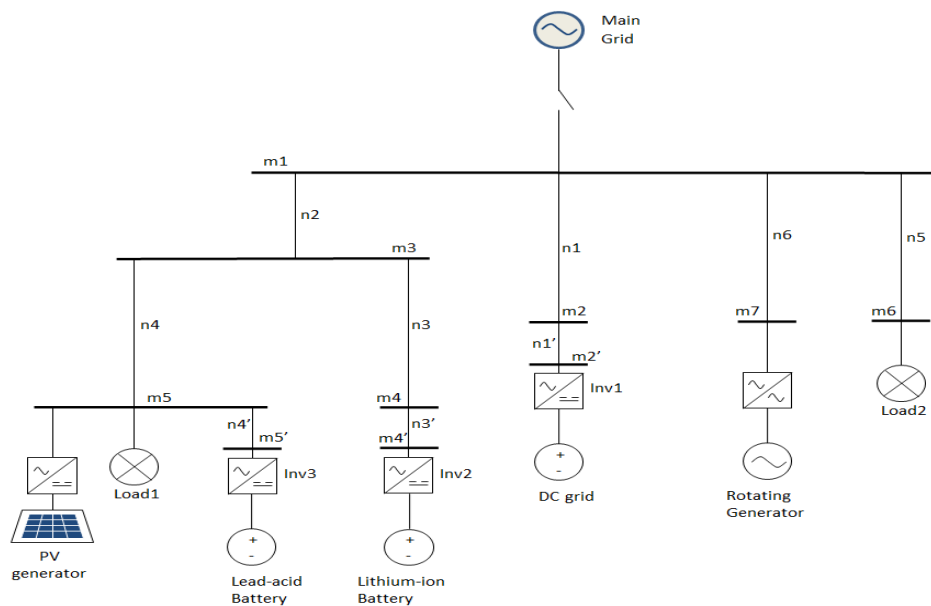
The RSE microgrid is extended over an area of about  $20000\text{ m}^2$ , is interconnected to the Medium Voltage (MV) Grid by means of a 800 kVA dedicated transformer (23 kV/400 V) and has an overall capability of 400 kW (active power) and 350 kVar (reactive power). Different types of DER generators are connected, as PV (PhotoVoltaic) Fields, Solar Dish with Stirling Engine, Wind Generator, Diesel Generator and Combined Heat and Power (CHP) natural gas generators and internal Combustion engine. The Microgrid has an overall storage capability of about 230 kWh based on different storage technologies as Lithium, Flow (redox), High temperature Nickel-Sodium Chloride (SoNick) and Lead (VLRA) batteries interconnected to the grid with dedicated converters. Resistive, Inductive and Capacitive Loads (overall capability of about 90 kW, 60 kVar inductive and 150 kVar capacitive are connected to the grid in order to simulate different typologies of actual users loads) and an electronic Load are also connected to the microgrid. A picture of the RSE Test Facility is illustrated in Figure 4.1, where the main units are highlighted. The microgrid is configurable (locally or remotely) at the interconnection board in order to obtain different grid topologies: radial grids and also meshed configurations. There is also the opportunity to extend feeders till one kilometer. The interconnection board (main bar and feeders) and all the DERs are provided with electrical measure equipment, set up to collect and analyze the experimental data derived from the field test. In addition to AC Microgrid, a Low Voltage DC Microgrid (400 V, 100 kW) is present and able to operate in islanding mode on DC side or interconnected to the AC grid by means of a bidirectional AC/DC converter.



Figure 4.1 Picture of the RSE microgrid

A Supervision and Control system has been developed in order to monitor and control all installed resources. Different Energy Management and control functions have been implemented and can be used in order to fulfil with the requested objective (economic optimization, renewable resources balancing, self-consumption, voltage control, state estimation). Resources control can be performed manually or in a full automated mode according to the different Microgrid control functions. New management and control functions (also from third parties) can be easily integrated to DER Test Facility Control System.

The RSE Microgrid has also a dedicated section to the study and the development of control algorithm for the island operation. This section of the Microgrid, depicted in Figure 4.2, is used to design and simulate the action of the secondary control level.



**Figure 4.2 Schematic of the RSE microgrid considered in the simulation.**

The grid is composed by 7 nodes (called m1, m2, etc in Figure 4.2) and 6 branches (called n1, n2, etc in Figure 4.2). This corresponds to an islanded small grid, which includes both controllable generators, storage units, renewable sources, and some loads through which it is possible to externally vary the amount of absorbed powers. The main microgrid elements are:

- Three Voltage Source Inverter connected in the node m5, m4 and m2 and controlled as a Grid Forming generator enhanced with a conventional droop control. The three Grid Forming Generators have the structure presented in CHAPTER 3 with an LCL output filter. The control of the voltage is so done on the capacitors terminal of the output filter, that are indicated in Figure 4.2 as the node m5', m4' and m2' respectively. The branches n4', n3' and n1' indicates the secondary inductance of the filter. As mentioned at the beginning of this chapter, these three inverters will be the actuators of the designed secondary control level.

- Two RL load connected in the node m5 and m6. Adjusting their internal impedances, these loads can absorb predefined values of active and reactive powers. These elements are extremely important to test the control strategies for different power situations, and they also allow to understand which power conditions would lead the network to possible collapses. Moreover, it should be noted that the imposed absorbed powers are defined at nominal conditions, meaning that the final power absorption will vary as voltages and frequency shift from their nominal values.
- One PV generator connected in the node m5 through a three phase Grid Following converter;
- One rotating generator, which in the real microgrid corresponds to a natural gas-fueled cogeneration source, connected in the node m7 through a three-phase Grid Following converter.

In the following table are enlisted the maximum active and reactive powers each microgrid element can absorb or generate. The Rotating Generator is usually utilized as an OFF/ON system able to provide a minimum active power of 25 kW and maximum one of 50 kW, this means that when the condition is on OFF the generated power is equal to 0 , while when it is ON the active power generated by the Rotating generator could be either 25 or 50 kW. This behavior is due to the use of the Rotating Generator in the microgrid system. This element is mainly utilized to provide power to the ESSs (Energy Storage System) presents in the microgrid, to re-establish their SOC (State of Charge) after it decreases down a certain lower bound.

**Table 4.1 Maximum power of microgrid devices.**

<i>Device</i>	<i>Max Active Power</i>	<i>Max Reactive Power</i>
<b>Load 1</b>	6 kW	0 kVar
<b>Load 2</b>	90 kW	60 kVar
<b>PV generator</b>	35 kW	21 kVar
<b>Inverter 1</b>	20 kW	20 kVar
<b>Inverter 2</b>	30 kW	30 kVar
<b>Inverter 3</b>	30 kW	30 kVar
<b>Rotating Generator</b>	50 kW	38 kVar

Although network interconnections are not active elements, they have a significant influence on the network variables' behavior. So the real line impedances have been considered in the design of the secondary control level and have been also implemented in the simulation environment. In Table 4.2, the impedances of each microgrid branch are resented.

**Table 4.2 List of line impedances parameters.**

<i>Line</i>	<i>Resistance</i>	<i>Reactance</i>
<b>n1</b>	42 mΩ	11 mΩ
<b>n2</b>	0.4 mΩ	0.4 mΩ
<b>n3</b>	18.5 mΩ	9.5 mΩ
<b>n4</b>	147 mΩ	29 mΩ
<b>n5</b>	13.6 mΩ	5 mΩ
<b>n6</b>	13 mΩ	6 mΩ
<b>n1'</b>	0	299 μΩ
<b>n4'</b>	0	444 μΩ
<b>n3'</b>	0	299 μΩ

As already mentioned, in the grid are present three Voltage Source Inverters that are controlled in Grid Forming mode with resistive droop law. Each of this device is connected at the DC side to an Energy Storage System (ESS); in particular, the inverter in m5' is connected to a Lead-acid Battery, the one in m4' to a Lithium-ion Battery and the last one in m2' to an autonomous DC grid (for this thesis work, we assume the DC grid composed only by the SoNick battery). The presence of battery in the microgrid system is considered in the simulation by the dynamics related to their SOC (State of Charge), which are function of the battery active power. The SOC dynamics have been chosen to be modelled by a discrete integrator system, which changes depending on whether the storage unit is on a charge or discharge condition:

$$SOC_{charge} = SOC_0 - \int \frac{\eta_{invcha} * \eta_{stocha}}{C_{max}} P(t) \quad (4.1)$$

$$SOC_{discharge} = SOC_0 - \int \frac{\eta_{invdis} * \eta_{stodis}}{C_{max}} P(t) \quad (4.2)$$

Where  $SOC_0$  represents the initial SOC,  $\eta_{inv}$  and  $\eta_{sto}$  are, respectively, the inverter and the battery yields and they change depending on whether the system is generating or absorbing power,  $C_{max}$  represents the maximum battery capacity [kWh], and, finally  $P(t)$  is the power generated or absorbed by the battery, taken with a positive sign in the former condition and negative in the latter.

In the following table are reported the parameters, used in simulations, of each battery and of the DC grid. The maximum capacity and the yields, in the case the system is charging or in the case it is discharging, are supposed equal. Finally, considering the two batteries, the values of maximum capacity are defined at nominal current, meaning that they could vary as the system output current shifts from its nominal value.

**Table 4.3 ESSs parameters.**

<i>ESS system</i>	<i>C<sub>max</sub></i>	<i>η<sub>inv</sub></i>	<i>η<sub>sto</sub></i>
<b>Lead-acid Battery</b>	45 KWh	0.9	0.9
<b>Lithium-ion Battery</b>	30 KWh	0.9	0.95
<b>DC grid</b>	20 KWh	0.9	0.9

### 4.3 Simulation specifications

The performances of the primary control level, first, and of the secondary one will be tested, by carrying out different simulations on a common microgrid working condition. Hence, before describing the elements that composed the secondary control level and showing its performances, a background of the simulation environment need to be provided.

The simulations refer to a defined scenario: the microgrid is working in the islanded operating mode and therefore the whole system need to be managed without the support of the main grid. It is recalled that the islanding event could be either intentional, due for example to economic reasons, or it can be due to a fault that occurred in the external grid, leading the microgrid to isolate itself in order to not be affected.

In the reported simulations, the microgrid in island mode will be tested for a pre-defined reactive and active power profile, conceived so to reproduce a possible real power behavior of the elements of the grid; thus loads and renewable sources will be supposed to vary their powers, during the entire simulation, in pre-determined instants of time and to pre-determined values. Obviously, as the corresponding powers change there will be an initial power unbalance between the total generated and absorbed power that will eventually result in a new transient for the network variables. The power trends for the unique uncontrollable unit present in the grid, the PV generator, have been designed in order to test the hierarchical microgrid control structure in different network conditions. Regarding the power absorption, it is recalled that two loads are present in the considered microgrid test case. One corresponds to the auxiliary cooling system of batteries, while the second corresponds to an RLC load, which can be regulated to absorb predefined values of active and reactive power.

In the following will be reported the active and reactive power profile implemented in this work. All the simulations are carried out, resorting to Matlab/Simulink simulation environment, and each of them will last for 200 sec.

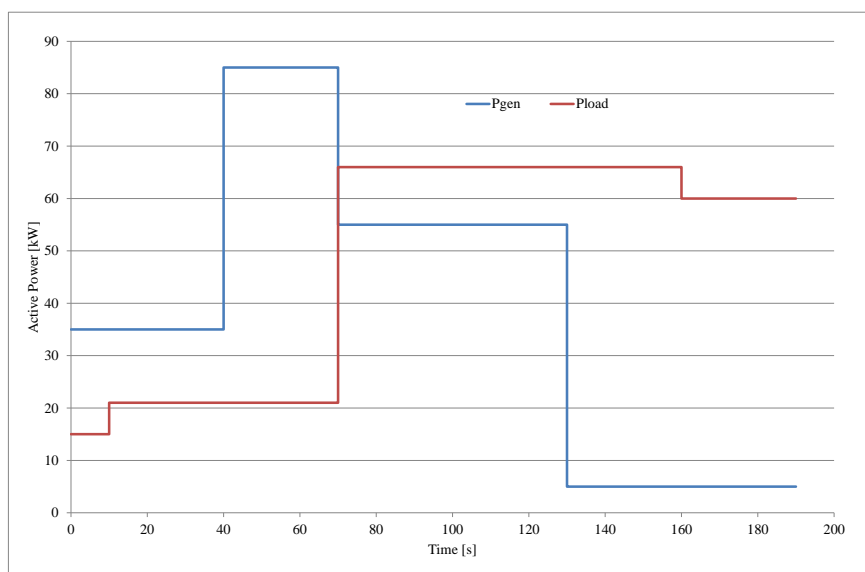


**Figure 4.3 Active power profile used for the secondary control simulations**

The active power profile, depicted in Figure 4.1, is the result of the variation of generated power from the PV generator and the Rotating generator, while the absorbed power one is due to the constant power absorption of the load in node m5 and the variable absorption of the RLC load.

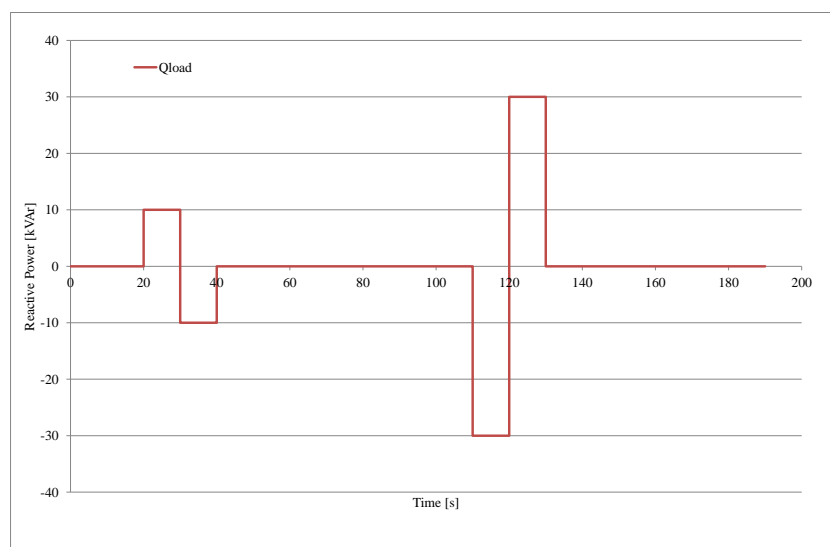


**Figure 4.4 Reactive power profile used for the secondary control simulations**

The reactive power profile, depicted in Figure 4.4, is determined by the RLC load, the unique microgrid element that is able to absorb or generate reactive power. It needs to be added that the final effective reactive and active power absorption will not be those showed in the figures but in reality they will vary as voltages and frequency shift from their nominal values. The power profile provided above

are just a simplification of what could be a plausible real scenario, designed just to test the performances of the designed secondary control strategy. However, it must be said, that this simplification does not belittle the effectiveness of the designed secondary control, since in the real world the powers don't vary as steps, but they presents a smoother transient. In the following table are reported the variations of reactive and active power and the corresponding time instants when these variations occur.

**Table 4.4 Active and reactive power variations in kW and kVar.**

<i>time</i>	<i>Ppv</i>	<i>Qpv</i>	<i>Pload1</i>	<i>Qload1</i>	<i>Pgen</i>	<i>Qgen</i>	<i>Pload2</i>	<i>Qload2</i>
<b>0</b>	35	0	0	0	0	0	15	0
<b>10</b>	35	0	6	0	0	0	15	0
<b>20</b>	35	0	6	0	0	0	15	10
<b>30</b>	35	0	6	0	0	0	15	- 10
<b>40</b>	35	0	6	0	50	0	15	0
<b>70</b>	5	0	6	0	50	0	60	0
<b>100</b>	5	0	6	0	50	0	60	0
<b>110</b>	5	0	6	0	50	0	60	- 30
<b>120</b>	5	0	6	0	50	0	60	30
<b>130</b>	5	0	6	0	0	0	60	0
<b>160</b>	5	0	0	0	0	0	60	0
<b>190</b>	5	0	0	0	0	0	60	0

## 4.4 Primary control: implementation and test

As discussed in the previous chapter, the primary control consists in two sequential sublayers, i.e. the inverter output control (Zero control level) and the droop control. The droop control provide the most significant contribute in the overall Primary level control action, since it is designed to vary the inverter output voltage amplitude and frequency from their nominal values, based on the power measured at the inverter output. For the purpose of this work, the conventional droop control approach has been adopted. This links the variations of active power to the variations of voltages and the variations of frequency to the variations of reactive power through a proportional control action. Being defined as a decentralized structure, this system is located at each of the three inverter controlled in Grid Forming mode. Its scheme is again represented in Figure 4.5.

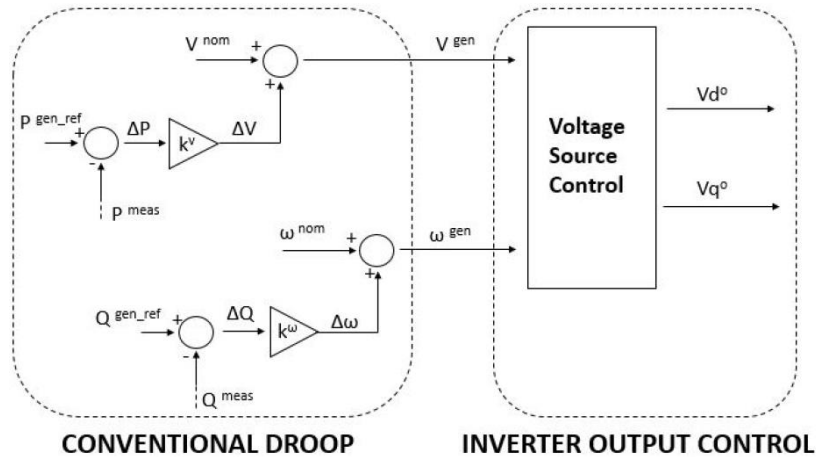


**Figure 4.5 Conventional Resistive Droop.**

The resistive configuration implies that the proportional gains must be chosen such that  $K_p^i < 0$  and  $K_Q^i > 0$ , where  $i \in (1,2,3)$  corresponds to  $i_{th}$  inverter, controlled in Grid Forming mode. There is not a fixed rule to choose the exact values of  $K_p^i$  and  $K_Q^i$ , although their magnitudes have a significant impact on the network since they express how the requested power is distributed among the generators. In this work the proportional gains have been defined as reported in equation (3.19). By setting the droop parameters as reported, the variation of generated or absorbed power of the inverter, that in the Conventional droop are a consequence of the deviation of the voltage amplitude and frequency values from the nominal on, will not be equally distributed but they will depend on the active and reactive power limits of each inverter. In this way, the bigger is the power a unit can absorb or generate the bigger will be the relative droop proportional gain.

Once the primary controllers for each of the three Voltage controlled inverter units have been designed, now the overall responses will be illustrated. These have been performed implementing in the simulation the powers profile, defined in previous sub-section. It must be added that for simulation reasons, the inverter output control dynamics have been disregarded; so the inverter, controlled in Grid Forming mode, is considered as an ideal programmable three-phase voltage generator, capable to vary the output voltage amplitude and frequency, according to the reference signals, provided by the droop control. This is a plausible simplification, since the inverter output control is able to track the frequency and amplitude references in about 0,02 s, as reported in the previous chapter. A schematic model of the Grid Forming inverter is reported in Figure 4.6.

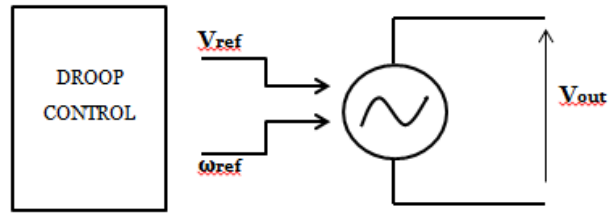


**Figure 4.6 Schematic representation of droop control and Inverter**

In the following, the performances of the primary control action are shown. The simulation is carried out with the powers profile, previously described, and with the droop coefficients exposed in Table 4.5.

**Table 4.5 Primary control droop gains**

<i>Inverter</i>	<i>Pmax</i>	<i>Pmin</i>	<i>Kp</i>
<b>Inv 1°</b>	20 KW	-20 KW	0.0016
<b>Inv 2°</b>	30 KW	-30 KW	0.0011
<b>Inv 3°</b>	30 KW	-30 KW	0.0011

In Figure 4.7 and in Figure 4.8 they are represented, respectively, the output active and reactive powers of the three inverters controlled in Grid Forming mode. As it can be seen, the power distribution is obviously not equal since it depends on the droop parameters. As above reported, the droop control has been designed such that the more power a unit can either generate or absorb, the larger will be the active and reactive power deviation from the references ( $P_{ref} = 0$ ,  $Q_{ref} = 0$ ).

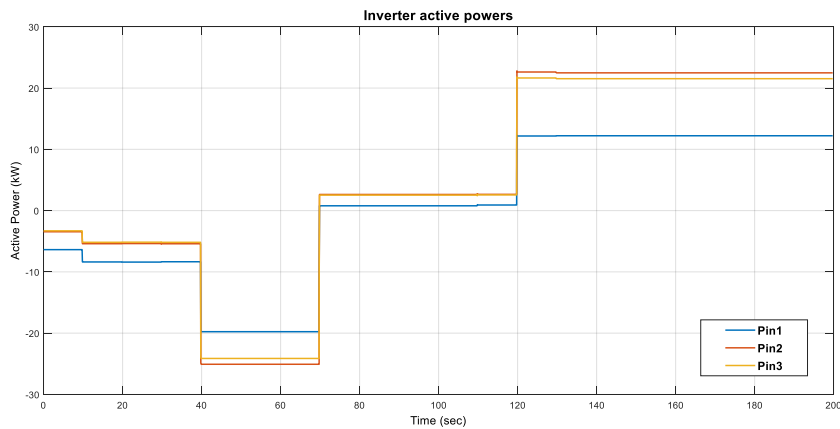


**Figure 4.7 Inverters output active powers**

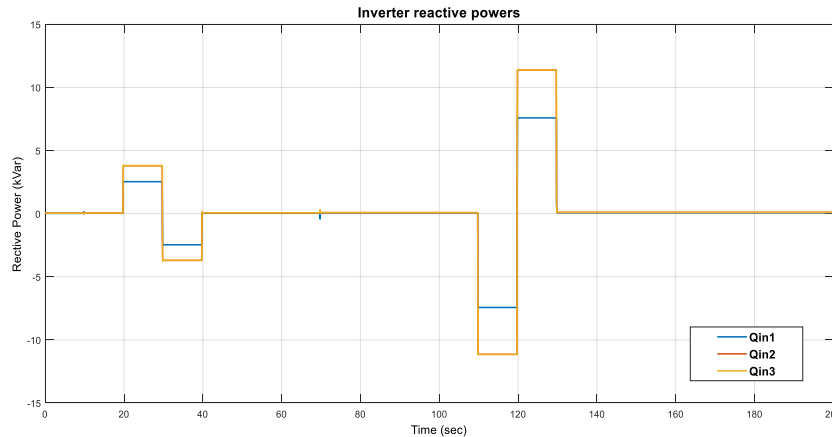


**Figure 4.8 Inverters output reactive powers**

With regard to the network variables, by looking at Figure 4.9, Figure 4.10 and Figure 4.11, it is possible to appreciate the effect of the primary control action. Indeed, the droop scheme is able to keep the network variables around realistic values, respecting the bound imposed by the regulation. However it can be surely noted that the nodal voltages don't keep their nominal value, which is 400 V (rms concatenated voltage rms value), and the frequency, eventually, return the nominal value of 50 Hz only because the final reactive power circulating in the microgrid is almost null. The restoration of the grid electric variables to their nominal values is a relevant feature, especially, for the frequency. In fact, it is recalled that, in case of a possible reconnection of the islanded microgrid to the main grid, it is strictly required that at the interconnection the two system are synchronized at the same frequency.

To recap, the primary controllers guarantee great performances in terms of stability of the microgrid, for unexpected peaks of generated or absorbed powers, but, still, they are not the best solution to manage an islanded microgrid. Pure proportional actions are in fact extremely efficient in ensuring a fast and considerable reduction of network variable deviations, but they are not able to make the network variables evolve close to their nominal values, especially for the microgrid frequency and the PCC (Point of Common Coupling) voltage magnitude. Moreover, through this simple structure is not possible to implement any resource management logic, talking for example the remaining states of charge of the batteries or some economic factors.

There is an additional degree of freedom that this control structure is not exploiting, which corresponds to actually vary the voltage magnitude and the frequency references of the three inverters, according to the network conditions. In this way in fact, the steady-state voltage and frequency deviations from their reference values can be furtherly decreased or increased, in order to implement a particular microgrid management strategy. These motivations lead to the design of a higher control layer, which could act on the microgrid, keeping the beneficial effects of the primary control.

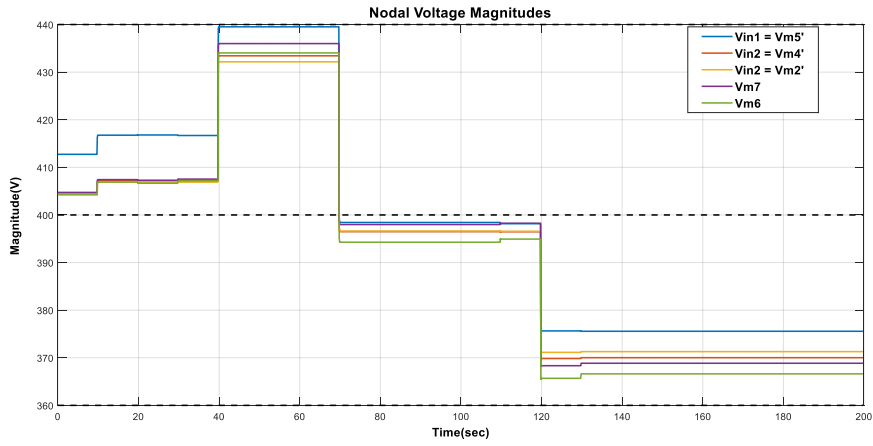


Figure 4.9 Nodal voltage response

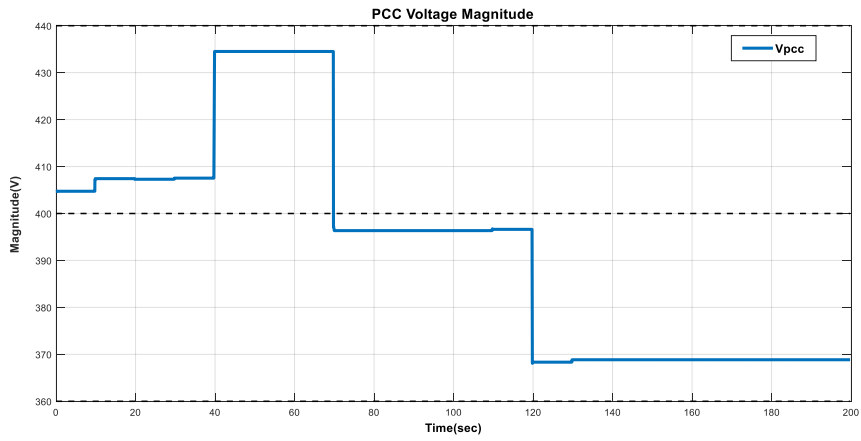


Figure 4.10  $V_{PCC}$  voltages response

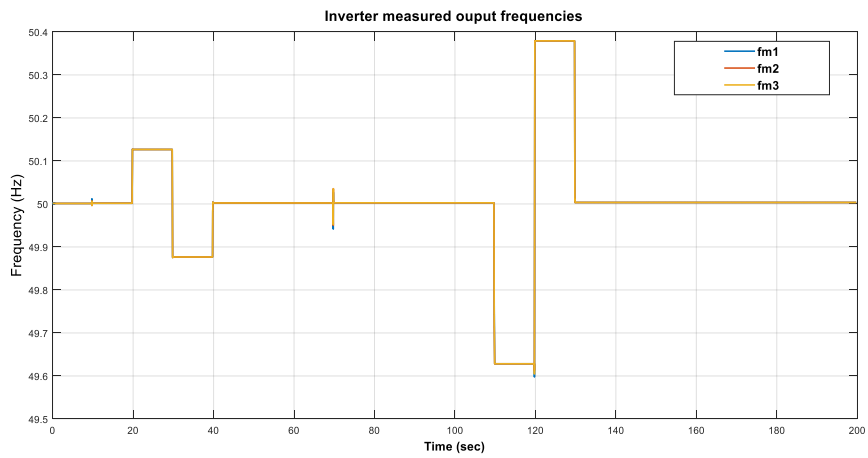


Figure 4.11 Inverters output frequencies

## 4.5 Secondary frequency control

In this sub-section the secondary frequency control will be described and then tested with the power profile defined in paragraph 4.3.

### 4.5.1 Control description

The objective of the secondary frequency control is to restore the microgrid frequency to its nominal value of 50 Hz, after the primary control action. The secondary frequency control level provide its contribute to the microgrid regulation by sending reference signals to the below control level, the primary one. There exists two ways to externally act on the primary control, that is by modifying the  $Q_{ref}$  value, in Figure 4.12 a), or by varying the reference frequency sign,  $\omega^{nom}$ , in Figure 4.12 b). The former case corresponds to shift the droop curve, shown in Figure 3.16, on the x-axis, the latter case, on the contrary, corresponds to shift droop characteristics up and down on the y-axis. In the designed frequency control, the  $Q_{ref}$  value will be considered constant and equal to 0,  $f_{ref}$ , instead, will vary according to the frequency control action.

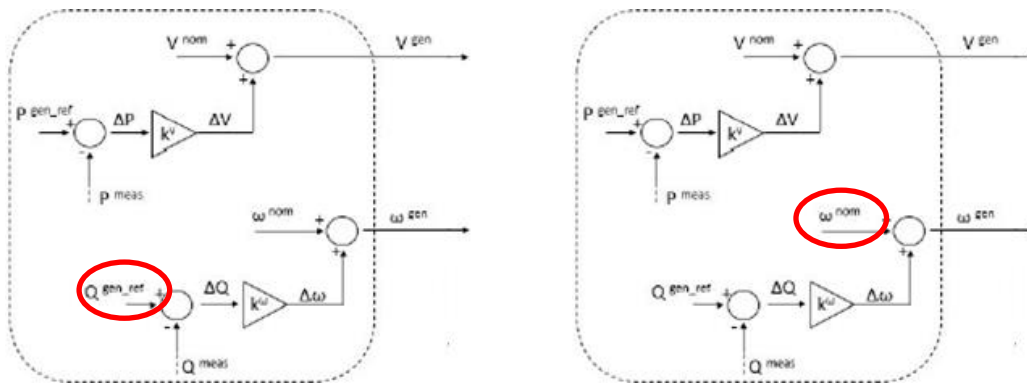


**Figure 4.12 Possible frequency secondary control actions**

The secondary frequency control action is provided for each of the three inverters by a PI regulator, operating as a centralized regulator. Figure 4.13 shows schematically the PI controller and the system under control. It is assumed in this case that the communication channels have a delay and that the MGCC (Microgrid Central Controller) doesn't have an instantaneous reaction, but it takes a small interval of time, in order to elaborate the gathered information and to apply the consequent control action. The sum of these two values of time represents the total delay  $\tau_d$ , equal to 1 sec. This parameter is purposely large, so to test the frequency control in the worst possible conditions. The frequency control usually requires a centralized frequency meter to estimate the MG operating frequency  $f_i$ , as

shown in Figure 4.13, where the SFC (Secondary Frequency Controller) is enclosed in a dashed box. For this work a PLL is used as frequency meter.

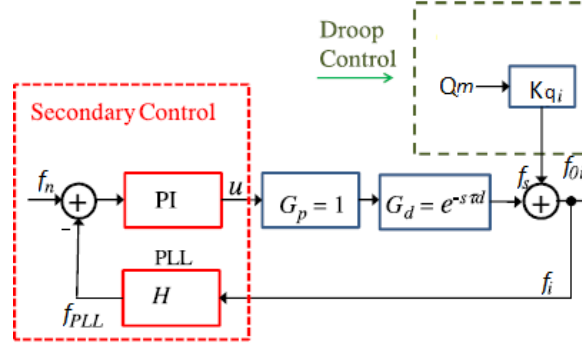


**Figure 4.13 Secondary frequency control scheme**

It can be seen from Figure 4.13 that the dynamics of the fast primary control system are neglected. Therefore, assuming that the control systems are decoupled, the characteristic equation of the controlled system plus the controller is obtained as

$$1 + e^{-s\tau d} G_p G_c H = 0 \quad (4.3)$$

where  $e^{-s\tau d}$  is the transfer function of the communication plus computation delay;  $G_c$  is the PI controller;  $H$  is the PLL transfer function, that here is modelled as a delay of 0.2 s ( $H = e^{-s0.2}$ ), since the MGCC interrogates the PLL to know the frequency measurement and receives information every 0.2 sec. Finally,  $G_p$  is the system plant transfer function. Using equation (4.3) and the Bode control techniques, the controller can be designed. However, the decoupling between the SCF and the primary control system can only be assumed when the SCF is well designed and tuned, i.e. equation (4.3) is only valid when  $f_{oi}$  (in Figure 4.13) could be considered as an external disturbance to the SCF. Moreover, if the communication delay is uncertain and changes in relative-large operating range, a conventional controller (usually a PI) could not be robust enough to ensure good and stable operation of the SFC in all the operating conditions. Hence a more robust strategy need to be implemented in order to take in consideration the worsening of the PI regulation due to an increasing of the time delay. For this reason, in this work, the PI controller is enhanced by the action of SP (Smith Predictor). A block diagram of a PI regulator plus a SP is shown in Figure 4.14. The complete control system is enclosed in the dashed box at the bottom of that graphic.

To implement the SP, good estimation of the transfer function of the plant ( $\widehat{G}_p(s)$ ) and delay ( $\widehat{G}_d(s)$ ), in a typical operating point are required. Using Figure 4.14, the closed loop transfer function between  $f_i(s)$  and  $f_n(s)$  is:

$$\frac{f_i(s)}{f_n(s)} = \frac{\frac{PI(s)G_p(s)G_d(s)}{1 + PI(s)G_p(s)H(s)}}{1 + \frac{PI(s)G_p(s)G_d(s)}{1 + PI(s)G_p(s)H(s)} (\hat{G}_p(s)\hat{H}(s)\hat{G}_d(s) - G_p(s)H(s)G_d(s))} \quad (4.4)$$

Assuming that  $\hat{G}_p(s)\hat{H}(s)\hat{G}_d(s) \approx G_p(s)H(s)G_d(s)$ , the transfer function in equation (4.4) is simplified to

$$\frac{f_i(s)}{f_n(s)} = \frac{PI(s)G_p(s)G_d(s)}{1 + PI(s)\hat{G}_p(s)\hat{H}(s)} \quad (4.5)$$

Therefore, when good estimates  $\hat{G}_p(s)$ ,  $\hat{G}_d(s)$ , and  $\hat{H}(s)$  are used, the delay  $e^{-\tau_d s}$  does not affect the close loop characteristic equation, i.e. the denominator of eq. (4.5). Using eq. (4.5), it is simple to design a controller using the Bode stability theory. To improve the controller performance when operating with a no exact plant model (or unknown system delay) a low pass filter could be used in the SP feedback.

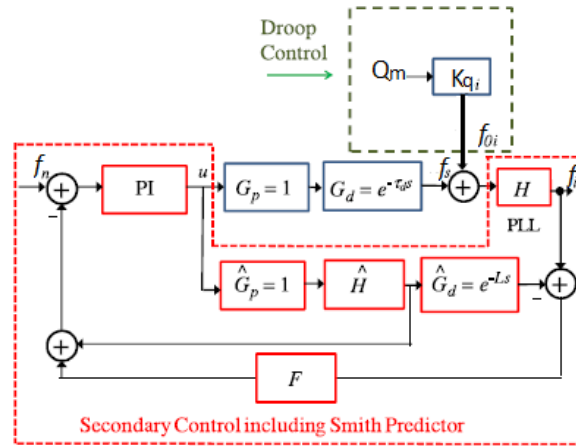


Figure 4.14 Secondary frequency control with SP

In the following a brief analysis on the performances of the PI controller, enhanced with a SP (Smith Predictor), is provided.

Using Figure 4.14, it can be shown that the dynamic behaviour of the SP based SCF is given by the following expressions:

$$\begin{aligned} f_i &= f_s + f_{oi} = f_s + f_n - K_{qi}Q_m \\ f_s &= G_d G_p P I e \\ e &= \omega_n - (\hat{H}\hat{G}_p P I e + F(H\omega_i - \hat{G}_p\hat{H}\hat{G}_d P I e)) \end{aligned} \quad (4.6)$$

Using the expression above, the secondary controller is described by:

$$\begin{aligned} \omega_s(1 + \hat{H}\hat{G}_pPI - F\hat{G}_p\hat{H}\hat{G}_dPI + G_dG_pFHPI) \\ = (G_dG_pPI - G_dG_pFHPI)\omega_n + G_dG_pFHPIK_{qi}Q_m \end{aligned} \quad (4.7)$$

Considering  $\hat{H} = H$ ,  $\hat{G}_p = G_p = 1$ ,  $G_d = e^{-\tau_d s}$ ,  $F = 1$ , and  $\hat{G}_d = e^{-Ls}$ , where  $L$  represents the estimation of the time delay  $\tau_d$ , the state representation is derived. Then, the state space model for the secondary control can be represented by

$$\begin{aligned} \dot{X}_{sf} &= A_{sf}X_{sf} + B_{sf}Q_m \\ X_{sf} &= [\Delta f_s^{(4)} \Delta \ddot{f}_s \Delta \dot{f}_s \Delta f_s] \end{aligned} \quad (4.8)$$

Matrixes  $A_{sf}$  and  $B_{sf}$  are represented in Appendix A.

**Table 4.6 Parameters for the eigenvalues test.**

<i>Parameters</i>	<i>Value</i>	<i>Unit</i>
<b>Kp_PI</b>	0.1	
<b>Ki_PI</b>	1	
<b>L</b>	0.5	sec
<b><math>\tau_{PLL}</math></b>	0.2	sec

In Figure 4.15, it is depicted how the eigenvalues of the secondary frequency controller closed-loop moves as the uncertainty on the time delay  $\tau_d$  increase. In order to carry out the test, the parameters in Table 4.6 have been used.

The eigenvalues of the system are computed and plotted by varying  $\tau_d$  of 0.3 sec from an initial value of  $\tau_d = 0.5$  sec, until an unstable condition is found with a delay of 4.7 sec.

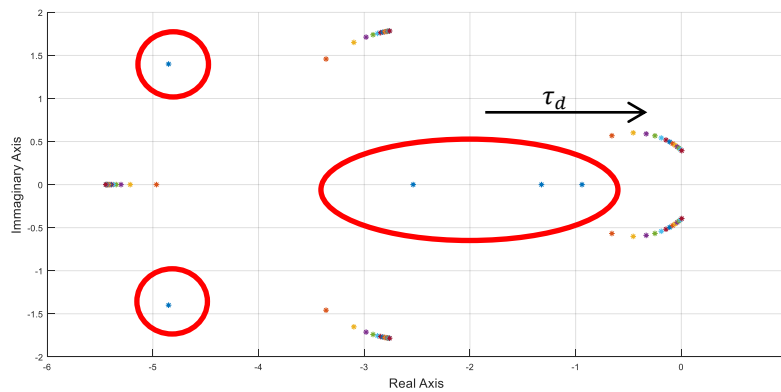


**Figure 4.15 Eigenvalues of the secondary control closed-loop.**

As it can be seen, the best response is obtained when  $\tau_d = 0.5 \text{ sec}$ , represented by the circled markers in the figure. This is due to the fact that the time delay estimation  $L$  is equal to the actual delay  $\tau_d$ . When the value of  $\tau_d$  is increased, and so the difference between the actual value and the estimated one is larger, the response of the system faces a worsening; it became oscillatory and, eventually, unstable as it can be noted from Figure 4.15.

### 4.5.2 Secondary frequency control simulation

In the following, they will be presented the numerical results of the designed secondary frequency control. Each inverter is controlled by the configuration described in the previous sub-section.

Since the frequency controller interrogates the PLL and applies its control action every 0.2 sec, all the PI regulators and the function that composed the SPs (Smith Predictors) are discretized through the Tustin or Trapezoidal method, with  $T_s = 0.2 \text{ sec}$ .

$$S = \frac{2z - 1}{T_s z + 1} \quad (4.9)$$

All the PI regulators are tuned in the same way and their coefficients, along with the other parameters involved in the simulation, are enlisted in the following table.

**Table 4.7 Frequency controller simulation parameters**

<i>Parameters</i>	<i>Value</i>	<i>Unit</i>
<b>Kp_PI</b>	0.1	
<b>Ki_PI</b>	1	
<b>L</b>	1	sec
<b><math>\tau_{PLL}</math></b>	0.2	sec
<b><math>\tau_d</math></b>	1	sec
<b>Ts</b>	0.2	sec

In Figure 4.16 and Figure 4.17, they are represented the active and reactive output powers of the inverters, when in the microgrid is implemented the designed SFC. As it can be seen, there isn't, obviously, significant variations from the results exposed for the primary control case.

In fact, as already mentioned, a powers distribution logic has not been implemented yet and so the output powers of the inverters depends only on the designed droop coefficients. In the following, a power distribution strategy will be designed and, in this case, the output powers value will change accordingly.

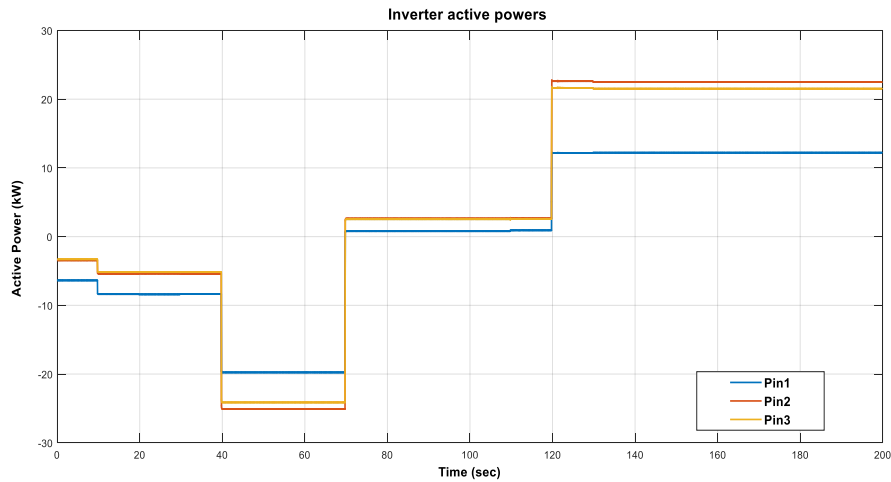


**Figure 4.16 SFC Active powers response**

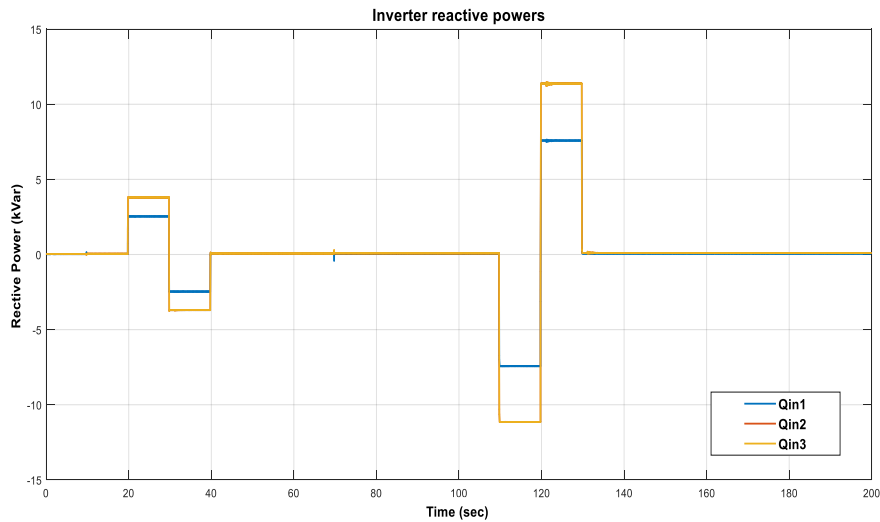


**Figure 4.17 SFC Reactive powers response**

In Figure 4.18, Figure 4.19 and Figure 4.20, the microgrid electrical variable responses are represented. As it can be noted, the nodal voltages neither change their trends respect to the previous case nor they are significantly affected by the action of the SFC. In fact, as already mentioned, the inverter, controlled in Grid Forming mode, and enhanced with the Droop control, provides a good

decoupling effect between the magnitude and the frequency value of the inverter output voltage. Regarding the measured frequencies of the three inverter, that is also the microgrid frequency, the effect of the SFC regulation can be clearly seen. The microgrid frequency returns to its nominal value (50 Hz) after a deviation, due to a peak of reactive power, is occurred. As it can be noted, the control action is not immediate but it presents a delay of 1 sec, as implemented, due to computation and communication. Tuned with the parameters above, the PI regulators are able to restore the output frequency of the inverters to 50 Hz in about 4 sec.

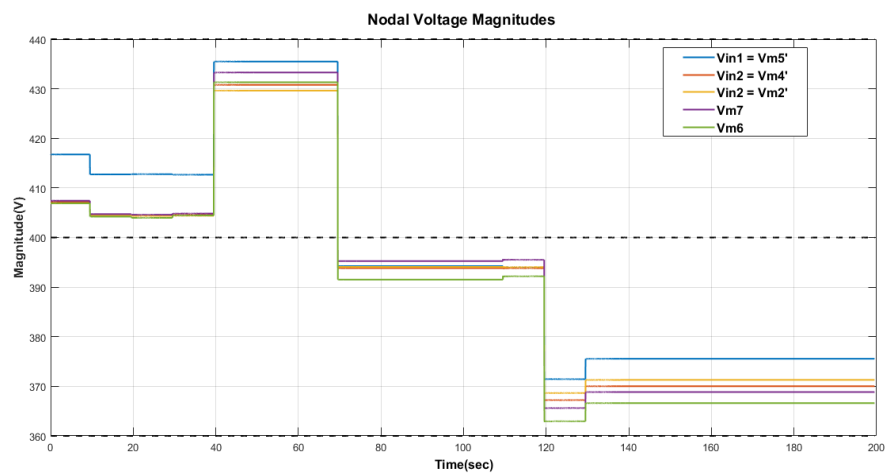


Figure 4.18 SFC nodal voltages response

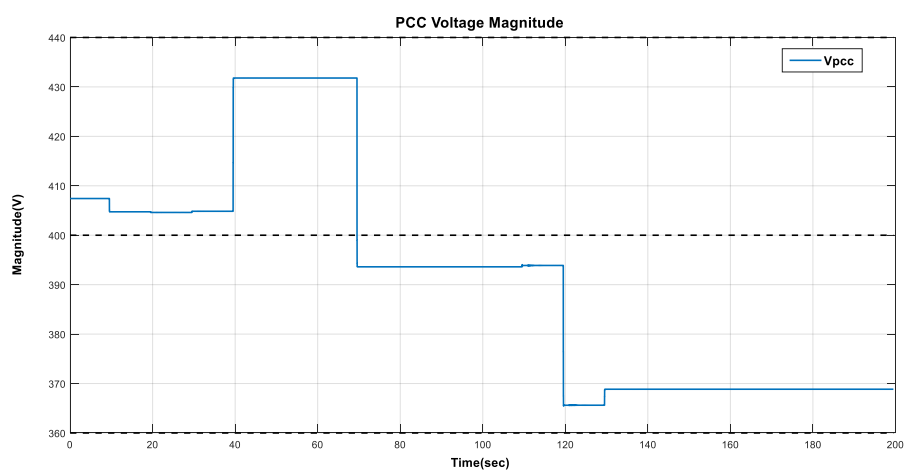
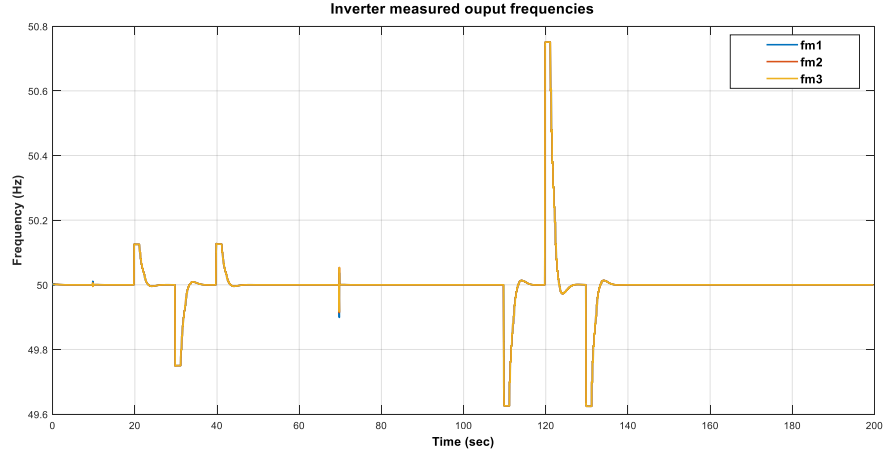


Figure 4.19 SFC  $V_{PCC}$  response



**Figure 4.20 SFC frequency response.**

In Figure 4.22 , it is represented the behaviour of the microgrid frequency in three cases: first, the case in which only the primary control level is implemented, the second case, in which the three inverters are regulated by PI+SP controllers and the final case, in which a modification of the  $K_q$  (Q-f droop gain) of each inverter is applied to the action of the PI+SP regulators.

The droop gain of the inverter  $i$ -th is modified according to the following criteria:

$$K_q^i = \frac{\min(f_{up}^i, f_{down}^i)}{Q_{max}^i} \quad (4.10)$$

where  $f_{up}^i = f_{max} - f_{ref}^i$  and  $f_{down}^i = f_{min} - f_{ref}^i$ , so they represent the difference between the upper or lower bound of the frequency, imposed by the norm, and the reference value of each converter. The reasons to apply a modification of the droop characteristic and the logic behind it can be explained by looking at Figure 4.21. When the microgrid frequency deviate from its nominal value, the PI+SP regulators act on the reference values  $f_{ref}$ , as already explained, to bring back it to 50 Hz. However, this control action presents a significant drawback; the droop line of the inverter is shift upward or downward, moving it to a new frequency working point. Hence, if two consecutive deviations occur, the second one results larger, as depicted in Figure 4.22, compared to the case in which only the Primary droop control is implemented in the microgrid and the  $f_{ref}$  is kept at 50 Hz. Therefore, the droop gain is changed in order to narrow the frequency deviation, as represented in Figure 4.21.

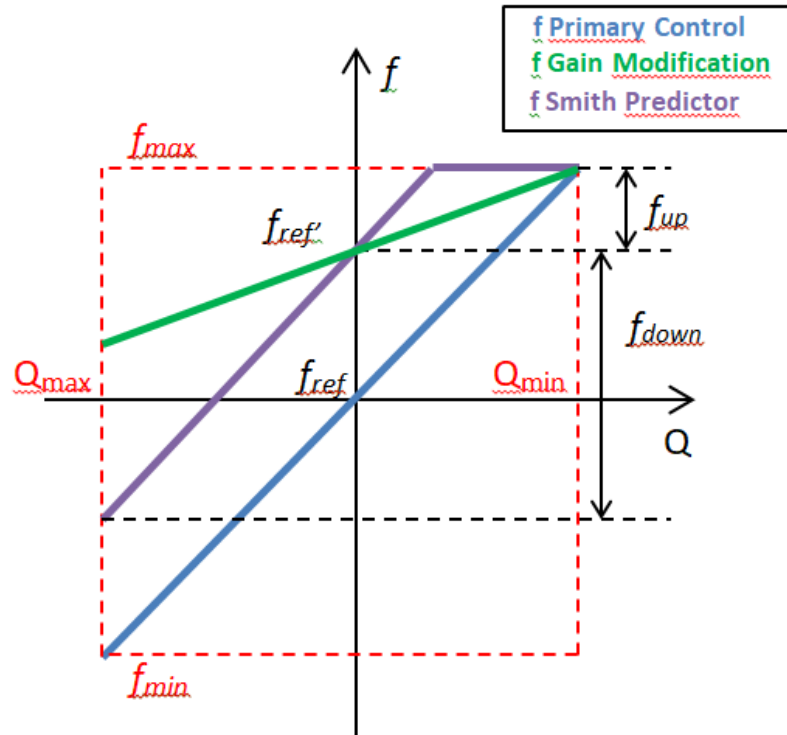


Figure 4.21 Droop gain modification

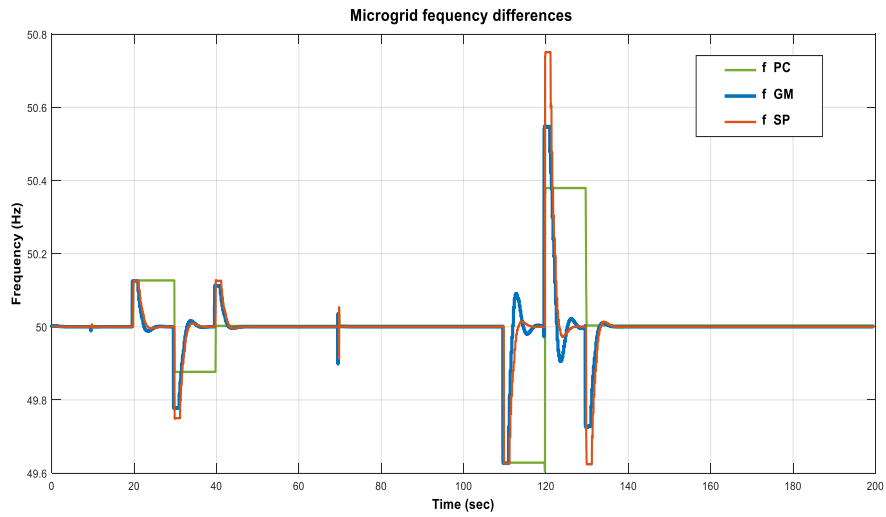


Figure 4.22 Microgrid frequency response with different control strategies

## 4.6 Secondary voltage control

In the following an optimal SVC (Secondary Voltage Control) is designed. This control strategy tries to minimize the voltage deviation of several selected buses in the microgrid and to accomplish a proportional distribution of the active power among the three voltage controlled inverters.

### 4.6.1 Secondary voltage control description

The main objective of the secondary voltage controller, designed in this work, is to restore the voltage of the PCC (Point of Common Coupling), that is the bus m1 in Figure 4.2, to its nominal value  $V_{PCC_n} = 400$ . At the same time, the secondary voltage control must take in consideration that the voltage of the other buses in the microgrid must be included in the range defined in CHAPTER 3; and that the three voltage controlled inverter must provide active power, according to a particular criteria.

As for the secondary frequency controller, the actuators of the secondary voltage controller are three inverters, controlled in Grid Forming form. In fact these devices, as already explained, are able to control the voltage amplitude of buses m1', m4' and m2', in Figure 4.2, and so they are able to affect the amplitude voltages of the remaining buses in the microgrid.

The secondary voltage controller, as the frequency one, regulate the microgrid through the control level immediately below, the primary level. It must be specified that, even if, the SFC and the SVC composed the MGCC of the microgrid, they don't affect each other, thanks to the decoupling action applied by the droop strategy, as describe in the previous chapter.

There exists two ways to externally act on the P-V droop characteristic of the primary level control without modifying its slope  $K_p$ . The first option is to vary the value of the active power reference, in Figure 4.23 a), that is equal to shift the P-V droop line on the x-Axis; the second option consists of properly modifying the voltage reference, in figure Figure 4.23 b), which means to shift the Droop line up and down on the y-Axis. In the designed voltage control, the  $P_{ref}$  value will be considered constant and equal to 0,  $V_{ref}$ , instead, will vary according to the chosen voltage control action.

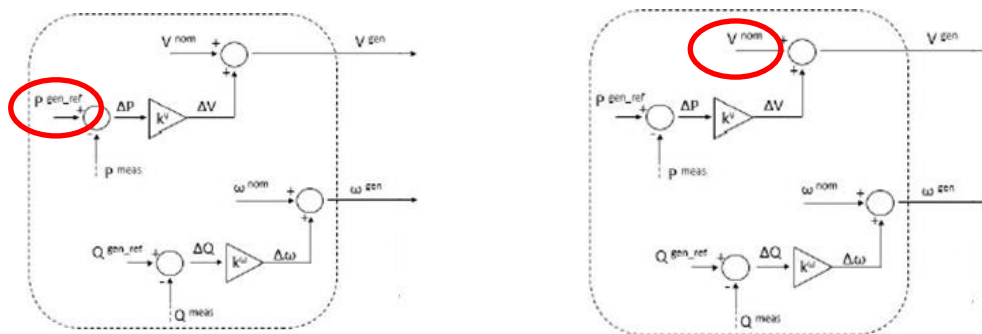


Figure 4.23 Possible secondary voltage control actions

As briefly mentioned above, the aim of the proposed optimal voltage control strategy is to restore the phase voltage amplitude of the PCC to its nominal value. To achieve this objective, a multiobjective function is designed, in order to force the output voltage amplitude of the inverters in m5', m4' and m2' to a particular value; and so, indirectly, control the voltage amplitude of node m1 (PCC). The adopted multi-objective function has the following quadratic form:

$$\min f = (V_{m5'_n} - V_{m5'})^2 + (V_{m4'_n} - V_{m4'})^2 + (V_{m2'_n} - V_{m2'})^2 \quad (4.11)$$

Ideally, every quadratic item is supposed to become zero after optimization, so when the argument of the multi-objective function is minimized to zero, the voltage magnitude of each controlled bus is closed to its voltage reference as follow:

$$\begin{aligned} V_{m5'_n} &= V_{m5'} \\ V_{m4'_n} &= V_{m4'} \\ V_{m2'_n} &= V_{m2'} \end{aligned} \quad (4.12)$$

During the process of solving the multi-objective function of the proposed optimal SVC strategy, several constraints must be satisfied, such that the control strategy doesn't only focus on the regulation of the voltages magnitude above, but take also into account the state of the entire microgrid.

First of all the active power provided by the three inverters, during the regulation of the voltage amplitude must not exceed the lower and the upper active power bounds of the device.

That is:

$$P_{MIN\_i} < P_{INVi} < P_{MAX\_i} \quad i = 1,2,3 \quad (4.13)$$

where  $P_{INVi}$  is the power provided by the  $i$ -th inverter of the three,  $P_{MAXi}$  and  $P_{MINi}$  represents, respectively, the upper and lower bounds of power.

The optimal strategy must also take into account that the voltage amplitude of buses that are not directly controlled by three Grid Forming inverters, must not exceeds the limits of voltage magnitudes, introduce in CHAPTER 3, as instances of the CEI 8-6 norm. Therefore:

$$\begin{aligned} V_{min} &< V_{m7} < V_{max} \\ V_{min} &< V_{m6} < V_{max} \end{aligned} \quad (4.14)$$

Once the optimization problem has been formulated, the multi-objective function (4.11) and the problem constraints (4.13) and (4.14) must be expressed in function of the control variables, that reference voltage values of the three invert in m5', m4' and m2',  $V_{ref1}$ ,  $V_{ref2}$  and  $V_{ref3}$ . For this purpose,

the droop laws, in equation (4.15), and the expression in (4.16), that derives from the radial configuration of the RSE microgrid [37], have been exploited.

$$\begin{aligned} V_{INV1} = V_{m5'} &= -K_{P1} * P_1 + V_{ref1} \\ V_{INV2} = V_{m4'} &= -K_{P2} * P_2 + V_{ref2} \\ V_{INV3} = V_{m2'} &= -K_{P3} * P_3 + V_{ref3} \end{aligned} \quad (4.15)$$

Where  $P_1$ ,  $P_2$  and  $P_3$  represent the measured output active powers of the inverters, and  $-K_{P1}$ ,  $-K_{P2}$  and  $-K_{P3}$  represents the droop gains, tuned as explained in CHAPTER 3.

$$\Delta V_{12} = V_1 - V_2 \cong \frac{RP_{T1} + XQ_{t1}}{3V_1} \quad (4.16)$$

The expression above is a way to express the voltage droop over a line, in a radial grid like taken into consideration for this work.  $P_{T1}$  and  $Q_{t1}$  represents the active and reactive power entering Node 1, as depicted in Figure 4.24, while  $V_1$  and  $V_2$  are the voltage magnitude of the two nodes of the line. X and R represent, respectively, the reactance and the resistance of the line.

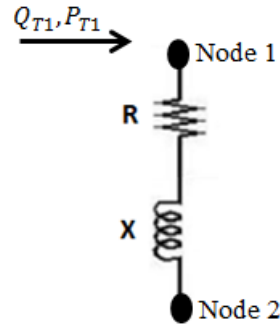


**Figure 4.24 Representation of a line**

In the following, the expressions in (4.11), (4.13) and in (4.14) are expressed in function desired value of the magnitude voltage of the PCC, by using the equations in (4.15) and (4.16).

$$\begin{aligned} V_{m5'_n} &= V_{PCC.n} - \frac{R_{n4}P_{T1} + X_{n4}Q_{t1}}{3V_{PCC}} - \frac{R_{n4'}P_{Tn4'} + X_{n4'}Q_{Tn4'}}{3V_{m5}} \\ V_{m4'_n} &= V_{PCC.n} - \frac{((R_{n3} + R_{n3'})P_{T2} + (X_{n3} + X_{n3'})Q_{T2})}{3V_{PCC}} \\ V_{m4'_n} &= V_{PCC.n} - \frac{((R_{n1} + R_{n1'})P_{T3} + (X_{n1} + X_{n1'})Q_{T3})}{3V_{PCC}} \end{aligned} \quad (4.17)$$

In the expressions (4.17),  $V_{PCC.n}$  is a constant value, in particular it represents the nominal value that the voltage magnitude of the PCC must reach due to the secondary voltage control action.  $P_{T1}$ ,  $P_{T2}$ ,

$P_{Tn4}$ , and  $P_{T3}$  are the measurements of the active powers entering the lines, as depicted in Figure 4.25, while  $Q_{T1}$ ,  $Q_{T2}$ ,  $Q_{Tn4}$ , and  $Q_{T3}$  are the measurements of reactive powers.  $V_{PCC}$  and  $V_{m5}$  are, respectively, the phase magnitude of the buses m1 (PCC) and m5'. As it can be seen from the expressions in (4.17) the voltage drop of the impedance of line n2 has been neglected, since the values of resistance and reactance involved are very small compared to the ones of the other lines (Table 4.2). The expression of  $V_{m5'n}$  is different from the others, since, in this region, the microgrid does not present anymore a radial configuration, but, on the contrary, the power flowing out line n4 is split between the inverter, the PV generator and the load 1.

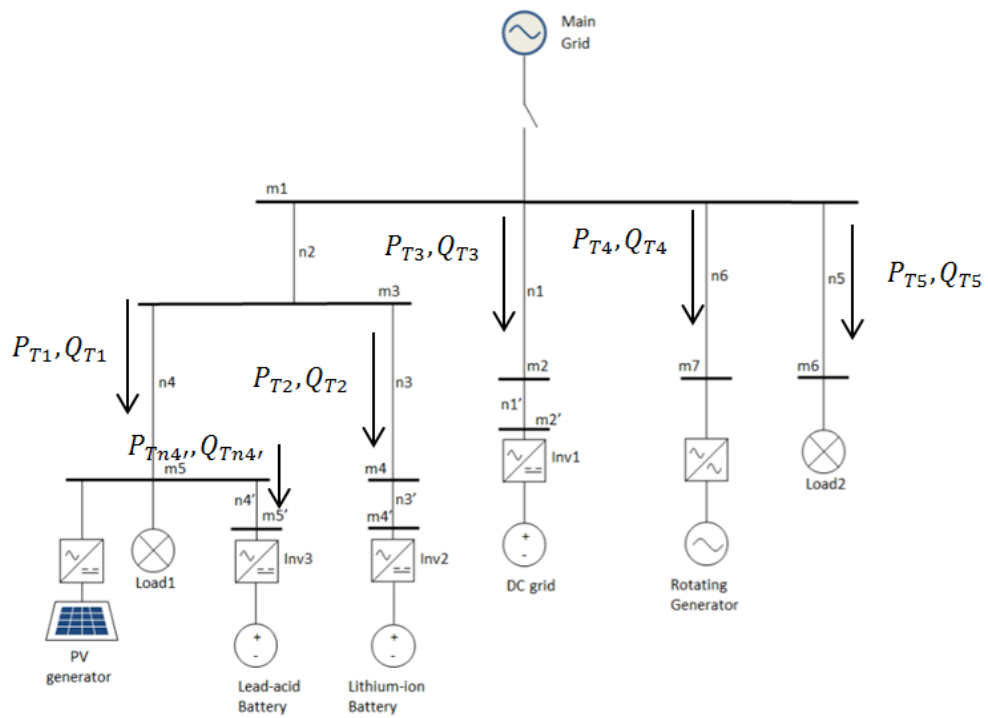


**Figure 4.25 Powers scheme of the microgrid.**

In the following, the elements involved in the optimal problem constraints are expressed in function of the control variables,  $V_{ref1}$ ,  $V_{ref2}$  and  $V_{ref3}$ .

$$V_{m7} = V_{INV1} + \frac{R_{n4}P_{T1} + X_{n4}Q_{T1}}{3V_{PCC}} + \frac{R_{n4'}P_{Tn4'} + X_{n4'}Q_{Tn4'}}{3V_{m5}} - \frac{R_{n6}P_{T4} + X_{n6}Q_{T4}}{3V_{PCC}} \quad (4.18)$$

$$V_{m7} = V_{INV2} + \frac{((R_{n3} + R_{n3'})P_{T2} + (X_{n3} + X_{n3'})Q_{T2})}{3V_{PCC}} - \frac{R_{n6}P_{T4} + X_{n6}Q_{T4}}{3V_{PCC}}$$

$$\begin{aligned}
 V_{m7} &= V_{INV3} + \frac{((R_{n1} + R_{n1'})P_{T3} + (X_{n1} + X_{n1'})Q_{T3})}{3V_{PCC}} - \frac{R_{n6}P_{T4} + X_{n6}Q_{T4}}{3V_{PCC}} \\
 V_{m6} &= V_{INV1} + \frac{R_{n4}P_{T1} + X_{n4}Q_{t1}}{3V_{PCC}} + \frac{R_{n4'}P_{Tn4'} + X_{n4'}Q_{Tn4'}}{3V_{m5}} \\
 &\quad - \frac{R_{n5}P_{T5} + X_{n5}Q_{T5}}{3V_{PCC}} \\
 V_{m6} &= V_{INV2} + \frac{((R_{n3} + R_{n3'})P_{T2} + (X_{n3} + X_{n3'})Q_{T2})}{3V_{PCC}} - \frac{R_{n5}P_{T5} + X_{n5}Q_{T5}}{3V_{PCC}} \\
 V_{m6} &= V_{INV3} + \frac{((R_{n1} + R_{n1'})P_{T3} + (X_{n1} + X_{n1'})Q_{T3})}{3V_{PCC}} - \frac{R_{n5}P_{T5} + X_{n5}Q_{T5}}{3V_{PCC}}
 \end{aligned} \tag{4.19}$$

By substituting (4.15) in the expressions above, the relation between the magnitude voltage values of node m7 and m6, and the control variable is obtained.

$$\begin{aligned}
 V_{m7} &= -K_{P1} * P_1 + V_{ref1} + \frac{R_{n4}P_{T1} + X_{n4}Q_{t1}}{3V_{PCC}} + \frac{R_{n4'}P_{Tn4'} + X_{n4'}Q_{Tn4'}}{3V_{m5}} \\
 &\quad - \frac{R_{n6}P_{T4} + X_{n6}Q_{T4}}{3V_{PCC}} \\
 V_{m7} &= -K_{P2} * P_2 + V_{ref2} + \frac{((R_{n3} + R_{n3'})P_{T2} + (X_{n3} + X_{n3'})Q_{T2})}{3V_{PCC}} \\
 &\quad - \frac{R_{n6}P_{T4} + X_{n6}Q_{T4}}{3V_{PCC}} \\
 V_{m7} &= -K_{P3} * P_3 + V_{ref3} + \frac{((R_{n1} + R_{n1'})P_{T3} + (X_{n1} + X_{n1'})Q_{T3})}{3V_{PCC}} \\
 &\quad - \frac{R_{n6}P_{T4} + X_{n6}Q_{T4}}{3V_{PCC}}
 \end{aligned} \tag{4.20}$$

$$\begin{aligned}
 V_{m6} &= -K_{P1} * P_1 + V_{ref1} + \frac{R_{n4}P_{T1} + X_{n4}Q_{t1}}{3V_{PCC}} + \frac{R_{n4'}P_{Tn4'} + X_{n4'}Q_{Tn4'}}{3V_{m5}} \\
 &\quad - \frac{R_{n5}P_{T5} + X_{n5}Q_{T5}}{3V_{PCC}} \\
 V_{m6} &= -K_{P2} * P_2 + V_{ref2} + \frac{((R_{n3} + R_{n3'})P_{T2} + (X_{n3} + X_{n3'})Q_{T2})}{3V_{PCC}} \\
 &\quad - \frac{R_{n5}P_{T5} + X_{n5}Q_{T5}}{3V_{PCC}} \\
 V_{m6} &= -K_{P3} * P_3 + V_{ref3} + \frac{((R_{n1} + R_{n1'})P_{T3} + (X_{n1} + X_{n1'})Q_{T3})}{3V_{PCC}} \\
 &\quad - \frac{R_{n5}P_{T5} + X_{n5}Q_{T5}}{3V_{PCC}}
 \end{aligned} \tag{4.21}$$

All the elements, involved in the equations above, are measurable quantities or known parameters. Hence, it results clear that without a complete knowledge of the structure of the microgrid and without a feasible communication system, able to carry out the information on the measurable variable, the secondary voltage controller, designed here, can't work properly.

This control strategy also doesn't allow the plug-and-play feature, since a modification of the microgrid structure implies the reformulation of the above expressions.

Since the optimization problem is quadrativ, the secondary voltage controller is implemented in Simulink through the Matlab function *quadprog*. This function is able to solve the optimization problem defined in (4.22) by means of either the Interior-Point- Convex algorithm or the Trust-Region-Reflective one, once the matrixes  $H, f, A, b, Aeq$  and  $beq$  are defined.

$$\min_x \frac{1}{2}x^T Hx + f^T x \text{ such that } \begin{cases} Ax \leq b, \\ Aeqx = beq, \\ lb \leq x \leq ub, \end{cases} \quad (4.22)$$

So the multi-objective function and the constraints, designed previously for the secondary voltage control, need to be rearranged, so to obtain a matrix expression of the problem as the one in (4.22).

## 4.6.2 Secondary voltage control simulation

In this subsection the performances of the designed voltage control are tested. This control along with the frequency one, previously described, composes the MGCC (MicroGrid Central Controller), the device put in charged of the secondary control action.

The designed voltage control action works in the following way: the MGCC every 6 sec gathers and elaborates the required measures in order to solve the optimal problem, defined in the previous subsection. Then, if the deviation of the PCC voltage magnitude respect to the nominal value is larger than 1 V, it computes the voltage references to send to the primary controllers.

This procedure is not immediate, but they must be considered a computational time delay and a communication line either when the Secondary Voltage control receives or delivers information. The computational delay is 0.8 sec, while the communication one is 0.2 sec.

In Figure 4.26 and Figure 4.27, the active and reactive measured output powers of the three inverters are represented. The reactive powers profile is the same of the other cases, while the active powers changed every time the voltage control action is applied. This is due to the nature of the voltage control action itself; the voltage of the nodes  $m5'$ ,  $m4'$  and  $m2'$  (Figure 4.25) are modified in order to restore the  $V_{PCC}$  to its nominal value, consequently the voltage droop lines  $n4'$ ,  $n3'$  and  $n1'$  increase or decrease along with the power absorbed or generated by the inverters.

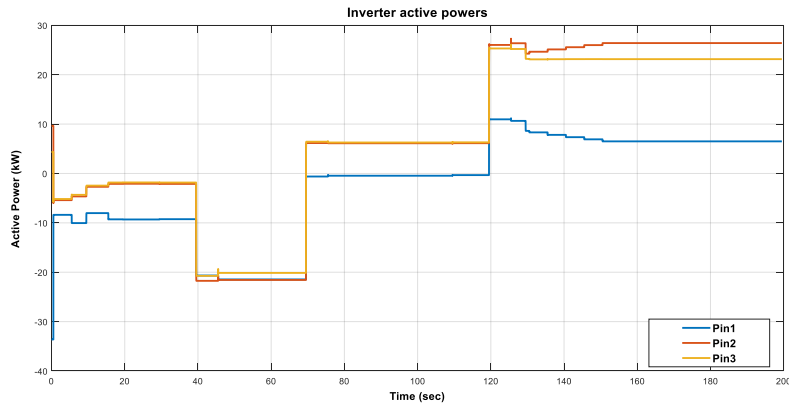


**Figure 4.26 SVC active powers response**

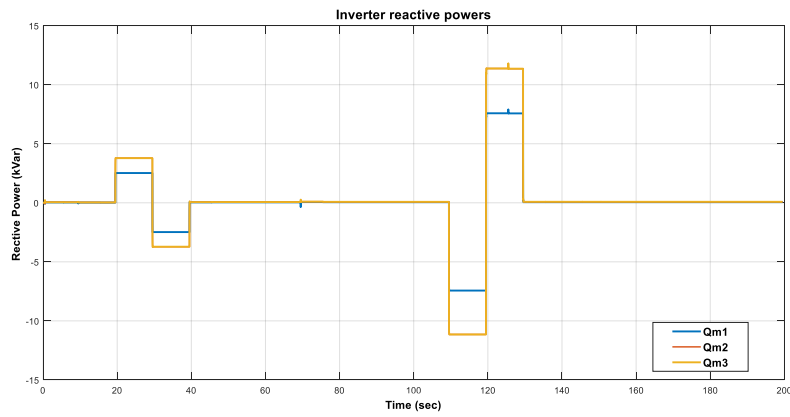


**Figure 4.27 SVC reactive powers response**

In Figure 4.28, Figure 4.29 and Figure 4.30 , they are shown the responses of the microgrid electrical variables to the action of the SVC. The voltage magnitude of the PCC is restored to its nominal value of 400 V after a deviation due to the regulation of the Primary level, at the same time also the deviations of the other nodal voltages of the microgrid are reduced. This outcome is due to the radial structure of the considered microgrid; in fact, the nodal voltages differ from the  $V_{pcc}$  value only for a drop, due to the impedance of the corresponding line. Hence, they practically follow the trend of the voltage magnitude of the PCC.

Regarding the microgrid frequency, depicted in Figure 4.30, it practically doesn't change respect to the case in which only the primary level control action is provided, since none frequency control is implemented. A slight disturbance can be noted when the voltage control action is performed, however it doesn't affect the stability of the microgrid or the performances of the SVC.

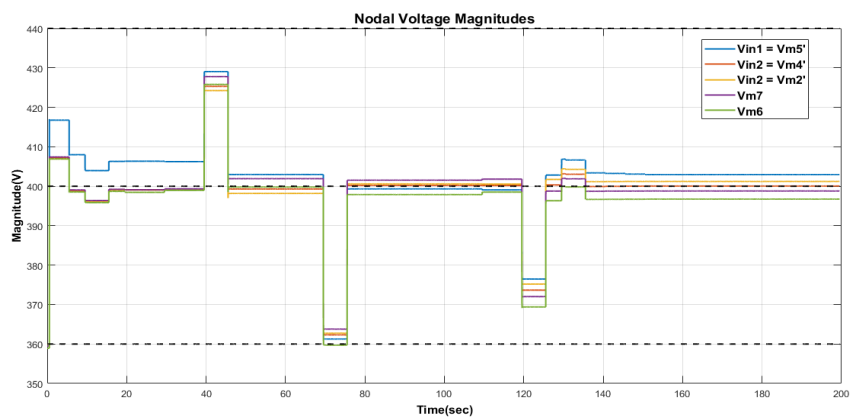


Figure 4.28 SVC nodal voltages response

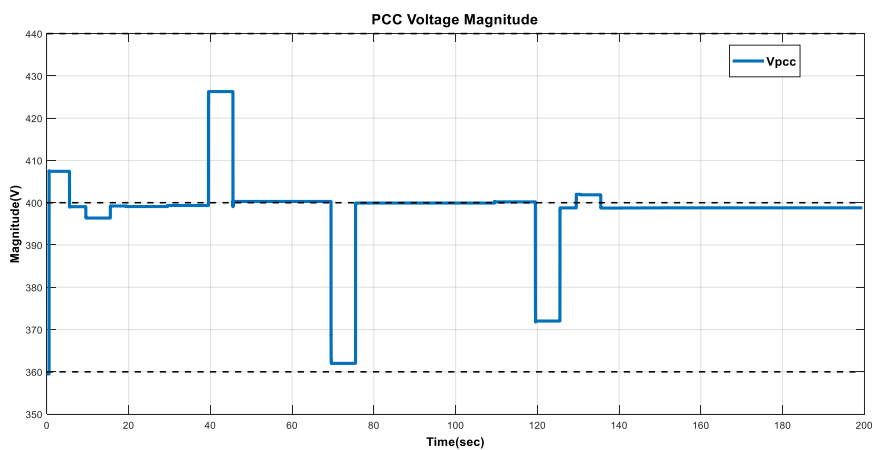


Figure 4.29 SVC PCC voltage response

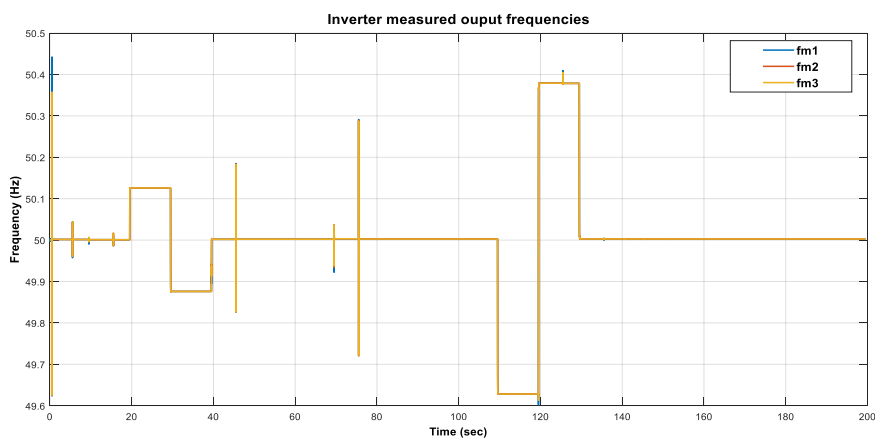


Figure 4.30 SVC microgrid frequency response

## 4.7 Overall secondary control level

The SFC and the SVC, described in the previous subsection, will be physically implemented through the MGCC, that is the electronic device, responsible of gathering the required information and of computing the control action. Obviously, the performances of the secondary designed control action depends both on the proper functioning of the down layers in the hierarchical control structure and of the measuring devices. It also very important to consider the performance of the used communication system, since a drop of information or a significant slowdown in the communication of it could affect the control action of both the SFC and the SVC, as already mentioned.

After a brief introduction, the results of the combined control actions of the secondary frequency control and of the voltage one are shown.

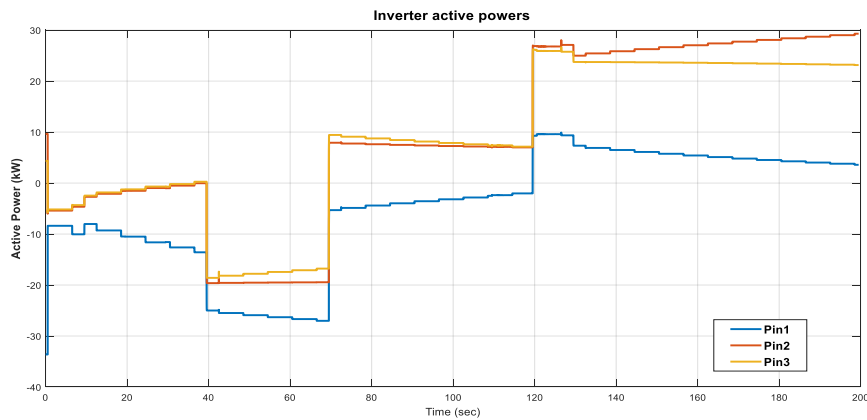


Figure 4.31 Overall secondary control active powers response

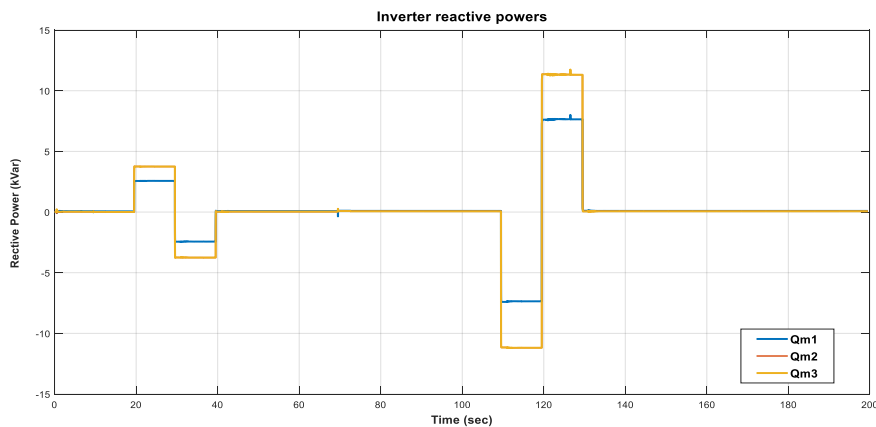


Figure 4.32 Overall secondary control reactive powers response

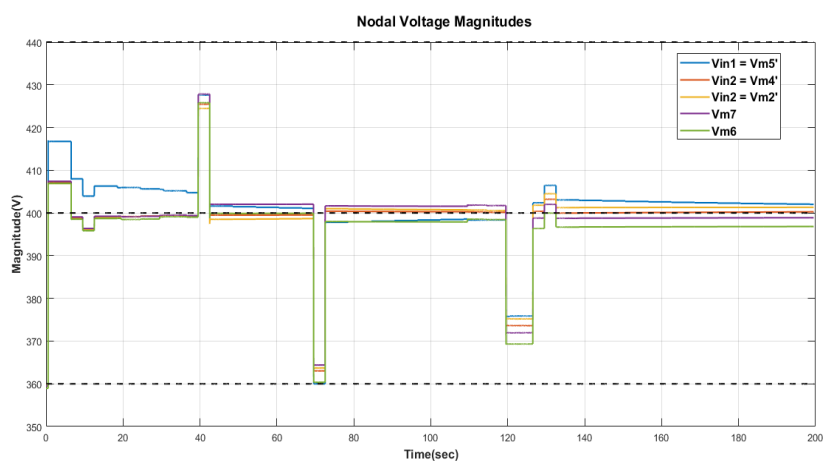


Figure 4.33 Overall secondary control nodal voltages response

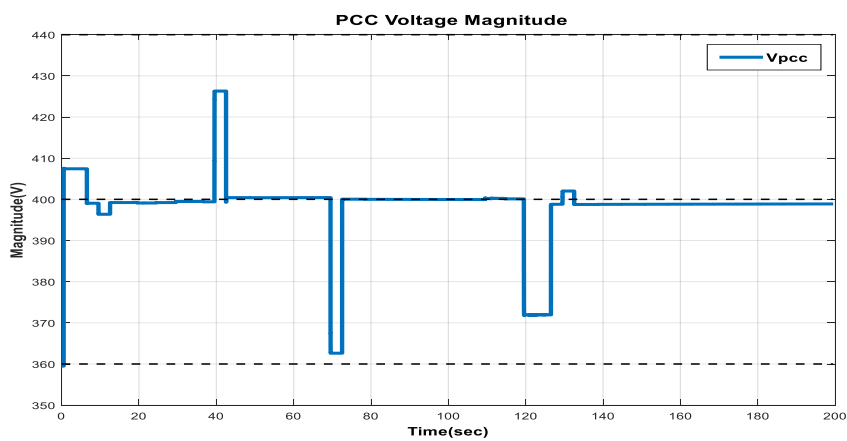


Figure 4.34 Overall secondary control PCC voltage response

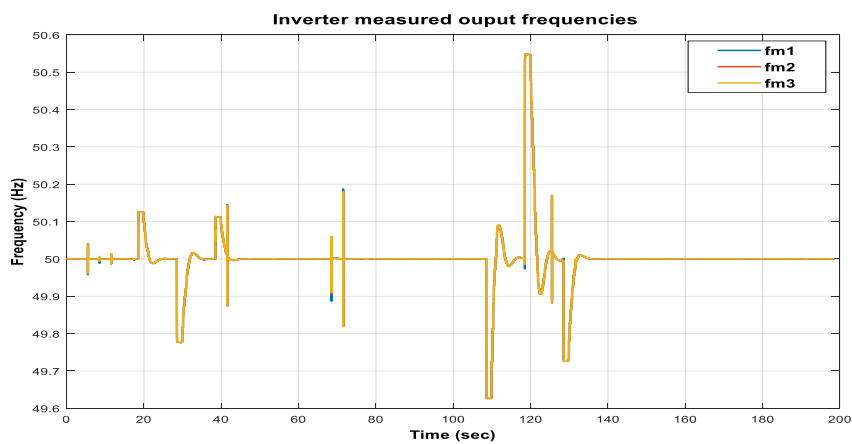


Figure 4.35 Overall secondary control microgrid frequency response

To sum up, starting from the description of the considered test case, the designed secondary control structure shows great improvements with respect to the case in which only a primary control action is implemented. Indeed, although the microgrid is subject to step variations of active and reactive powers, the network variables never exceed the bounds imposed by the norm and, eventually, they are restored to their nominal values.

#### 4.7.1 Secondary control considering the SOC<sub>s</sub> of the ESSs

Until now no considerations have been made on the State of Charge of the ESSs presents in the microgrid. As already explained, the three inverters, which represent the actuators of the designed hierarchical control structure, have at the DC side a Storage System. In particular, the inverter in m5' is connected to a Lead-Acid battery, the one in m4' to Lithium-Ion battery and the final one to a DC grid, that is modelled in this work as a battery.

The batteries guarantee a continuous flow of power as long as their State of Charge is limited in a certain range, usually 0.1-0.9. When these bounds are exceeded, the battery and consequently the inverter stop working normally, so disabling any control actuation. Hence, some kind of SOC<sub>s</sub> management strategy need to be considered, in the designing of the microgrid control action.

In order to include a SOC management strategy in the hierarchical control already designed, the Secondary Voltage Control is slightly modified, while the other elements of the overall control are kept unchanged. In particular, new equality constraints are added to the optimization problem, defined in the previous section. This modification forces the inverters to generate or absorb active power, taking into account the SOC of their respective DC sources.

$$0.1 < SOC_i < 0.9 \quad (4.23)$$

$$\begin{aligned} P_i &= P_{TOT} * \frac{SOC_i}{SOC_{TOT}} & \text{if } P_{TOT}^m > 0 \\ P_i &= P_{TOT} * \frac{(1 - SOC_i)}{3 - SOC_{TOT}} & \text{if } P_{TOT}^m < 0 \end{aligned} \quad (4.24)$$

where  $P_{TOT}^m$  is the sum of the measured output active powers of the inverters,  $SOC_{TOT}$  the sum of the measured state of charge of the storage, while  $P_{TOT}$  represents the sum of the active powers of the inverter when the SVC action is performed, this value depends on the control variables. The equations above need to be expressed in function of the control variables  $V_{ref1}$ ,  $V_{ref2}$  and  $V_{ref3}$ , as it has been done for the rest of the optimization problem elements. To express the eq. (4.23) in function of the

control variables, the equation (4.1) and (4.2) are discretize in the following way:

$$\begin{aligned}
 SOC_{charge} &= SOC_0 - K_{bcharge}^i * \left( \frac{(P_m^i(t) + P_m^i(t-1)) * 2}{T_s} + INT_{P^i}(t-1) \right) \\
 SOC_{charge} &= SOC_0 - K_{bdischarge}^i * \left( \frac{(P_m^i(t) + P_m^i(t-1)) * 2}{T_s} + INT_{P^i}(t-1) \right)
 \end{aligned} \tag{4.25}$$

In the equation above, the integral of the measured active power of the single inverter is computed as the trapezoidal area between two consecutive power samples.  $T_s$  represents the time interval between the two samples,  $INT_{P^i}(t-1)$  is the integral value computed at the previous time instant, while  $K_{bcharge}^i$  and  $K_{bdischarge}^i$  are constant parameters that include both the inverter and battery yields, along with the maximum capacity of the battery. Since the dynamics of eq. (4.1) and eq. (4.2) depend on the parameter  $C_{max}$  (maximum capacity), which is very small, they are very slow. Therefore, eq. (4.25) represents a good approximation of the actual power integral.

In order to expand equations (4.24) and (4.25) in function of the control variables, the droop characteristics, expressed in (4.15), are exploited. Therefore:

$$\begin{aligned}
 SOC_{charge}^i &= SOC_0 - \frac{K_{bcharge}^i}{K_p^i} * \left( \frac{(V_{INVi}(t) + V_{INVi}(t-1)) * 2}{T_s} \right. \\
 &+ INT_{V^i}(t-1) \left. \right) + \frac{K_{bcharge}^i}{K_p^i} * \left( \frac{(V_{refi}(t) + V_{refi}(t-1)) * 2}{T_s} + INT_{Vref}^i(t-1) \right) \\
 SOC_{discharge}^i &= SOC_0 - \frac{K_{bdischarge}^i}{K_p^i} * \left( \frac{(V_{INVi}(t) + V_{INVi}(t-1)) * 2}{T_s} \right. \\
 &+ INT_{V^i}(t-1) \left. \right) + \frac{K_{bdischarge}^i}{K_p^i} * \left( \frac{(V_{refi}(t) + V_{refi}(t-1)) * 2}{T_s} + INT_{Vref}^i(t-1) \right)
 \end{aligned} \tag{4.26}$$

where  $V_{INVi}$  represents the measured output voltage magnitude on the  $i$ -th inverter and  $V_{refi}$  is its output reference voltage value, as well as the control variable of the SVC (Secondary Voltage Control).  $K_p^i$  is the droop gain of the P-V characteristic and, in the case of the Secondary Voltage Control, represents a constant parameter.

$$\begin{aligned}
 \frac{(V_{INVi} - V_{refi})}{K_{pi}} &= \left( \sum_{j=1, j \neq i}^3 \frac{(V_{INVi+j} - V_{refi+j})}{K_{pi+j}} \right) + \frac{(V_{INVi} - V_{refi})}{K_{pi}} \\
 &\quad * \frac{SOC_i}{SOC_{TOT}} \quad \text{if } P^m_{TOT} > 0
 \end{aligned}
 \tag{4.27}$$

$$\begin{aligned}
 \frac{(V_{INVi} - V_{refi})}{K_{pi}} &= \left( \sum_{j=1, j \neq i}^3 \frac{(V_{INVi+j} - V_{refi+j})}{K_{pi+j}} \right) + \frac{(V_{INVi} - V_{refi})}{K_{pi}} \\
 &\quad * \frac{SOC_i}{SOC_{TOT}} \quad \text{if } P^m_{TOT} > 0
 \end{aligned}$$

Looking at the equations above, it can be explained the logic behind the new constraints introduced. Eq. (4.26) imposes that the control variable values must be chosen in order to keep the SOC of the batteries in the limitations. This is not a stringent condition, since when the SOC of one of the three ESSs reach a critical value, such as, for example, 0.2 or 0.8, the Rotating Generator can be switched on if the storage system must be recharge or off if the SOC is too high. In addition to this the other limitations both on the maximum and minimum active power of the inverter, and on the nodal voltages range, prevent peaks of absorption or generation that could push the SOC to exceed the bounds. For this reasons, the constraints in (4.26) is usually never violated.

More significant is the constraint, expressed by Eq.(4.27). This one, in fact, imposes that the optimization algorithm must compute the voltage reference values, that minimize the multi-objective function  $f$  (4.22) and, at the same time, allow an SOC-wise distribution of the active power among the inverters. This means that each inverter will generate or absorb active power, according to the current SOC of the respective battery. Therefore, according to this logic, the battery that has the minimum SOC value will absorb more power, on the contrary, the one with the maximum SOC will absorb less. The same principle is valid in generation conditions: the battery with the maximum State of Charge will generate more active power, the one with a smaller value will generate less. Eventually, the ESSs of the microgrid will reach a condition in which their SOC values will be very similar. This is a favorable scenario, since it prevents that faults of the storage systems could critically affect the performances of the hierarchical control. As a matter of fact, if, for example, among the three batteries, two have an SOC value less than 0.3 and the other has a SOC equal to 0.8, due to an incoherent distribution of the active powers; if this last one stop working for a fault, the control action on the microgrid could be compromise, since the working ESSs don't have enough energy to provide the active power, required by the control. Hence, an active power distribution needs to provided, even at the cost of a not perfect regulation of the PCC voltage magnitude.

In the following, they will be presented the performances of the designed secondary control level, when it is tested over the powers profile adopted until now, but with the addition of the new constraints

to the optimization problem. Two tests have been carried out: in the first test, the initial value of the SOC is equal, in the second one, each battery has a different initial SOC.

Only the graphs that represent the active powers and nodal voltages response and the SOC behavior will be shown, since neither the reactive powers nor the microgrid frequency are affected by the described modification.

To better see the effects of the new constraints, the value of maximum capacity listed in Table 4.3 are multiplied by 10. In Table 4.8, instead, they are listed the initial value of State of Charge of the batteries for the two tests.

**Table 4.8 Initial SOC**

<i>Parameters</i>	<i>% SOC1</i>	<i>% SOC2</i>	<i>% SOC3</i>
<b>Balanced SOC</b>	50	50	50
<b>Unbalanced SOC</b>	30	50	70

In Figure 4.36, are represented the measured active output powers of the inverters. Since they begin the test, with the same value of SOC, throughout the whole simulation they provide almost the same amount of active power. This behavior is accordant to the new constraint just described. In fact, according to eq. (4.27) the inverters must provide an active power amount proportional to the SOC of their batteries, which in this case is equal. Besides, looking at Figure 4.39, it can be noted that the ESSs charge and discharge with nearly the same rate.

Regarding the nodal voltages, looking at Figure 4.38, it can be seen that they are all included in the established voltage range. The PCC voltage magnitude, in Figure 4.37, is restored to the nominal value by the action of the voltage control for almost the entire simulation, except for the last seconds.

This is due to the fact that the Optimization algorithm is trying to compute the voltage references and, at the same time, is trying to distribute the active power according to the current SOC of the batteries. This is impossible, since the first inverter has reached its maximum output active power value. To overcome this problem, the Rotating Generator could be activated, in order to relieve the load of active power on the inverters.

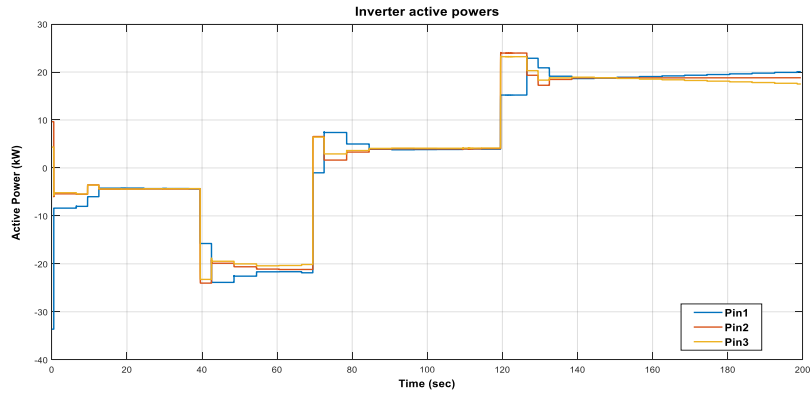


Figure 4.36 Balance SOCs active powers response

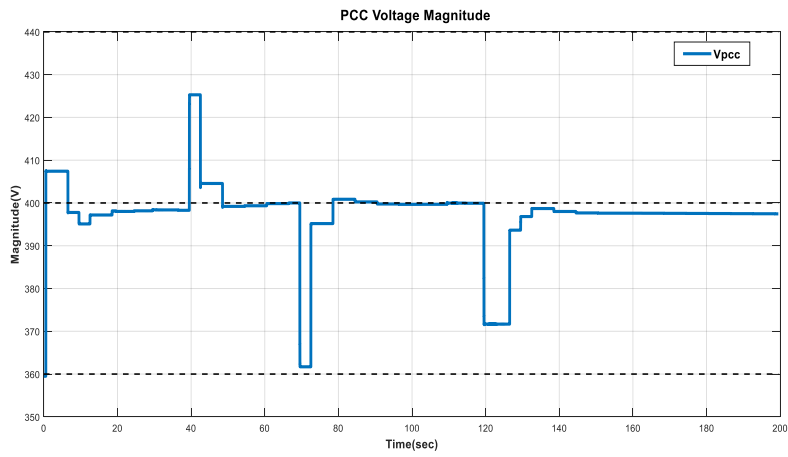


Figure 4.37 Balanced SOCs PCC voltage response

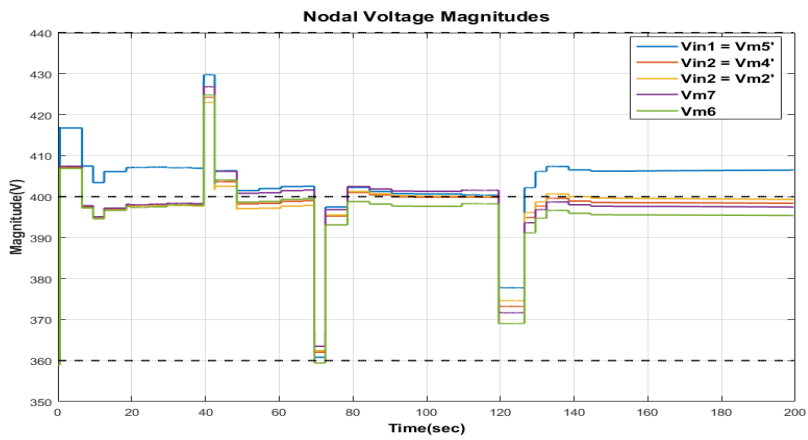
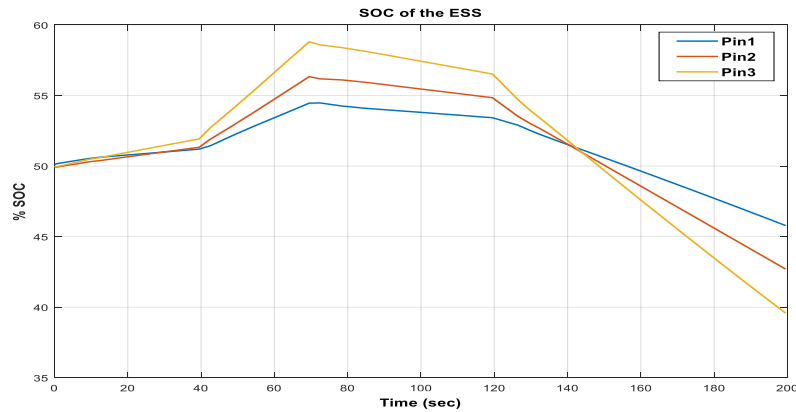


Figure 4.38 Balanced SOCs nodal voltages response



**Figure 4.39** Balance SOC's response

In the following, the results of the second test, performed with different initial SOC values, are presented.

The simulations are carried out, omitting the condition of maximum and minimum active powers on the inverters. This assumption is due to the initial conditions of the microgrid; in fact, the large difference among the initial values of the state of charge, could compromise the performances of the optimization algorithm. However, in a real scenario, it is unusual to find a situation with such a significant unbalance among the SOC's.

In Figure 4.40, they are represented the active powers of the three inverters. As it can be seen, compared to the previous case, the amount of generated and absorbed active power is different for each inverter.

In particular, the ESSs with the lower SOC level will absorb a larger and generate a smaller amount of active power, compared to the other storage systems. The opposite logic is valid for the ESS with the higher SOC level. This behavior will eventually lead to a situation in which the SOC value of all the batteries is almost equal.

As it can be seen in Figure 4.42, also in this case the SVC is not able to completely restore the PCC voltage magnitude to its nominal value, reducing the voltage deviation to about 2V. However, this deviation is the minimum possible one, considering the condition imposed on the active powers. This is an acceptable compromise in order to achieve a generated or absorbed active power distribution, which takes into account the state of charge of the ESSs.

In Figure 4.43, it can be seen the action condition imposed by the proportional power equality constraint. In a time interval of 80 sec, the third battery reduces its state of charge to the 55%, instead the battery one and two, respectively, to 43% and 30%.

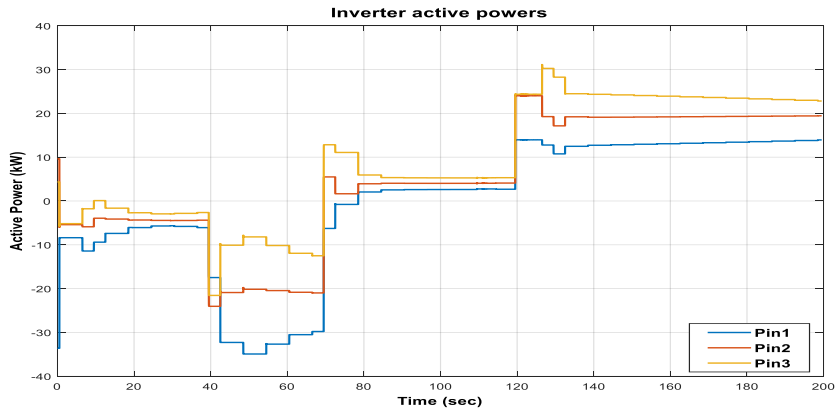


Figure 4.40 Unbalanced SOCs active powers response

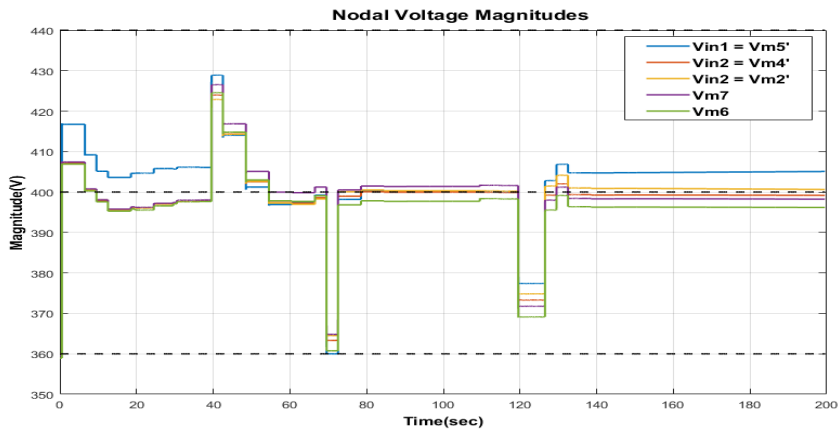


Figure 4.41 Unbalanced SOCs nodal voltages response

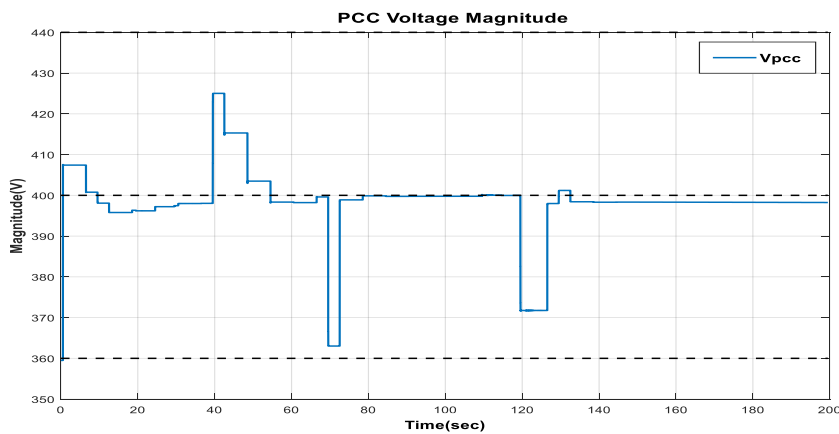
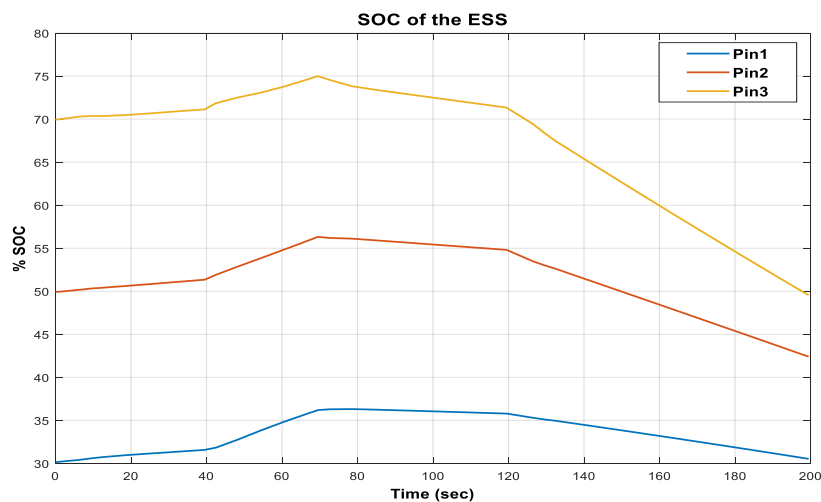


Figure 4.42 Unbalanced PCC nodal voltages response



**Figure 4.43 Unbalanced SOC response**

## 4.8 Conclusions

In this chapter the microgrid test case has been presented and the performances of the designed control structure have been discussed. To sum up, it has been demonstrated that the implementation of the described secondary control layer gives considerable improvements since the network variables do not significantly deviate from their nominal values. Moreover, it allows to implement a power distribution strategy, that takes into consideration the SOC of the ESSs presented in the microgrid.



# CONCLUSION AND FUTURE DEVELOPMENTS

With the increasing spreading of generating system based on renewable source and of power converters, new and more efficient ways to control the energy production and distribution need to be explored. In this context, an interest in Microgrid design and control is growing more and more. The microgrid concept, a cluster of renewable sources, storage units and loads, represents an appealing alternative for overcoming the challenges of integrating Distributed Energy Resource units, including renewable energy sources, in the current power systems; and, at the same time, to reduce power losses and improve power quality. These features can be obtained only through the development of robust and reliable control systems, in particular for what concerning the islanded mode of the inverters base microgrid. A microgrid can work either connected to the main grid, in grid-connected mode, or can separate from it and work alone, in islanded-mode. Major issues occur exactly in this case; the stochastic nature of both renewable sources and loads could create unbalances between the total generated power and the absorbed one. While in the grid-connected mode any power mismatch is compensated by a power exchange with the main grid, unbalance in islanded mode has a considerable impact on the network electrical variable, which can significantly deviate from their nominal value. Moreover in islanded mode, the stabilizing effect guaranteed by rotating machine inertia is missing. Droop controls implemented on the different converters, according to a distribute control approach, acting as voltage generators or Grid Forming mode, provide a solution to the stability problem of the microgrid.

The main objective of this work is to design a centralized controller for the coordination of the energy storage systems, interfaced to the microgrid through voltage controlled voltage source inverters. The control objective is to restore the frequency of the microgrid to its nominal value of 50 *Hz* and to keep, as close as possible, the nodal voltage magnitudes to a nominal value of 400 V, after a renewable source or load disturbance. Moreover, a power distribution logic among the storage systems is implemented, in order to take into account their state of energy. To this purpose, this dissertation has been developed as described in the following.

In the first chapter, a complete overview of the future microgrid context has been presented, describing the main issues involving this new electrical paradigm. These are more relevant, as already explained, in the so called islanding operating mode, where frequent unbalances between the total generated and requested power can occur.

In the second chapter, a review of the second level control state-of-the-art is discussed. In particular, the drawbacks of the primary control level and the motivations for the implementation of a further control layer are enlightened. The drawbacks of a classical PI regulator, as secondary controller, are discussed and, at the end of the chapter, the advantage and disadvantages of each secondary control methods reviewed, are listed.

The third chapter covered the design and testing of a primary layer that has the function to reduce the deviations of the electrical variables of the microgrid, due to unbalances of power. This primary level has a decentralize structure and it is based on the *Droop Control* method. In the final part of this chapter, it is reported that this control layer is not enough to ensure that the network variables evolve around the nominal values, important feature specially for the microgrid frequency, and that, therefore, a second control level is needed.

Finally, in the last chapter the secondary control level is implemented and tested over a predefine power profile. The secondary layer, as already described, is composed by two control action: one on the the frequency references and one on the voltage references of the three voltage control inverters, present in the microgrid. The frequency action is performed by three PI regulators, enhanced with Smith Predictors, in order to overcome problems due to time delays. Moreover, the stability of this secondary frequency controller has been studied for different value of the time delay. The voltage control action, instead, is performed by an optimal control. The multi-objective function  $f$  and the constraints of the optimization problem are computed, taking in consideration the particular configuration of the RSE microgrid. After a first description, the SVC and SFC are tested over a made-up active and reactive powers profile, focusing on the advantages and drawbacks of each one, when they work alone or in combination. In the final part of the chapter, the optimal problem is modified, in order to include in the voltage control action a power management strategy that takes into account the SOC of the ESSs of the microgrid. The modified Secondary controller is then tested on the same powers profile and the improvements, respect to the previous cases, are underlined.

The main innovations developed in this work are:

- The development of a secondary control level that acts on the frequency and voltage references, instead of a the reactive and active power ones, as it is supposed in the most part of the reviewed literature.
- The development of a PI+SP controller for the regulation of the microgrid frequency and the development of an optimal control for both the regulation of the nodal voltages and the management of the SOC of the storage systems present in the microgrid.

Possible future developments, that could be investigated, are the analysis of the performances and the validation of the proposed hierarchical control structure, when it is implemented on the physical devices that actually compose the microgrid present at RSE. The study of a more complex hierarchical control structure, which consists in more than two layers, and that it is able to vary both the voltage and frequency reference values and the droop proportional gains according to some predefined objectives. A new optimization problem could be designed and studied, with different multi-objective function and different constraints, that take into account other aspects and new goals for the microgrid control. Finally, the proposed control system has been designed to manage the microgrid only in islanded condition, and it does not consider neither the islanding nor the reconnecting event. The hierarchical control structure could be actually improved so that it is performed both in island and in grid-connected mode, ensuring an efficient regulation in both conditions.



## APPENDICES



## APPENDIX A

### Matrix A of the Secondary Frequency Control System

$$A = \begin{bmatrix} a_{11} & a_{12} & a_{13} & a_{14} & a_{15} \\ 1 & 0 & 0 & 0 & 0 \\ 0 & 1 & 0 & 0 & 0 \\ 0 & 0 & 1 & 0 & 0 \\ 0 & 0 & 0 & 1 & 0 \end{bmatrix}$$

$$a_{11} = -\frac{L\tau_d + 2L\tau_{PLL} + L\tau_d\tau_{PLL} + 2\tau_d\tau_{PLL} + KpL\tau_d}{L\tau_d\tau_{PLL}};$$

$$a_{12} = -\frac{2L + L\tau_d + 2L\tau_{PLL} + 2\tau_d + 4\tau_{PLL} + 2\tau_d\tau_{PLL} + 2KpL + KpL\tau_d + 2Kp\tau_d + KiL\tau_d}{L\tau_d\tau_{PLL}};$$

$$a_{13} = -\frac{2L + 4 + 2\tau_d + 4\tau_{PLL} + 4Kp - 2Kp\tau_d + 6KpL + 2KiL + KiL\tau_d + 2Ki\tau_d}{L\tau_d\tau_{PLL}};$$

$$a_{14} = -\frac{4Kp + 4Ki - 2Ki\tau_d + 6KiL + 4}{L\tau_d\tau_{PLL}};$$

$$a_{15} = -\frac{4Ki}{L\tau_d\tau_{PLL}};$$



# Bibliography

- [1] Directive 2009/28/EC of the European Parliament and of the Council of 23 April 2009 on the promotion of the use of energy from renewable sources and amending and subsequently repealing Directives 2001/77/EC and 2003/30/EC (OJ L 140, 5.6.2009, p. 16–62).
- [2] S.Acquistapace, “ Modelling and control of a low voltage inverter based micorgrid”, Master thesis, Politecnico di Milano, Dipartimento di Energia, A.A. 2015-2016
- [3] V.Verma and G. G. Talpur, “Decentralized master-slave operation of microgrid using current controlled distributed generation sources”, Proc. IEE int. Conf. Power Electron. Drives Energy Syst. (PEDES), Bangalore, India, pp. 1-6, 2012.
- [4] C.Wang, “Theoretical analysis and simulation Microgrid”, Nov 2013.
- [5] N.Cai and J.Mitra, “ A decentralized control architecture for a microgrid with power electronics interfaces”, *Proc. Of the 42th Annual North America*, Alinton, TX, Sep. 2010.
- [6] Y.Hang H.Li, P.Shen, E.A.A.Coelho, J.M. Guerrero, “Review of Active and Reactive Power Sharing Strategies in Hierarchical Controlled Microgrids”, *IEEE Transaction on Power Electronics*.
- [7] D. E. Olivares et al., "Trends in Microgrid Control," in *IEEE Transactions on Smart Grid*, vol. 5, no. 4, pp. 1905-1919, July 2014.
- [8] T. Morstyn; B. Hredzak; V. G. Agelidis, "Control Strategies for Microgrids with Distributed Energy Storage Systems: An Overview," in *IEEE Transactions on Smart Grid* , vol.PP, no.99, pp.1-1.
- [9] A. Morotti and A. Spreafico, “Predictive control of voltages and frequency in islanded microgrid” Master’s thesis, Politecnico di Milano, Dipartimento di Energia, A.A. 2012-2013.
- [10] A. La Bella, S. Raimondi Cominesi, C. Sandroni and R. Scattolini, "Hierarchical Predictive Control of Microgrids in Islanded Operation," in *IEEE Transactions on Automation Science and Engineering*, vol. 14, no. 2, pp. 536-546, April 2017.

- [11] F. Pilo, G. Pisano and G. G. Soma, "Neural Implementation of MicroGrid Central Controllers," 2007 5th IEEE International Conference on Industrial Informatics, Vienna, 2007, pp. 1177-1182.
- [12] S. Shokoohi, F. Sabori and H. Bevrani, "Secondary voltage and frequency control in islanded microgrids: online ANN tuning approach," 2014 Smart Grid Conference (SGC), Tehran, 2014, pp. 1-6.
- [13] E. J. Agnoletto, R. V. A. Neves, R. F. Bastos, R. Q. Machado and V. A. Oliveira, "Fuzzy secondary controller applied to autonomous operated AC microgrid," 2016 European Control Conference (ECC), Aalborg, 2016, pp. 1788-1793.
- [14] H. R. Chamorro and G. Ramos, "Microgrid central fuzzy controller for active and reactive power flow using instantaneous power measurements," 2011 IEEE Power and Energy Conference at Illinois, Champaign, IL, 2011, pp. 1-6.
- [15] X. Yang, Y. Du, J. Su, L. Chang, Y. Shi and J. Lai, "An Optimal Secondary Voltage Control Strategy for an Islanded Multibus Microgrid," in *IEEE Journal of Emerging and Selected Topics in Power Electronics*, vol. 4, no. 4, pp. 1236-1246, Dec. 2016.
- [16] C. M. Colson, M. H. Nehrir and S. A. Pourmousavi, "Towards real-time microgrid power management using computational intelligence methods," *IEEE PES General Meeting*, Minneapolis, MN, 2010, pp. 1-8.
- [17] C. M. Colson, M. H. Nehrir and C. Wang, "Ant colony optimization for microgrid multi-objective power management," 2009 IEEE/PES Power Systems Conference and Exposition, Seattle, WA, 2009, pp. 1-7.
- [18] C. Schwaegerl, L. Tao, P. Mancarella, and G. Strbac, "A multi-objective optimization approach for assessment of technical, commercial and environmental performance of microgrids," *Eur. Transact. On Electrical Power*, vol. 21, no. 2, pp. 1269–1288, 2011.
- [19] E. Alvarez, A. C. Lopez, J. Gómez-Aleixandre and N. de Abajo, "On-line minimization of running costs, greenhouse gas emissions and the impact of distributed generation using microgrids on the electrical system," 2009 IEEE PES/IAS Conference on Sustainable Alternative Energy (SAE), Valencia, 2009, pp. 1-10.
- [20] H. Kanchev, D. Lu, B. Francois and V. Lazarov, "Smart monitoring of a microgrid including gas turbines and a dispatched PV-based active generator for energy management and emissions reduction," *2010 IEEE PES Innovative Smart Grid Technologies Conference Europe (ISGT Europe)*, Gothenburg, 2010, pp. 1-8.
- [21] D. He, D. Shi and R. Sharma, "Consensus-based distributed cooperative control for microgrid voltage regulation and reactive power sharing," *IEEE PES Innovative Smart Grid Technologies, Europe*, Istanbul, 2014, pp. 1-6.
- [22] W. Ni, I. B. Collings, J. Lipman, X. Wang, M. Tao and M. Abolhasan, "Graph theory and its applications to future network planning: software-defined online small cell management," in *IEEE Wireless Communications*, vol. 22, no. 1, pp. 52-60, February 2015.
- [23] A. Micallef, M. Apap, C. Spiteri-Staines and J. M. Guerrero, "Secondary control for reactive power sharing in droop-controlled islanded microgrids," *2012 IEEE. International Symposium on Industrial Electronics*, Hangzhou, 2012, pp. 1627-1633.

- [24] S. Liu, X. Wang and P. X. Liu, "Impact of Communication Delays on Secondary Frequency Control in an Islanded Microgrid," in *IEEE Transactions on Industrial Electronics*, vol. 62, no. 4, pp. 2021-2031, April 2015.
- [25] A. Micallef, M. Apap, C. Spiteri-Staines, J. M. Guerrero and J. C. Vasquez, "Reactive Power Sharing and Voltage Harmonic Distortion Compensation of Droop Controlled Single Phase Islanded Microgrids," in *IEEE Transactions on Smart Grid*, vol. 5, no. 3, pp. 1149-1158, May 2014.
- [26] R. E. Mackiewicz, "Overview of IEC 61850 and Benefits," *2006 IEEE PES Power Systems Conference and Exposition*, Atlanta, GA, 2006, pp. 623-630.
- [27] Meiqin Mao, Fengming Mei, Peng Jin and Liuchen Chang, "Application of IEC61850 in energy management system for microgrids," *2014 IEEE 5th International Symposium on Power Electronics for Distributed Generation Systems (PEDG)*, Galway, 2014, pp. 1-5.
- [28] X. Lu, K. Sun, J. Guerrero and L. Huang, "SoC-based dynamic power sharing method with AC-bus voltage restoration for microgrid applications," *IECON 2012 - 38th Annual Conference on IEEE Industrial Electronics Society*, Montreal, QC, 2012, pp. 5677-5682.
- [29] Y. Guan, J. C. Vasquez and J. M. Guerrero, "Coordinated Secondary Control for Balanced Discharge Rate of Energy Storage System in Islanded AC Microgrids," in *IEEE Transactions on Industry Applications*, vol. 52, no. 6, pp. 5019-5028, Nov.-Dec. 2016.
- [30] <http://www.fipa.org/>
- [31] Erhong Wang, Jinglei Tang and Yimin He, "Intelligent Group Decision Support Systems based on Multi-Agent System," *2012 6th International Conference on New Trends in Information Science, Service Science and Data Mining (ISSDM2012)*, Taipei, 2012, pp. 129-132.
- [32] Q. Li, F. Chen, M. Chen, J. M. Guerrero and D. Abbott, "Agent-Based Decentralized Control Method for Islanded Microgrids," in *IEEE Transactions on Smart Grid*, vol. 7, no. 2, pp. 637-649, March 2016.
- [33] A. Bidram, A. Davoudi and F. L. Lewis, "Two-layer distributed cooperative control of multi-inverter microgrids," *2014 IEEE Applied Power Electronics Conference and Exposition - APEC 2014*, Fort Worth, TX, 2014, pp. 2364-2371.
- [34] V. Nasirian, Q. Shafiee, J. M. Guerrero, F. L. Lewis and A. Davoudi, "Droop-Free Distributed Control for AC Microgrids," in *IEEE Transactions on Power Electronics*, vol. 31, no. 2, pp. 1600-1617, Feb. 2016.
- [35] L. Jingang, Z. Hong, H. Wenshan and L. Xiaoqing, "Distributed secondary control for reactive power sharing of inverter-based DGs in microgrids," *2015 34th Chinese Control Conference (CCC)*, Hangzhou, 2015, pp. 8990-8995.
- [36] C. A. Gross, T. A. Roppel. "Fundamental of electrical Engineering". CRC Press,2012.
- [37] G.Pasini, "Corso di Impianti Elettrici Industriali".